uOttawa

L'Université canadienne
Canada's university

FACULTÉ DES ÉTUDES SUPÉRIEURES ET POSTOCTORALES

uOttawa

L'Université canadienne
Canada's university

FACULTY OF GRADUATE AND POSDOCTORAL STUDIES

Kathy-Sarah Focsanéanu
AUTEUR DE LA THÈSE / AUTHOR OF THESIS

Ph.D. (Chemistry)
GRADE / DEGREE

Faculty of Chemistry
FACULTÉ, ÉCOLE, DÉPARTEMENT / FACULTY, SCHOOL, DEPARTMENT

Applications of Physical Organic Chemistry:
Two Examples of 'Weakly-bound' Dimers

TITRE DE LA THÈSE / TITLE OF THESIS

J.C. Scaiano
DIRECTEUR (DIRECTRICE) DE LA THÈSE / THESIS SUPERVISOR

CO-DIRECTEUR (CO-DIRECTRICE) DE LA THÈSE / THESIS CO-SUPERVISOR

EXAMINATEURS (EXAMINATRICES) DE LA THÈSE / THESIS EXAMINERS

Tony Durst

Derek Pratt

John Pezacki

Jim Wright

Gary W. Slater
Le Doyen de la Faculté des études supérieures et postdoctorales / Dean of the Faculty of Graduate and Postdoctoral Studies

Applications of Physical Organic Chemistry: Two Examples of 'Weakly-Bound' Dimers

Kathy-Sarah Focsanéanu

A thesis submitted to the
Faculty of Graduate and Postdoctoral Studies
in partial fulfillment of the requirements for the degree of
Doctor of Philosophy
in the Ottawa-Carleton Chemistry Institute
Department of Chemistry, University of Ottawa

uOttawa

L'Université canadienne
Canada's university

Candidate	Supervisor
Kathy-Sarah Focsanéanu	Professor J. C. Scaiano

Your file Votre référence
ISBN: 978-0-494-49350-2
Our file Notre référence
ISBN: 978-0-494-49350-2

To my husband and my family,
for their unfailing support, encouragement, and love.

Abstract

This thesis describes two projects involving novel applications of physical organic chemistry.

The first project involved investigation into a series of nitrile-substituted benzyl radicals and their remarkable persistence and attenuated reactivity towards oxygen. Following the characterization of these species by time-resolved spectroscopic techniques, we anticipated that, through radical-radical recombination reactions, they could successfully employed in carbon-carbon bond formation *via* the application of the Persistent Free Radical Effect (PFRE).

In general, radical-radical coupling reactions are inadequate for organic synthetic purposes as they tend to yield complex product mixtures. However, this restriction may be circumvented through use of the PFRE, a kinetic phenomenon that leads to cross-product formation in coupling reactions between persistent and transient radicals.

It is possible to exploit this effect as a synthetic tool through the use of a "radical buffer", in which persistent radicals are generated thermally from dimeric derivatives of the aforementioned persistent carbon-centred radicals. If a transient radical is then introduced photochemically, it will recombine selectively with the persistent radical species. This process is demonstrated in the steady-state photolysis and laser flash photolysis studies of dibenzyl ketone with 2,2,3,3-tetraphenylsuccinonitrile to produce 2,3,3-triphenylproprionitrile. Therefore, by carefully choosing persistent/transient radical pairs, this method may be applied as a simple and effective alternative for more complex organic syntheses.

In subsequent experiments, we found that, along with novel carbon-carbon bond formation, involvement of the persistent carbon-centred radicals could also be applied to other systems, such as the photodecomposition of a pesticide, and the trapping of peroxyl and hydroperoxyl radicals.

The second project investigated the use of pyrene fluorescence quenching as a technique to detect electron-deficient compounds. The photophysical properties of

pyrene in dilute and concentrated solutions have been a topic of intense research interest for many years and the dynamic equilibrium between the monomer and excimer forms has been largely elucidated. However, the effect of certain fluorescence quenchers on the ratio of emission from the two species remained largely unexplored. Time-resolved and steady-state fluorescence techniques were employed to study the quenching behaviour of concentrated pyrene solutions. It was found that certain quenchers, namely electron-poor compounds, were able to efficiently quench both the monomer and excimer species, with bimolecular quenching rate constants approaching diffusion control. As a consequence, by monitoring the monomer-to-excimer fluorescence ratio, it is possible to identify and quantify these compounds. Therefore, this characteristic allows for potential security-related applications, including the detection of explosives and for rapid screening of complex samples suspected of containing explosives.

The concept of differential monomer-to-excimer fluorescence quenching was then extrapolated to other systems that we found intriguing. For example, it was found that, in addition to nitroaromatics, molecular oxygen also quenches both species with rate constants approaching diffusion-control; thus, this methodology can also feasibly be applied to sensing dissolved oxygen. As well, we explored the effect of constrained media on differential quenching, including the use of gas-permeable silicone films and supramolecular materials (zeolites), both heavily-loaded with pyrene, with the idea that these materials could potentially be developed as cheap and disposable sensor materials.

Acknowledgements

I have had the extreme pleasure of spending the last nine years of my life - four as an undergraduate and five as a graduate student - as a member of the Scaiano Research Group at the University of Ottawa. As a result, there is a multitude of people who are due many, many thanks.

First, thank you, Tito, for accepting me into your group so long ago, when I was freshly graduated from high school. You have been an amazing mentor, an unflagging supporter, a (nearly) shameless cheerleader, and a second father. It is a testament to your excellence as a scientist and as a supervisor that students like myself (and there are many others) return to your labs summer after summer, year after year, to work with you. Thank you also to Elda for welcoming me (back) into your family.

Thank you Mom and Dad for your endless love, support, and encouragement - and of course, for a 'rent-free' room during my student career! Thank you Marie-Nicole, Richard, and my gorgeous nieces Hannah and Laura for the stream of cards, emails and phone calls, and for the lovely drawings that adorn my desk: they never fail to make me smile, and they make Halifax feel not so far away. I also wish to thank my husband's family for welcoming me with open arms: I am truly grateful for your support and words of encouragement, and I am so proud to belong to such a loving and close family.

Thank you to Prof. Tony Durst, for his foundation and continuing promotion of the Undergraduate Research Scholarship at the University of Ottawa. Due to your program, I discovered a passion for chemistry, and without it, I would not be where I am today. Your dedication to such an innovative and unique program is inspiring, and it is a boon to all students who are fortunate enough to participate in it.

After nine years in the Scaiano Group, I have worked alongside so many amazing people. Many thanks to past and present members of the group, who have made my time as an undergraduate and graduate student an unforgettable experience. First, thank you to Sonia Corrent and Annie Shaw for guiding me through my very first

summer in the group. To Gonzalo Cosa, I owe many thanks. I learned so much during our two summers together: including how to keep a neat and tidy lab bench! I am also overwhelmingly grateful to Michelle Chrétien, who was a wonderful (and patient) friend: you are a beautiful person and I am in your debt. My fellow graduate students, Larisa Mikelsons, Marie Laferrière, Marius Ivan, Mathieu Frenette, Jessie Blake, Mark Perry, Kathy McGilvray, Paul Billone, Laetitia Rene-Boisneuf, and Steve Maguire: thanks for the many laughs, the many thoughtful conversations, and of course, for the friendship. Long live the Scaiano Group Quote Board!

To the many, many postdocs who passed through our lab doors, I am grateful for sharing your knowledge and experience with me. In particular, I'd like to thank Carolina Aliaga, Alexis Aspée, and Enrique Font-Sanchis for our many fruitful discussions and collaborations. I'd also like thank the two undergraduate students I had the privilege of supervising: thank you Marco Llamazares and Marie-Josée Drouin-Dion, for your enthusiasm and hard work: I can only hope you learned from me as much as I did from you! A deeply felt thanks to Betty Yakimenko for granting my endless 'little favours': your patience with the innumerable demands from the group is to be praised!

To my friends, thank you for your love and support...and yes, I'm finally finished! You can stop asking now!

To my husband, Waleed Jubran: it has been quite a journey, and I'm so grateful to have had you by my side the entire time. Thank you for turning my world 'right-side-up'.

Finally, I'd like to acknowledge the generous financial support I've received from NSERC and the University of Ottawa.

Table of Contents

List of Figures

List of Schemes

List of Tables

List of Abbreviations and Symbols

ΔOD	change in sample absorbance before and after laser excitation
Φ_f	fluorescence quantum yield
τ	lifetime (= k^{-1})
<S>	occupancy, defined as the number of molecules per zeolite cavity
A	pre-exponential factor
AIBN	2,2′-azo*bis*isobutyronitrile
BA	benzaldehyde
BDE	bond dissociation energy
BP	benzophenone
CCD	charge capture device
DBK	dibenzylketone
DCB	1,4-dicyanobenzene
DMF	dimethylformamide
DNA	deoxyribonucleic acid
DPE	diphenylethane
$^1E^*$	first singlet excited state of the excimer form of pyrene
EI	electron impact
EPA	United States' Environmental Protection Agency
F_E	fluorescence emission from the excimer form of pyrene
F_M	fluorescence emission from the monomer form of pyrene
FV	fenvalerate
GC	gas chromatography

HMX	octahydro-1,3,5,7-tetranitro-1,3,5,7-tetrazocine
HOMO	highest occupied molecular orbital
HPLC	high performance liquid chromatography
I	absorption or emission intensity (arbitrary units)
k	rate constant
K_{eq}	equilibrium constant
K_{SV}	Stern-Volmer constant
LC	liquid chromatography
LED	light-emitting diode
LFP	laser flash photolysis
LUMO	lowest unoccupied molecular orbital
$^1M^*$	first singlet excited state of the monomer form of pyrene
mp	melting point
***m*PPA**	*m*-phenoxyphenylacetonitrile
MS	mass spectrometry
nLFP	nanosecond laser flash photolysis
NMR	nuclear magnetic resonance
P•	persistent radical
PAH	polycyclic aromatic hydrocarbon
PDA	photodiode array
PDMS	polydimethylsiloxane
PFRE	Persistent Free Radical Effect
PMT	photomultiplier tube
ppm	parts per million

PTI	Photon Technology International, Inc.
^{1}Py•	first singlet excited state of pyrene
Py	pyrene
Q	quencher
Q_A	electron-accepting quencher
Q_D	electron-donating quencher
R•	carbon-centred radical
RDX	hexahydro-1,3,5-trinitro-1,3,5-triazine
RO•	alkoxyl radical
ROO•	alkylperoxyl radical
SDS	sodium dodecyl sulfate
T•	transient radical
T_c	critical temperature for the formation of a dynamic equilibrium
TEMPO	2,2,6,6-tetramethyl-piperidine-1-oxyl free radical
TNT	2,4,6-trinitrotoluene
TP	triphenylphosphine
T-P	cross –reaction product between radicals T• and P•
TPO	triphenylphosphine oxide
TPP	2,2,3-triphenylpropionitrile
TPS	1,1,2,2-tertrasuccinonitrile
TTL	transistor-transistor linked
UVA	ultraviolet radiation ranging from 315-400 nm.
UVB	ultraviolet radiation ranging from 280-315 nm.
UVC	ultraviolet radiation ranging from 100-280 nm.

UV-vis ultraviolet-visible

YAG yttrium-argon-garnet

Abbreviations for the quenchers used in Chapters 6 and 7 can be found in Appendix 6A.

Chapter 1. Introduction

Chapter 1. Introduction

In the last decade, the field of physical organic chemistry has witnessed leaps in innovation and a shift from basic to applied research: taking fundamental concepts of physical organic chemistry and applying them to exciting areas such as supramolecular chemistry, molecular recognition, materials chemistry and nanotechnology.

This thesis describes two successful applications of physical organic chemistry. The first project investigated the possible application of a kinetic phenomenon to deliberate and selective carbon-carbon bond formation mediated by radical-radical recombination reactions. The second project involved employing knowledge about pyrene, a highly-studied fluorophore, to a novel methodology to detect electron-deficient materials.

1.1 Organic Synthesis Mediated by the Persistent Free Radical Effect

In general, radical-radical coupling reactions are considered to be inadequate for organic synthetic purposes as they tend to yield complex product mixtures. However, this restriction may be circumvented *via* the use of the Fischer-Ingold Persistent Free Radical Effect (PFRE), a kinetic phenomenon that leads to cross-product formation in coupling reactions between persistent and transient radicals. This section will describe persistent radicals, dimers prepared from persistent carbon-centered radicals, the operation of the PFRE, and how the PFRE may be applied to practical organic synthesis.

1.1.1. Defining 'Persistence'

When describing typical carbon-centred radicals, the adjective "stable" is frequently employed to indicate the relative potential energies of the radical species. For example, Scheme 1.1 illustrates the stabilities of the primary, secondary, and tertiary radicals generated from homolytic cleavage of the various C-H bonds in 1-methylbutane.[1] Of these three reactions, the greatest energy must be supplied to produce the primary alkyl radical; this radical thus has the greatest potential energy. Since the relative stability of a chemical species is inversely proportional to its potential energy, the secondary and tertiary radicals are therefore more stable radicals.

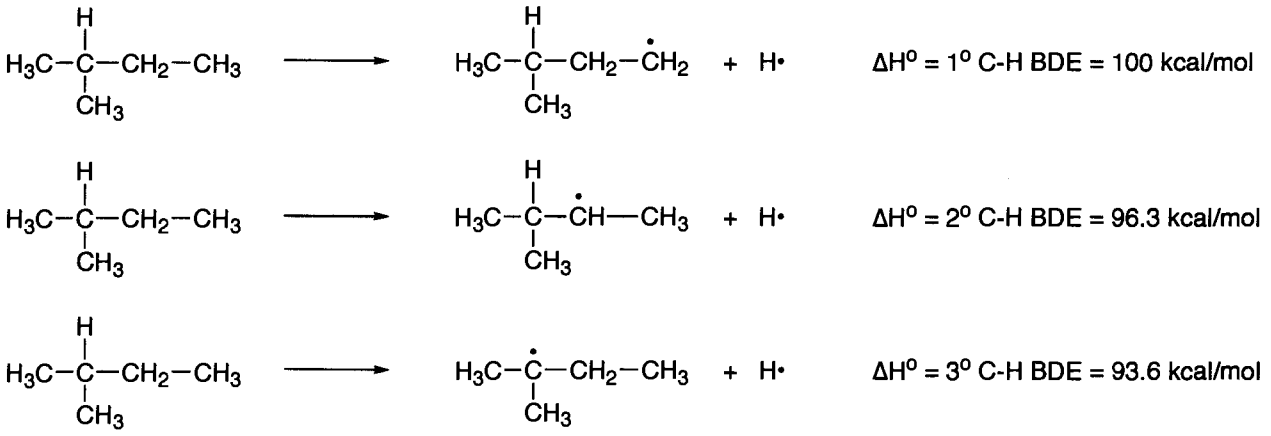

Scheme 1.1. Primary, secondary, and tertiary alkyl radicals generated from 1-methylbutane. BDE = bond dissociation energy.

In general, there are four factors which contribute to the thermodynamic stability of radicals:[2]

1. Hyperconjugation: usually used to explain alkyl radical stabilities, this effect is interpreted as the interaction between a singly-occupied 2p orbital at the carbon

radical centre with the filled σ and empty σ* of a C-H (or a C-C) bond on an alkyl substituent. Increasing the number of substituents increases this stabilization, resulting in the trends illustrated in Scheme 1.1.

2. Mesomerism: this effect is observed for radicals in which the unpaired electron is conjugated with unsaturated systems (*e.g.* allylic or benzylic radicals), thus allowing for multiple resonance structures to be drawn. In general, radical stabilization increases with the number of its possible resonance forms.
3. Hybridization: this refers to the effect of hybridization at the carbon radical centre, where destabilization increases with the s character of the orbital. For example, in the phenyl radical, the unpaired electron is in a sp^2 orbital, and so is considerably less stable than a dialkylmethyl radical, where the electron is in a pure p orbital.
4. Captodative effect: this is observed for radicals with two substituents, XR•Y, capable of exerting electronic effects, where the stabilization energy contributed by these groups is not strictly additive (*i.e.* E_s (XR•H) + E_s(HR•Y) ≠ E_s(XR•Y)). When the two substituents are of the same type (both electron-donating or electron-withdrawing), the resulting stabilization energy is less than the sum of the two effects taken individually; this is referred to as an *antagonistic* effect. Conversely, if one group is an electron-donor while the other is an electron-attractor, the stabilization is greater then the sum of the two separate effects; this is referred to as a *synergistic* or *captodative* effect.

While one of these effects affords a radical some stability, a combination of two or more provides significant stabilization for a carbon-centred radical, thus weakening the relevant C-H bond.

Unfortunately, for many years, the term 'stable' was also applied to radicals that displayed unusually long lifetimes. This led to a degree of ambiguity regarding the kinetic parameters of certain radical species. For example, primary, secondary, and even tertiary benzylic radicals are considered to be stable radicals due to their multiple possible resonance structures. However, benzylic radicals are generally *not* long-lived species: these radicals usually undergo self-termination reactions at close to the diffusion-controlled limit.[3]

In an effort to avoid confusion when applying adjectives to certain carbon-centered radicals, Ingold and Griller proposed in 1976 the usage of the term "persistent" to describe radicals with significantly longer lifetimes than a methyl radical under similar conditions.[4] Conversely, those radicals that display rapid decay can be accurately designated as 'transient' radicals. Ingold and Griller thus stated that the term 'stable' is more appropriately a thermodynamic parameter, and suggested that 'stabilized' radicals R• are those whose C-H bond strength is less than that of the C-H bond strength of the corresponding alkane analogue.

Ingold and Griller then established the two general criteria for a persistent radical to be attenuated self-reaction (*i.e.* resistance to recombination) and an attenuated reactivity with oxygen (so that they may be prepared and handled under general laboratory conditions).

The classic example of a persistent carbon-centred radical is the triphenylmethyl radical, first described by Gomberg in 1900 (Scheme 1.2).[5] This radical exists in solution in equilibrium with its head-to-tail dimer, where the persistence of this and other similar radicals have been attributed to electronic and steric factors.

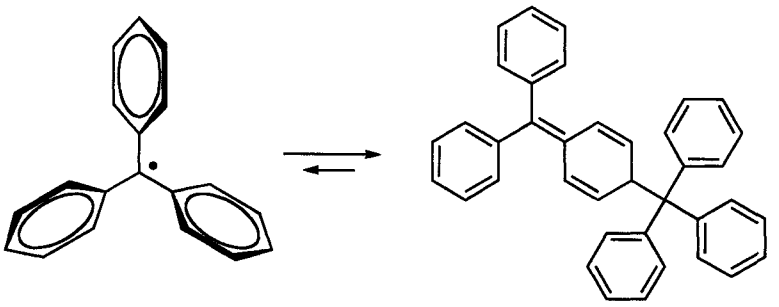

Scheme 1.2. The persistent triphenylmethyl radical co-exists in solution with its head-to-tail dimer.

1.1.2. Carbon-Centred Radicals and Persistence

Recently, the Scaiano group investigated several lactones and cyano-substituted compounds as potential antioxidants (Scheme 1.3).[6-9] These molecules all behaved as excellent H-donors: the benzylic C-H bonds in **1** and **4** were readily abstracted by *tert*-butoxyl radicals with rate constants on the order of ~10^7 $M^{-1}s^{-1}$. For the radical species generated from the coumaranone derivatives **2** and **3**, the observation of a kinetic solvent effect on the rate of hydrogen abstraction led to the conclusion that the active H-donor was actually the enol form, with O-H abstractions comparable to the benzylic C-H bonds.[10]

Surprisingly, the resulting carbon-centered radicals were remarkably long-lived, with half-lives in the hundreds of microseconds, and they displayed a greatly

attenuated reactivity towards oxygen (*i.e.* essentially negligible on the time scale of laser flash photolysis). The results for radical **1** and other α-cyanobenzylic radicals are described in Chapter 3 of this thesis.

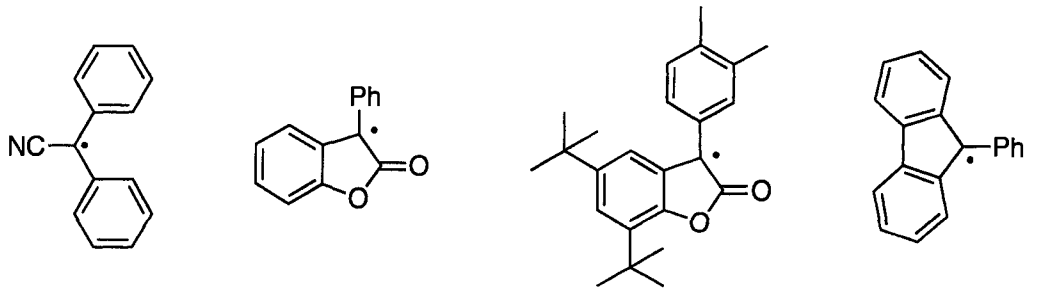

1 **2** **3** **4**

Scheme 1.3. Persistent carbon-centered radicals investigated in the Scaiano group.

Geometry optimization calculations revealed that these radicals were generally planar and spin distribution calculations showed that the heteroatoms contributed significantly to the overall spin density. In some cases, this contribution was as much as 25%, with less than 50% spin density at the carbon radical centre itself. Therefore, it was proposed that there are essentially five factors which influence radical persistence and electrophilic attack by oxygen: 1) resonance stabilization, 2) unpaired spin delocalization on a heteroatom, 3) favorable stereoelectronic effects (*e.g.* planarity), 4) the presence of electron-withdrawing and/or electron-donating groups (especially in cases in which the captodative effect is operating), and 5) steric effects. This list is not in order of importance nor is it a checklist: it is the combination of some or all of these criteria which render a carbon-centered radical persistent and/or unreactive towards oxygen.

1.1.3. Dimers of Persistent Carbon-Centred Radicals

Dimers of the persistent carbon-centered radicals shown in Scheme 1.3 were prepared from their corresponding monomers (Scheme 1.4).[11]

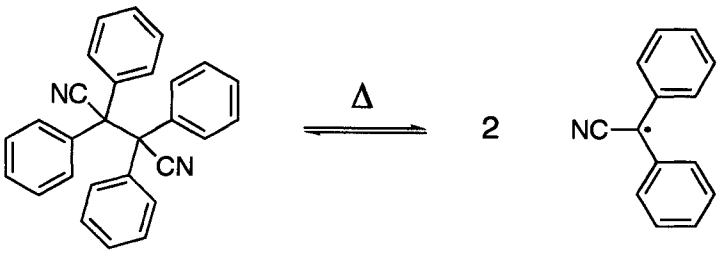

Scheme 1.4. Dimers prepared from the persistent carbon-centered radicals are in thermal equilibrium with the radical species.

The UV-visible absorption spectra revealed that, in toluene solution, the dimers are in thermal equilibrium with the radical species. Frenette *et al.* determined that these molecules have bond dissociation energies of 15-26 kcal/mol and an average bond length of 1.6Å for the central C-C bond. Thus, even at room temperature, a small fraction of the radical species will be present in equilibrium with the dimer.

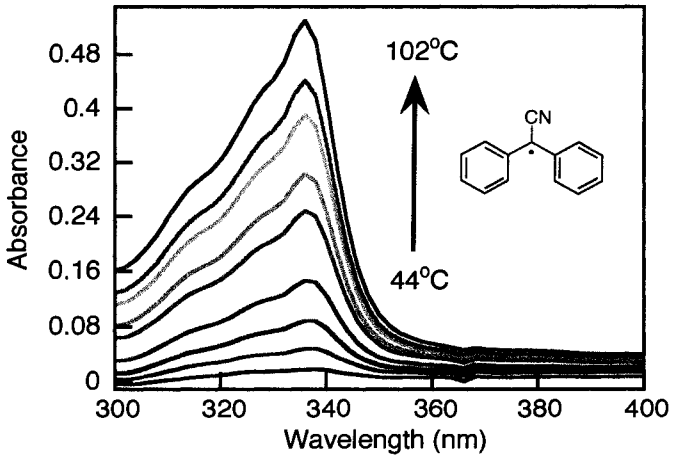

Figure 1.1. UV-visible absorption spectrum of the α-cyanodiphenylmethyl radical, generated thermally from its respective dimer. Adapted from Reference 12.

Most interestingly, these dimers showed no significant decomposition upon prolonged irradiation or heating while in solution. This apparent stability was attributed to the fact that the radical species are unreactive towards molecular oxygen and virtually unreactive towards possible side reactions such as hydrogen abstraction from solvents like toluene. Thus, the usual fate of the radicals is to simply recombine to reform the dimer; the term *dynamic stability* was used to describe this behaviour.[11] Ultimately, it was this characteristic that led us to investigate how the dynamic stability might be affected by the introduction of a second radical species, and the resulting product distribution from radical-radical recombination reactions.

1.1.4. Radical-Radical Recombination Reactions

Radical-radical recombination reactions are not generally considered to be useful for organic synthesis purposes because these termination reactions tend to yield complex mixtures of products.[12] For example, consider the free radical combination reactions involving two different radicals, A• and B•. Ignoring all other possible side reactions (rearrangements, fragmentations, hydrogen abstractions, etc.), this system can lead to three different combination products, as shown in Scheme 1.5.

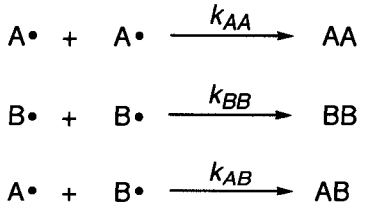

Scheme 1.5. Free radical combination reactions.

In these reactions, we normally expect the cross-combination reaction (forming AB) to reflect statistics as the geometric mean of the self-reaction rate constants[13-15], *i.e.*

$$k_{AB} = 2\sqrt{k_{AA}k_{BB}} \quad (1.1)$$

In general, radical-radical reactions are very fast when they involve unhindered radical centers leading to the formation of a strong sigma bond, making the reaction highly exothermic. In solution, the maximum rate constant achievable is one quarter of the diffusion-controlled rate constant (~10^{10} $M^{-1}s^{-1}$), reflecting spin statistical factors.[16] In these cases (*i.e.* $k_{AA} = k_{BB} = ¼\ k_{diff}$) the observed product ratio would reflect simple statistics, where [AA]:[BB]:[AB] would equal 1:1:2. Thus, even in the simplest of systems, the maximum yield of a cross-reaction product is only 50%. Therefore, due to these limitations, radical-radical recombination reactions are generally not considered to be useful synthetic tools. However, we hypothesized that such reactions could prove practical by applying the kinetic phenomenon known as the Fischer-Ingold Persistent Free Radical Effect.

1.1.5. The Fischer-Ingold Persistent Free Radical Effect (PFRE)

In 1985, Hanns Fischer was intrigued by some unusual experimental observations, such as the photochemical behavior of methylcobalamine: it was essentially photostable in the absence of radical traps, but highly unstable in the presence of methyl radical scavengers (Scheme 1.6)[17]. If methyl radicals are formed, why is ethane not a significant product? A discussion with Keith U. Ingold proved illuminating for Fischer, and led to a significant contribution to the field of physical organic chemistry.

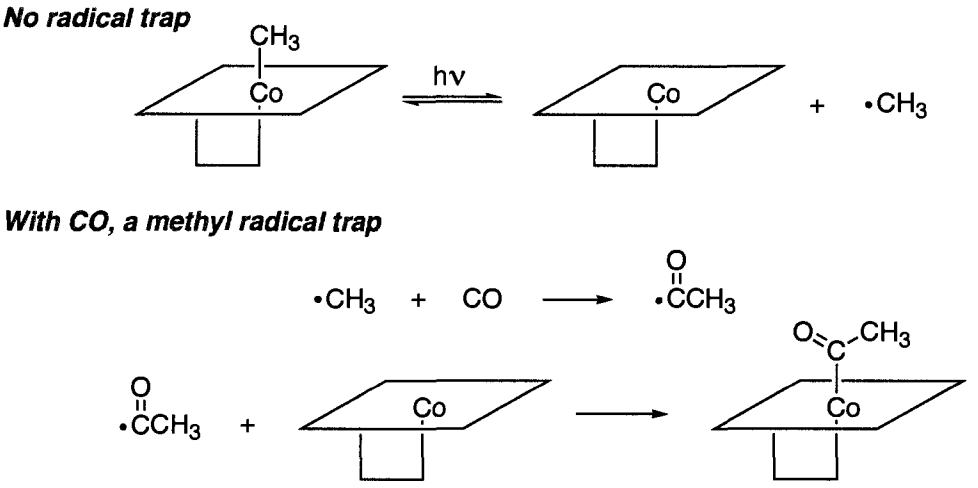

Scheme 1.6. Methylcobalamine is photostable in solution in the absence of methyl radical traps, but forms acetylcobalamine in the presence of carbon monoxide.

In his seminal 1986 paper, Fischer credited his discussion with Ingold for the mechanistic suggestion that led to today's understanding of the Fischer-Ingold Persistent Free Radical Effect.[18] Fischer took the concepts underlying Ingold's suggestion and developed a full kinetic model for the interpretation of experimental data. In a 2001 review on this kinetic phenomenon and its applications[19], Fischer went further in his acknowledgment of previous, independent descriptions of the effect by Bachmann[20] and Perkins[21].

The PFRE is a kinetic phenomenon that controls product formation in systems involving radical-radical recombination reactions. It is normally examined in systems where transient (T•) and persistent radicals (P•) are generated simultaneously, frequently from a single precursor:

$$\text{Source} \xrightarrow{k} \text{T}\bullet + \text{P}\bullet \qquad (1.2)$$

We would expect these radicals to undergo the following recombinations:

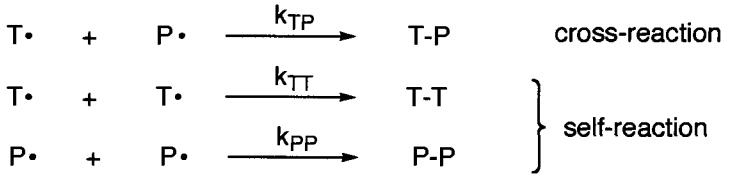

Scheme 1.7. Radical-radical recombinations involved in the PFRE.

However, by definition, persistent radicals are resistant to dimerization, or *self-reaction*. Thus, the rate constant for the self-reaction of P•, k_{PP}, must be very small relative to the rate constants for the other two reactions, or:

$$k_{TP}, k_{TT} >> k_{PP} \tag{1.3}$$

It is this inequality that establishes the conditions necessary for the operation of the PFRE: each time two T• radicals undergo self-reaction, there is a corresponding accumulation of two unreacted P• radicals. As a result, the concentration of persistent radical increases rapidly in the system; the sole reaction pathway available to these P• radicals is the cross-reaction with T•. Since the rate of the cross-reaction is directly proportional to the concentration of P•,

$$Rate_{TP} = k_{TP}[T\bullet][P\bullet] \tag{1.4}$$

the cross-reaction accelerates, suppressing the self-reaction of T• to form T-T. The end result is the dominant formation of the cross-reaction product, T-P. Thus, the system is 'self-adjusting' in that the accumulation of P• continues until the kinetic condition favouring cross-reaction is established. After this point, T• and P• are consumed in stoichiometric amounts.

This can be seen graphically in Figure 1.2: T-T is formed initially, but then its concentration remains constant when T-P begins to form ([P-P] remains small through the whole reaction).

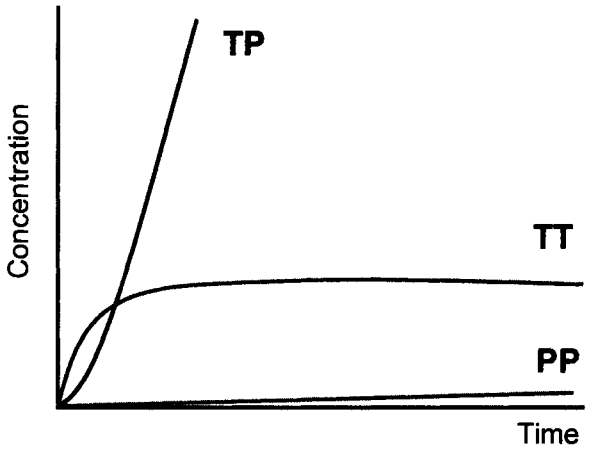

Figure 1.2. Schematic representation of the PFRE at short timescales. Note that [T-P] increases when the self-reaction to form T-T is suppressed; [P-P] remains very small at all times.

The operation of the persistent free radical effect thus inspired us (and others) to realize that indeed, radical-radical recombination reactions can be used in effective organic synthesis, as long as we require the radical intermediates to be *disciplined*: in other words, we have some knowledge regarding the kinetic behaviour of these species. The Fischer-Ingold persistent free radical effect has since been applied to several systems,[19, 22-30] including living free radical polymerization,[31-38] and more than likely, there are dozens of reactions buried in the literature that could benefit from re-interpretation based on the Fischer-Ingold effect.

1.1.6. The Synthetic Concept

Inspired by the operation of the persistent free radical effect, we devised a novel synthetic method for selective carbon-carbon bond formation mediated by radical-radical recombination reactions. Although the PFRE is normally examined in systems where the two different radicals are generated simultaneously from a single precursor, in this technique, the supply of persistent and transient radicals was independently controlled: persistent radicals were produced thermally from their aforementioned dimers while transient radicals were generated *in situ* photochemically, as shown in the modified PFRE scheme below.

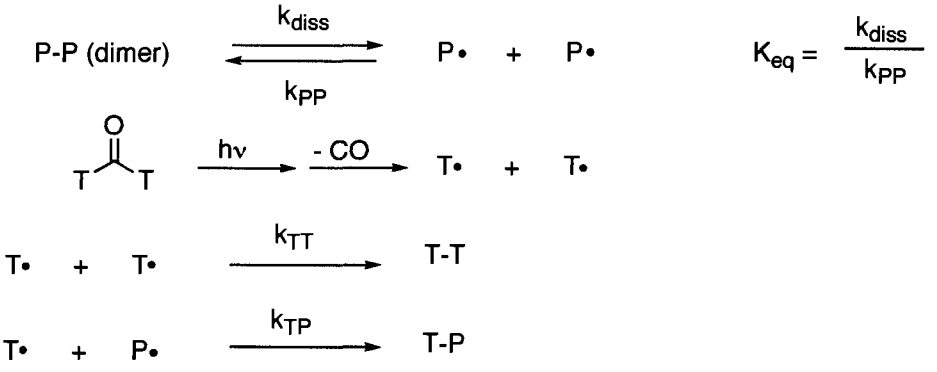

Scheme 1.8. Modified PFRE scheme, where the persistent and transient radicals are generated thermally and photochemically, respectively.

As shown in Scheme 1.8, transient radicals can be generated from Norrish Type I cleavage and subsequent decarbonylation from a symmetrical ketone.[16] In this case, we used dibenzylketone (DBK) as the source of transient radicals. The photochemistry of DBK is well-known:[39, 40] steady-state photolysis in toluene using UVB lamps leads to 1,2-diphenylethane (DPE) as the only significant product, formed by combination of two benzyl radicals according to Scheme 1.9.

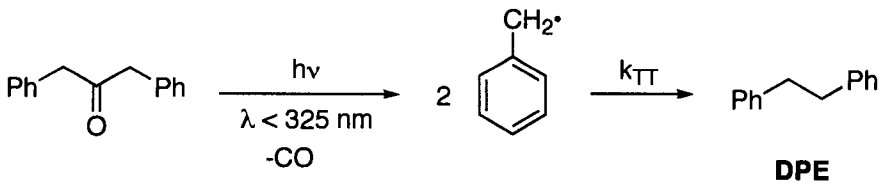

Scheme 1.9. The photochemistry of dibenzylketone.

Therefore, by combining the photoreaction of Scheme 1.9 and the thermal equilibrium of Scheme 4, we obtain a simple, yet effective one-pot synthesis of 2,2,3-triphenyl-propionitrile, TPP, as illustrated in Scheme 1.10.[41]

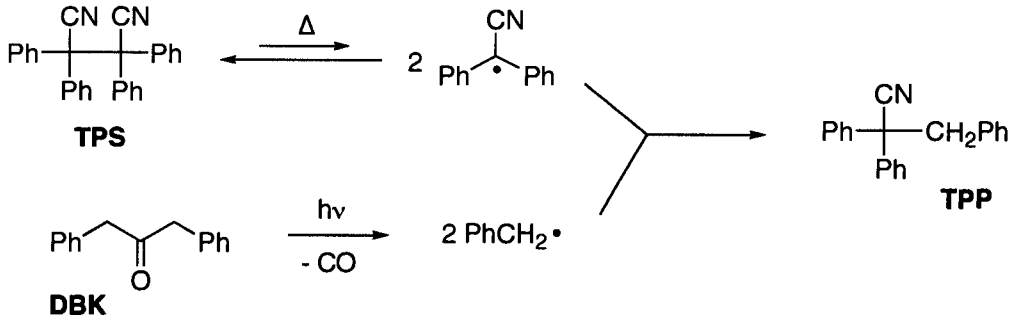

Scheme 1.10. Organic synthesis using the PFRE. Benzyl radicals are produced photochemically from DBK, while diphenylcyanomethyl radicals are generated thermally from the dimer, TPS.

A sort of "radical buffer" results, with the persistent radicals trapping the transient radicals to form the cross-reaction product, while the dimer (through the equilibrium of Scheme 1.4) keeps the supply of radicals available. Although other examples of synthesis employing the PFRE are described in the literature, we believe this method to be the first to involve C-C bond formation through independent control of persistent and transient radicals.

1.2 Detection of Electron-Deficient Compounds by Pyrene Fluorescence Quenching

The photophysical properties of pyrene in dilute and concentrated solutions have been the topic of intense research interest for many years and the dynamic equilibrium established between the monomer and excimer forms has been largely elucidated. However, the effect of certain fluorescence quenchers on the ratio of emission from the two species remained largely unexplored. Investigation revealed that electron-deficient molecules interact with the charge-transfer excimer complex as well as the pyrene monomer. This characteristic allows for the potential identification and quantification of electron-deficient compounds, leading to possible security-related applications, including the rapid screening of complex samples suspected of containing explosives. This section will introduce the basic photophysical properties of pyrene, its interactions with electron deficient molecules, and possible analytical applications.

1.2.1. The Fluorophore Pyrene

Pyrene is a rigid, planar alternant polycyclic aromatic hydrocarbon (PAH) that has received intense and widespread attention as a practical fluorophore because it offers several advantages: it absorbs strongly in the UV region (with extinction coefficients on the order of 10^4 $M^{-1}s^{-1}$), it fluoresces intensely (with a quantum yield Φ_F ~0.65), it has a fairly long-lived singlet excited state (up to 475 ns in dilute solutions), and the intensities of the bands in its fluorescence spectra are sensitive to the polarity of its environment.[42] As well, pyrene exists in equilibrium with an excited-state complex, known as the excimer (*vide infra*), in moderately concentrated solutions. Consequently,

pyrene and its derivatives appear in thousands of research articles, representing an unmatched range of sensing and reporting applications that would be impossible to list here.

As a result of such extensive and insightful research, the photophysical properties of pyrene are well-established. Figure 1.3 shows the normalized absorption and fluorescence spectra of a dilute (4 μM) solution of pyrene in ethanol. The fine-structured bands in the fluorescence spectrum correspond to emission from the first singlet excited state of pyrene, ^{1}Py*. In general, the fluorescence spectra of PAHs are mirror images of the absorption spectra, where the 0,0 band (representing absorption and emission between the lowest vibrational levels of the ground and excited states of the molecule) may or may not be present in the fluorescence spectrum due to self-absorption.[16, 43] Planar, rigid PAHs fluoresce quite strongly ($\Phi_f > 0.5$) relative to their non-planar counterparts due to their less efficient radiationless deactivations from the singlet excited state.[44]

The $\pi^* \rightarrow \pi$ emission spectrum of pyrene shows five well-resolved major vibronic bands between 370 and 400 nm. These peaks are usually labeled I, II, III, IV, and V.

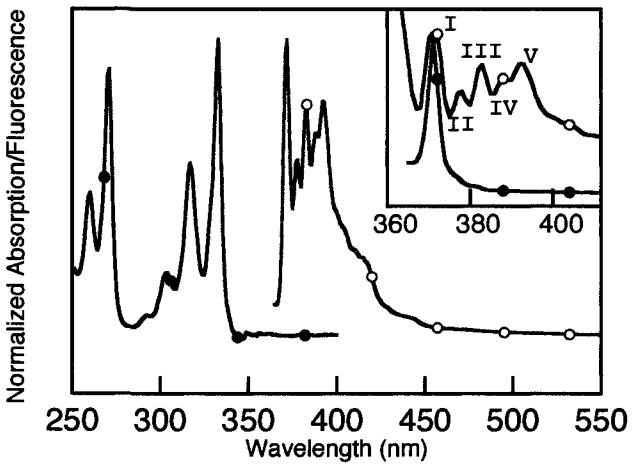

Figure 1.3. Normalized absorption (●) and fluorescence (O) spectra of pyrene, 4μM in ethanol. Inset: Zoom view of the 0,0 band region.

As mentioned above, the fluorescence spectra of PAHs are often sensitive to solvent polarity: the intensity of the first vibronic band (I) undergoes significant enhancement with increasing solvent polarity relative to the third band (III) due to coupling of the electronic and vibronic states. Measurement of the ratio of emission intensities of the vibronic bands (I/III) in different solvents leads to the formation of the so-called Py-scale of solvent polarity.[45, 46] As a result, pyrene or similar derivatives are frequently used to probe local polarity, such as within lipid bilayers or micelles.[47]

1.2.2. The Pyrene Excimer

In 1955, Förster and Kasper were the first to report the fluorescence spectra of moderately concentrated solutions of pyrene showing two distinct emission bands.[48, 49] The fine structured band below 400 nm corresponds to emission from the singlet excited state monomer, $^1M^*$.[42] The broad, structureless band centered around 470 nm is

emission due to the formation of 'excited dimers', or *excimers*, a term first introduced in 1962 by Stevens.[50]

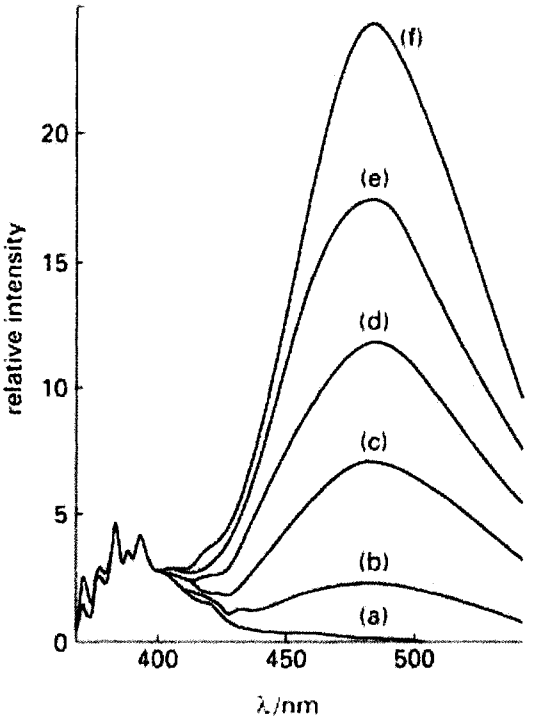

Figure 1.4. *Fluorescence spectra of pyrene solutions in cyclohexane, normalized at 392 nm.* (a) $1x10^{-4}$ M (b) $1x10^{-3}$ M (c) $3.25x10^{-3}$ M (d) $5.5x10^{-3}$ M (e) $7.75x10^{-3}$ M (f) $1x10^{-2}$ M. The band appearing around 480 nm corresponds to the pyrene excimer. From Reference 59.

The excimer $^1E^*$ is a relatively stable excited-state charge-transfer complex between one excited molecule of pyrene and another in its ground state, where the distance between the two pyrenes is roughly equivalent to that between layers of graphite (~3 to 4 Å).[42]

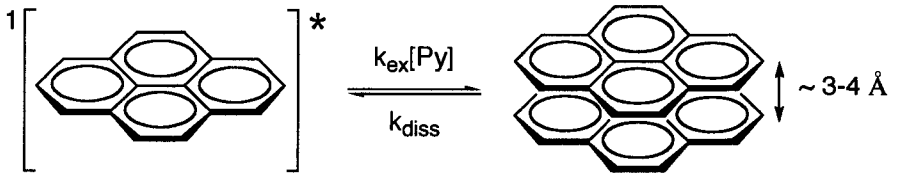

Scheme 1.11. Excimer formation in moderately concentrated solutions of pyrene.

The pyrene excimer is a collision complex, stabilized by a charge-transfer interaction relative to an analogous collision between two ground-state pyrene molecules. This can be explained *via* simple molecular orbital interaction theory (Figure 1.5).[16, 43]

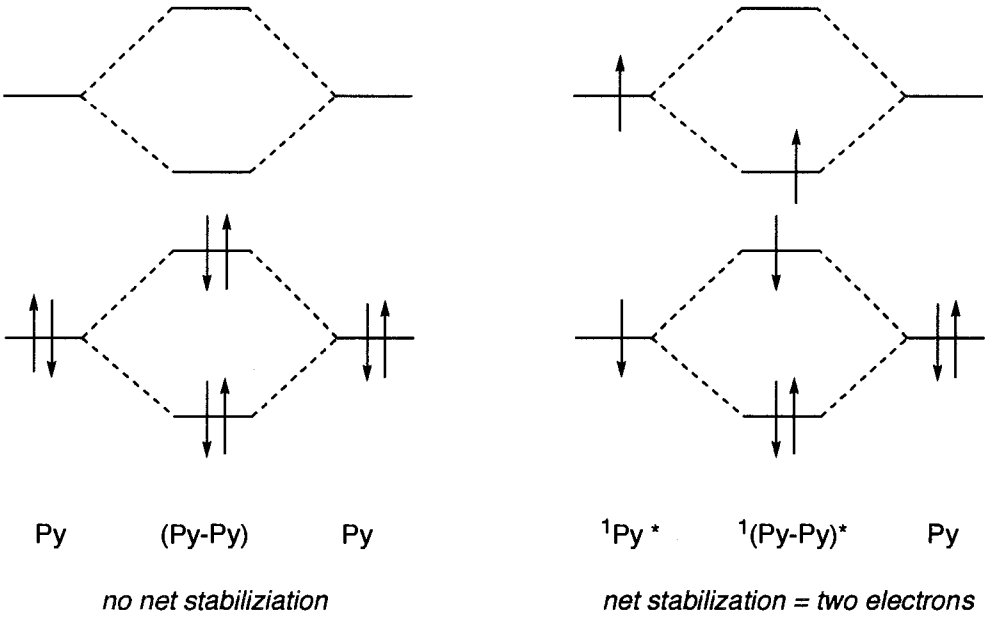

Figure 1.5. Molecular orbital interactions between two ground state pyrenes *versus* a ground state with an excited state pyrene.

When two ground-state pyrenes approach each other, two electrons are stabilized and two electrons are destabilized, leading to no net gain in energy, and thus the molecules dissociate. However, in the excimer, three electrons are stabilized and

only one electron is destabilized, resulting in an overall stabilization of two electrons. This corresponds to a binding energy for the pyrene excimer of 38-42 kJ/mol in non-viscous solvents.[51-54]

1.2.3. The Monomer-Excimer Equilibrium

Since the 1950s, the monomer-excimer equilibrium has been thoroughly investigated, in both solution and the solid state.[42, 55-58] Using a variety of steady-state and time-resolved spectroscopic techniques, researchers have made the pyrene excimer one of the most well-understood excited-state species. This section serves to highlight a fraction of the mound of data regarding the pyrene monomer-excimer equilibrium that has been amassed in the intervening decades.

Scheme 1.12 displays the formation and deactivation pathways for the monomer (M) and excimer (E) forms of pyrene. The initial observation that the ratio of excimer to monomer fluorescence (F_E/F_M) was directly proportional to the solution's concentration led to the realization that formation of the excimer species was not due to excitation of ground state dimers (also confirmed by absorption spectra). Förster demonstrated that excimer formation was also proportional to the solvent viscosity, illustrating that excimerization is indeed a diffusion-controlled process.[48, 49]

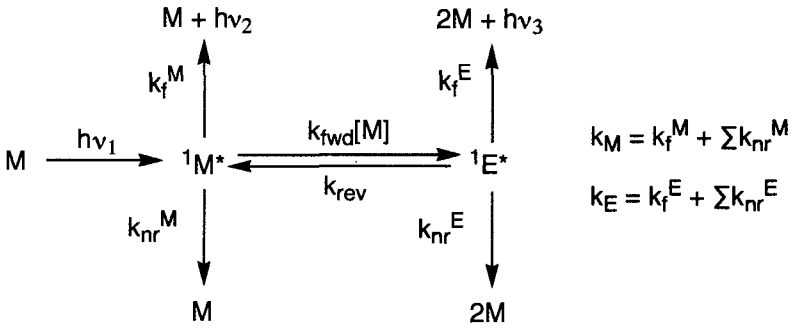

Scheme 1.12. Decay pathways for the monomer (M) and excimer (E) forms of pyrene; k_f = fluorescence rate constant, k_{nr} = sum of rate constants for non-radiative processes.

Under photostationary conditions (where $d[^1M^*]/dt = d[^1E^*]/dt = 0$), the following equilibrium relations are obtained:

$$K_{eq} = \frac{[^1E^*]}{[^1M^*][M]} = \frac{k_{fwd}}{k_{rev} + k_E} \tag{1.5}$$

where k_E is the observed decay rate constant for the excimer species including both radiative and nonradiative pathways. For a 4 mM solution of pyrene, Birks determined the rate constants for excimerization and de-excimerization, k_{fwd} and k_{rev}, to be 7×10^9 $M^{-1}s^{-1}$ and 0.6×10^7 s^{-1}, respectively.[42] In solution at room temperature, he also found that the decay of the excimer species is approximately three times faster than the rate of de-excimerization ($k_E \sim 2 \times 10^7$ s^{-1}). Thus, the photostationary requirements are not met and the monomer-excimer equilibrium is not established under these conditions.

However, at higher temperatures, a dynamic equilibrium is possible, with excimers dissociating to regenerate ground state and excited state pyrene molecules. This dynamic equilibrium is possible when

$$k_{fwd}[^1M^*], k_{rev} >> k_M, k_E \qquad \therefore K_{eq} \rightarrow \frac{k_{fwd}}{k_{rev}} \tag{1.6}$$

This condition is satisfied above a critical temperature T_c, which depends on the excimer binding energy and solvent viscosity. For most compounds in low viscosity solvents, T_c is below room temperature; for pyrene, however T_c is at or above room temperature, as illustrated by Birks' observations.[42]

1.2.4. Pyrene Fluorescence Quenching

Along with using the I/III band intensities to indicate solvent polarity and excimer formation to monitor solvent viscosity, pyrene fluorescence quenching has also been used as an effective analytical tool. Some recent applications in analytical chemistry include: detecting NO in NO-releasing oxygen-sensing polymer films,[59] probing the heterogeneous microenvironments of the C18 stationary phase in capillary electrochromatography,[60] and measuring intracellular molecular oxygen concentrations.[61]

Deactivation of the pyrene monomer and excimer singlet excited states is regulated by the competition between radiative and non-radiative pathways. While the rate constant for fluorescent decay (k_F) is largely insensitive to the molecular environment, rate constants for non-radiative processes are readily influenced by perturbations resulting from interactions between pyrene and solvent or quencher molecules. Thus, increasing the strength or number of these interactions results in more efficient non-radiative decay and hence the observed fluorescence quenching.

For PAHs, the most widely accepted theory for fluorescence quenching involves an electron- or charge-transfer mechanism, where the fluorophore acts as an electron donor or acceptor in a complex with the quencher.[62] In this mechanism, the fluorophore

and quencher encounter each other in solution and undergo partial or full electron transfer. A rapid back electron transfer then occurs, returning the fluorophore and its quencher back to their respective ground states.[63]

The charge transfer is illustrated in Figure 1.6A using frontier molecular orbital theory: an electron-donating quencher (Q_D) undergoes partial or full electron transfer from its HOMO to the half-filled HOMO of $^1Py^*$ while an acceptor quencher (Q_A) will engage in partial or full electron transfer from the half-filled LUMO of $^1Py^*$ to its LUMO. Therefore, the efficiency of quenching is proportional to the ionization potential of Q_D or the electron affinity of Q_A. In general, nitro-substituted compounds are known to selectively quench alternant polycyclic aromatic hydrocarbons (by acting as the electron acceptor) whereas alkyl amines act as electron donors and quench non-alternant PAHs.[64-68]

While the pyrene monomer is readily quenched by both electron rich and electron poor substrates in polar media according to the above mechanism, the pyrene excimer is said to be stabilized against electron-transfer quenching. This is illustrated in Figure 1.6B: for the excimer, Q_D undergoes partial or full electron transfer to ψ_2 while Q_A undergoes partial or full electron transfer from ψ_3. Since ψ_2 is raised and ψ_3 is lowered relative to the HOMO and LUMO of the pyrene monomer, respectively, electron transfer to ψ_2 or from ψ_3 will thus be more difficult for the excimer species for a given quencher.[69]

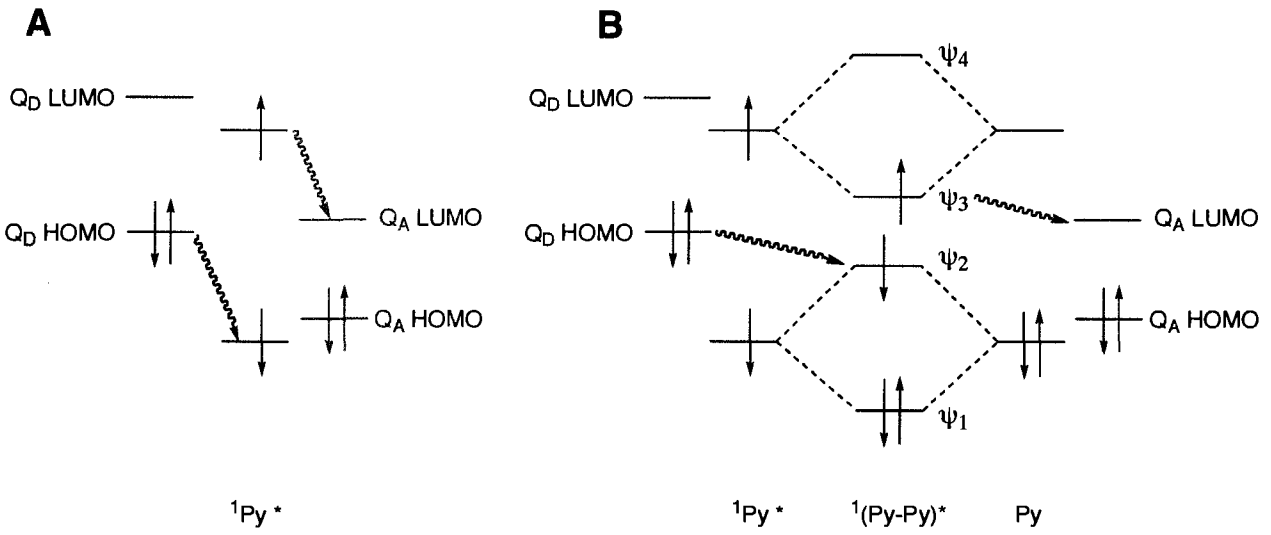

Figure 1.6. Fluorescence quenching by electron donating (Q_D) and electron-accepting (Q_A) quenchers: (A) Pyrene monomer. (B) Pyrene excimer.

The research described in this thesis revealed that a certain class of highly-electron deficient compounds, namely nitroaromatics, effectively *does* quench excimer fluorescence. Since these nitrated molecules are known and used for their explosive properties, we anticipated that a detection method based on excimer fluorescence quenching would have potential security applications.

1.2.5. Explosives

Explosives are a class of highly energetic materials. The decompositions of these materials are extremely exothermic chain reactions, releasing enormous amounts of heat and gas, typically within a fraction of a second.

Prior to the middle of the nineteenth century, explosive materials were limited to naturally-occurring nitrate or perchlorate salts. Christian F. Schönbein's accidental discovery of nitrocellulose in 1846 led to the development of other nitrated materials, such as shock-sensitive nitroglycerin (later modified into a stable form as dynamite by

Alfred Nobel). Towards the turn of the century, progress in the field of organic chemistry led to the discovery of nitroaromatic explosives, such as picric acid (**1**) and 2,4,6-trinitrotoluene (**2**). Today, the majority of commercial or military-grade explosives use hexahydro-1,3,5-trinitro-1,3,5-triazine (RDX, **3**) or octahydro-1,3,5,7-tetranitro-1,3,5,7-tetrazocine (HMX, **4**) as the primary explosive.

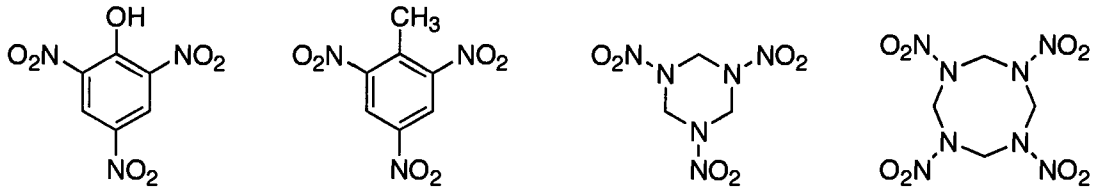

1 **2** **3** **4**

Scheme 1.13. Common explosive organic compounds.

While energetic materials are the result of several different kinds of functional groups (such as perchlorates or peroxides), the vast majority of commercially available or military-grade explosives use nitrated derivatives as the primary explosive. Since the nitro group is highly electron-withdrawing, these are, in general, electron-deficient compounds. However, the methods used to detect these materials do not take advantage of this common trait; instead, detection technology often relies on time-of-flight mass spectrometry or chromatographic techniques.

1.2.6. Explosives detection

Explosives detection methods can, in general, be divided into two separate categories. 'Real-time' detection methods are those associated with security applications, such as landmine clearance or airport security. In these methods,

quantification and/or identification of the explosive is often not critical. Instead, these are screening techniques, where a simple yet accurate positive or negative response for the presence of explosive materials is desired. Alternatively, laboratory detection methods are normally associated with 'after-the-fact' applications such as forensic investigations or environmental monitoring. In these cases, accurate quantification and identification of the explosive compound is highly desirable.

The research described in this thesis may contribute to the development of a novel laboratory detection method that could complement or even replace current accepted techniques.

1.2.7. The EPA8330 Method

The most commonly used laboratory protocol for the detection of nitroaromatic and nitramine compounds is known as the EPA8330, developed by the U.S. Environmental Protection Agency.[70, 71] In this method, water, soil, or sediment samples (following the appropriate sample preparation techniques) are injected into a reverse-phase HPLC with UV-visible absorption detection. Similar methods employ capillary liquid chromatography to separate and identify sample mixtures.[72] Table 1.1 shows the explosive compounds and their approximate detection limits.[73]

Although sensitivity is high, it is a time-consuming technique, requiring up to three calibrations per operational day. Also, it offers little selectivity towards electron-deficient compounds, especially when these compounds are part of complex mixtures.

Table 1.1. Explosive compounds and their approximate detection limits for the EPA8330 method. From reference 74.

Compound	Abbreviation	Approx. Detection Limit (μg/L)
Octahydro-1,3,5,7-tetranitro-1,3,5,7-tetrazocine	HMX	13.0
Hexahydro-1,3,5-trinitro-1,3,5-triazine	RDX	0.84
1,3,5-Trinitrobenzene	1,3,5-TNB	0.26
1,3-Dinitrobenzene	1,3-DNB	0.11
Methyl-2,4,6-trinitrophenylnitramine	Tetryl	4.0
Nitrobenzene	NB	6.4
2,4,6-Trinitrotoluene	TNT	0.11
4-Amino-2,6-dinitrotoluene	4-Am-DNT	0.060
2-Amino-4, 6-dinitrotoluene	2-Am-DNT	0.035
2,4-Dinitrotoluene	2,4-DNT	0.31
2,6-Dinitrotoluene	2,6-DNT	0.020
2-Nitrotoluene	2-NT	12.0
3-Nitrotoluene	3-NT	8.5
4-Nitrotoluene	4-NT	7.9

1.2.8. A Modification to EPA8330 Method

In 2001, McGuffin and Goodpaster illustrated a possible modification to the EPA8330 method.[65] Following separation by HPLC, they introduced a constant flow of the fluorophore pyrene *via* a mixing tee. They replaced the absorption spectrophotometer with a fluorescence spectrophotometer, thus monitoring the emission from pyrene at ~390 nm. As the components of the sample eluted from the column, they quenched the fluorescence signal, resulting in inverted chromatograms (Figure 1.7). By monitoring fluorescence quenching instead of UV-visible absorption, improved sensitivity was achieved, along with a significant increase of the signal-to-noise ratio.

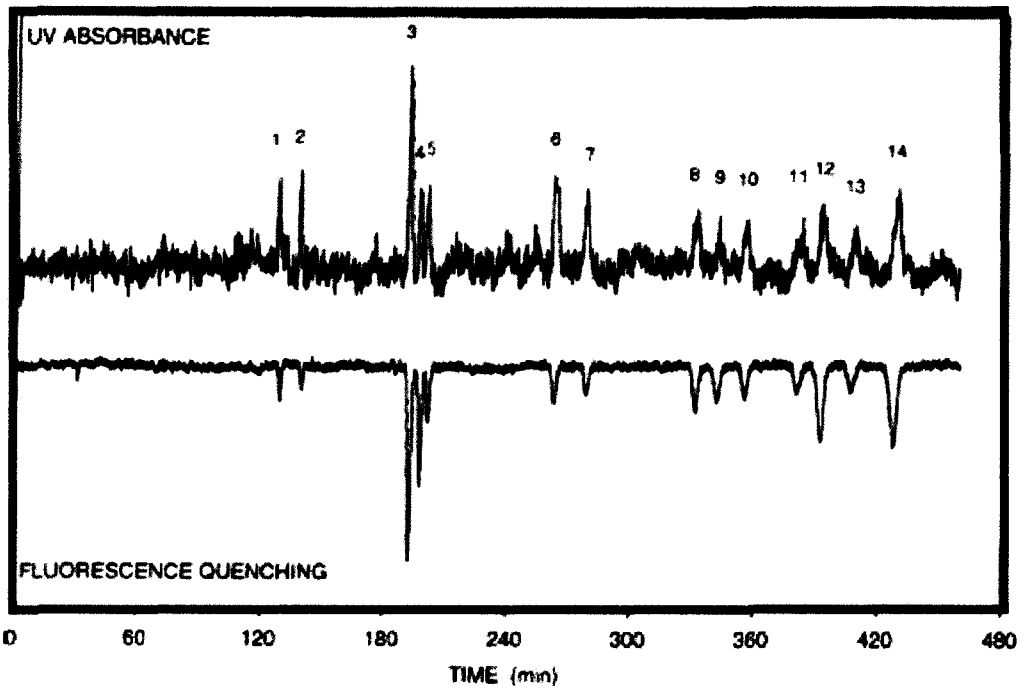

Figure 1.7. Comparison of the sensitivity of UV-visible and fluorescence quenching detection methods with a 3.0 mg/mL solution of explosives and their degradation products. (1) RDX, (2) HMX, (3) 1,3-DNB, (4) 1,3,5-TNB, (5) NB, (6)2-Am-4,6-DNT, (7) 2-Am-2,6-DNT, (8) 2,4-DNT, (9) 2,6-DNT, (10) 2,-NT, (11) 4-NT, (12) 2,4,6-TNT, (13) 3-NT, AND (14) Tetryl. Adapted from Reference 66.

McGuffin and Goodpaster concluded that their method represented a significant improvement over the conventional technique, noting that previously ambiguous signals were readily resolved. For example, the domestically manufactured military-grade explosive C4 uses RDX as the primary explosive. However, it also contains a trace amount of HMX, introduced during the synthesis of RDX. Using the fluorescence quenching technique, this residue of HMX in the commercial explosive was easily identifiable and quantifiable. Thus, the authors remarked that this method could be particularly useful for identification of post-blast residues in forensic investigations.

1.2.9. Potential Analytical Application of Pyrene Fluorescence Quenching

Following our investigation into the interactions between electron-deficient molecules and the pyrene monomer and excimer, we thus realized that, by recording the monomer fluorescence quenching concurrent with acquisition of the monomer-to-excimer fluorescence ratio (F_M/F_E) clear discrimination between general and electron-deficient quenchers would be possible. Experimentally, this would require the use of a multiwavelength fluorescence detector (such as a diode array), rather than a single wavelength detector. We anticipate that, while this method responds to all electron-deficient molecules (thus leading to false positives), it would not lead to false negatives, and as such, represents an attractive screening technique for security-related applications.

1.3 Summary

While the two concepts of physical organic chemistry outlined in this chapter seem utterly dissimilar, in essence, this thesis describes two successful applications of 'weakly-bound dimers'. In the first case, covalently bonded dimers of persistent carbon-centered radicals are used in the deliberate and selective carbon-carbon bond formation mediated by the Persistent Free Radical Effect. The second case involves employing fluorescence quenching of the excited-state dimer of pyrene to develop a novel methodology to detect electron-deficient materials. Ultimately, these two projects demonstrate how fundamental concepts of physical organic chemistry may be applied to practical uses, from organic synthesis to molecular detection.

1.4 References

1. Solomons, T. W. G., *Organic Chemistry*. 6th Ed. ed.; John Wiley & Sons, Inc.: New York, 1996.

2. Fossey, J.; Lefort, D.; Sorba, J., *Free Radicals in Organic Chemistry*. John Wiley & Sons: New York, 1995.

3. Chatgilialoglu, C., Electronic Absorption Spectra of Free Radicals. In *Handbook of Organic Photochemistry*, Scaiano, J. C., Ed. CRC Press: Boca Raton, Florida, 1989; Vol. II, pp 3-11.

4. Griller, D.; Ingold, K. U., Persistent Carbon-Centered Radicals. *Acc. Chem. Res.* **1976,** 9, 13-18.

5. Gomberg, M., An Instance of Trivalent Carbon: Triphenylmethyl. *J. Am. Chem. Soc.* **1900,** 22, 757.

6. Aliaga, C.; Aspee, A.; Scaiano, J. C., A new method to study antioxidant capability: Hydrogen transfer from phenols to a preflourescent nitroxide. *Org. Lett.* **2003,** 5, 4145-4148.

7. Bejan, E. V.; Font-Sanchis, E.; Scaiano, J. C., Lactone-derived Carbon-centered Radicals: Formation and reactivity with Oxygen. *Org. Lett.* **2001,** 3, (25), 4059-4062.

8. Font-Sanchis, E.; Aliaga, C.; Focsaneanu, K.-S.; Scaiano, J. C., Greatly Attenuated Reactivity of Nitrile-Derived Carbon-centered Radicals toward Oxygen. *Chem. Commun.* **2002,** (15), 1576-1577.

9. Scaiano, J. C.; Martin, A.; Yap, G. P. A.; Ingold, K. U., A Carbon Centered Radical Unreactive Towards Oxygen: Unusual Radical Stabilization by a Lactone Ring. *Org. Lett.* **2000,** 2, (7), 899-901.

10. Aliaga, C.; Stuart, D. R.; Aspée, A.; Scaiano, J. C., Solvent Effects on Hydrogen Abstraction Reaction from Lactones with Antioxidant Properties. *Org. Lett.* **2005,** 7, 3665.

11. Frenette, M.; Aliaga, C.; Font-Sanchis, E.; Scaiano, J. C., Bond Dissociation Energies for Radical Dimers Derived from Highly Stabilized Carbon-Centered Radicals. *Org. Lett.* **2004,** 6, (15), 2579-2582.

12. Chatgilialoglu, C., Basic Concepts of Carbon-Carbon Bond Formation. In *Radicals in Organic Synthesis*, Renaud, P.; Sibi, M. P., Eds. Wiley-VCH: New York, 2001; Vol. Volume 1: Basic Principles, p 31.

13. Blake, H. R.; Henderson, J. F.; Kutschke, K. O., *Can. J. Chem.* **1961,** 39, 1920.

14. Garland, L. J.; Bayes, K. D., Rate Constants for Some Radical-Radical Cross-Reactions and the Geometric Mean Rule. *J. Phys. Chem.* **1990,** 94, 4941.

15. Kerr, J. A.; Trotman-Dickenson, A. F., The reactions of alkyl radicals. In *Prog. React. Kinet.*, Porter, G., Ed. 1961; Vol. 1, p 105.

16. Turro, N. J., *Modern Molecular Photochemistry.* University Science Books: Sausalito, 1991.

17. Kräutler, B., Acetyl-cobalamin from photoinduced carbonylation of methyl-cobalamin. *Helv. Chim. Acta* **1984,** 67, 1053.

18. Fischer, H., Unusual Selectivities of Radical Reactions by Internal Suppression of Fast Modes. *J. Am. Chem. Soc.* **1986,** 108, (14), 3925-3927.

19. Fischer, H., The Persistent Radical Effect: A Principle for Selective Radical Reactions and Living Radical Polymerizations. *Chem. Rev.* **2001,** 101, 3585-3610.

20. Bachmann, W. E.; Wiselogle, F. Y., The relative stability of pentaarylethanes. III. The reversible dissociation of pentaarylethanes. *J. Org. Chem.* **1936,** 1, 354.

21. Perkins, M. J., The thermal decomposition of phenylazotriphenylmethane in p-xylene. *J. Chem. Soc.* **1964,** 5932.

22. Alajarin, M.; Vidal, A.; Ortin, M.-M.; Bautista, D., Persistent radical effect in the intramolecular addition of benzylic radical onto ketenimines: selective cross-coupling of α-(indol-2-yl)-benzyl radicals with the 1-cyano-1-methylethyl radical. *New. J. Chem.* **2004,** 28, 570-577.

23. Magnus, P.; Venable, J. D.; Shen, L.; Lynch, V., Some reactions of persistent benzofuranone radicals related to the 'old' diazonamide structure. *Tet. Lett.* **2005,** 46, 707-710.

24. Renaud, P.; Sibi, M. P., *Radicals in Organic Synthesis, Vol. 1 and 2.* Wiley-VCH: New York, 2001.

25. Sanjuán, A.; Aguirre, G.; Alvaro, M.; García, H.; Scaiano, J. C.; Chrétien, M. C.; Focsaneanu, K.-S., Product studies and laser flash photolysis of direct and 2,4,6-triphenylpyrylium-zeolite Y photocatalyzed degradation of fenvalerate. *Photochem. Photobiol. Sci.* **2002,** 1, 955-959.

26. Studer, A., The Persistent Radical Effect in Organic Synthesis. *Chem. Eur. J.* **2001,** 7, 1159-1164.

27. Studer, A., Tin-free radical chemistry using the persistent radical effect: alkoxyamine isomerization, addition reactions, and polymerizations. *Chem. Soc. Rev.* **2004,** 33, 267-273.

28. Wetter, C.; Studer, A., Microwave-assisted free radical chemistry using the persistent radical effect. *Chem. Commun.* **2004,** 174-175.

29. Zard, S. Z., *Radical Reactions in Organic Synthesis.* Oxford University Press: Oxford, 2003.

30. Rüegge, D.; Fischer, H., Unusual Selectivities of Radical Reactions. Experimental Studies on Alkyl versus Phenoxyl Reaction Systems. *Int. J. Chem. Kinet.* **1989,** 21, 703-714.

31. Garcia Ballesteros, O.; Maretti, L.; Sastre, R.; Scaiano, J. C., Kintetics of Cap Separation in Nitroxide-regulated "Living" free radicla Polymerization: Application of a Novel Methodology Involving a prefluorescent Probe Nitroxide Switch. *Macromolecules* **2001,** 34, 6184-6187.

32. Georges, M. K.; Veregin, R. P. N.; Kazmaier, P. M.; Hamer, G. K., Nitroxide Stable Free Radical Mediated Polymerization: Autopolymerization. *Polymer Preprints (ACS)* **1994,** 35, (2), 870-871.

33. Georges, M. K.; Veregin, R. P. N.; Kazmaier, P. M.; Hamer, G. K.; Saban, M., Narrow polydispersity Polystyrene by a Free Radical Polymerization Process - Rate Enhancement. *Macromolecules* **1994,** 27, 7228-7229.

34. Moad, G.; Rizzardo, E.; Salomon, D. H., A product study of the nitroxide inhibited thermal polymerization of styrene. *Polymer Bull.* **1982,** 6, (11-12), 589-593.

35. Rizzardo, E.; Serelis, A. K.; Salomon, D. H., Initiation mechanisms in radical polymerizations: Reaction of cumyloxy radicals with methyl methacrylate and styrene. *Aust. J. Chem.* **1982,** 35, 2013-2024.

36. Skene, W. G.; Belt, S. T.; Connolly, T. J.; Hahn, P.; Scaiano, J. C., Decomposition Kinetics, Arrhenius Parameters and Bond Dissociation Energies for Alkoxyamines of Relevance in "Living" Free Radical Polymerization. *Macromolecules* **1998,** 31, (25), 9103-9105.

37. Skene, W. G.; Scaiano, J. C.; Yap, G. P. A., An Improved Mimetic Compound for Styrene 'Living' Free Radical Polymerization. An Initiator Containing the 'Penultimate' Unit. *Macromolecules* **2000,** 33, (10), 3536-3542.

38. Fischer, H., The Persistent Radical Effect in "Living" Radical Polymerization. *Macromolecules* **1997,** 30, (19), 5666-5672.

39. Engel, P. S., Photochemistry of Dibenzyl Ketone. *J. Am. Chem. Soc.* **1970,** 92, 6074-6076.

40. Lunazzi, L.; Ingold, K. U.; Scaiano, J. C., Absolute Rate Constants for the Decarbonylation of the Phenylacetyl Radical. *J.Phys.Chem.* **1983,** 87, 529-530.

41. Focsaneanu, K.-S.; Aliaga, C.; Scaiano, J. C., Clean Photochemical Synthesis Mediated by Radical-Radical Reactions: Radical Buffer or the Persistent Free Radical Effect? *Org. Lett.* **2005,** 77, (22), 4979-4982.

42. Birks, J. B., *Photophysics of Aromatic Molecules.* Wiley-Interscience: New York, 1970.

43. Gilbert, A.; Baggott, J., *Essentials of Molecular Photochemistry.* Blackwell: Oxford, 1991.

44. Dabestani, R.; Ivanov, I. N., A compilation of physical, spectroscopic and photophysical properties of polycyclic aromatic hydrocarbons. *Photochem. Photobiol.* **1999,** 70, 10.

45. Dong, D. C.; Winnik, M. A., The Py scale of solvent polarities. *Can. J. Chem.* **1984,** 62, 2560.

46. Nigam, S.; Rutan, S., Principles and Applications of Solvatochromism. *Applied Spec.* **2001,** 55, 362.

47. Barenholtz, Y.; Cohen, T.; Haas, E.; Ottolenghi, M., Lateral organization of Pyrene-labeled Lipids in Bilayers as Determined from the Deviation from Equilibrium between Pyrene Monomers and Excimers. *J. Bio. Chem.* **1996,** 271, (6), 3085-3090.

48. Förster, T.; Kasper, K., Der Konzentrationsumschlag des Fluoreszenz des Pyrens. *Z. Phys. Chem. (N.F.)* **1954,** 1, 274.

49. Förster, T.; Kasper, K., Ein Konzentrationsumschlag der Fluoreszenz des Pyrens. *Z. Electrochim.* **1955,** 59, 976.

50. Stevens, B., *Spectrochim. Acta* **1962,** 18, 439.

51. Duhamel, J.; Winnik, M. A.; Baros, F.; André, J. C.; Martinho, J. M. G., Diffusion Effects on Pyrene Excimer Kinetics: Determination of the Excimer Formation Rate Coefficient Time Dependence. *J.Phys. Chem.* **1992,** 96, (24), 9805-9810.

52. Duhamel, J.; Yekta, A.; Winnik, M. A., Excimer Lifetime Recovery: Application to Microheterogeneous Systems. *J. Phys. Chem.* **1993,** 97, 2759-2763.

53. Stevens, B., Influence of Environment on the Radiative and Radiationless Transition Rates of the Pyrene Excimer. *Adv. Photochem.* **1971,** 8, 161.

54. Winnik, F. M., Photophysics of Preassociated Pyrenes in Aqueous Polymer Solutions and in Other Organized Media. *Chem. Rev.* **1993,** 93, 587-614.

55. Birks, J. B.; Alwattar, A. J. H., Influence of Environment on the Radiative and Radiationless Transition Rates of the Pyrene Excimer. *Chem. Phys. Lett.* **1971,** 11, (1), 89-92.

56. Birks, J. B.; Dyson, D. J.; Munro, I. H., 'Excimer' fluorescence II. Lifetime studies of pyrene solutions. *Proceedings of the Royal Society of London. Series A, Mathematical and Physical Sciences* **1963,** 275, 575-588.

57. Birks, J. B.; Seifert, H. G., Double-Photon Excitation of Excimer Fluorescence of Pyrene Solutions. *Phys. Lett.* **1965,** 18, (2), 127-128.

58. Birks, J. B.; Christophorou, L. G., *Spectrochim. Acta* **1963,** 19, 401.

59. Schoenfisch, M. H.; Huiping, Z.; Frost, M. C.; Meyerhoff, M. E., Nitric Oxide-Releasing Fluorescence-Based Oxygen Sensing Polymeric Films. *Anal. Chem.* **2002,** 74, (23), 5937-5941.

60. He, Y.; Geng, L., In Situ Time-Resolved Fluorescence Spectroscopy in the Frequency Domain in Capillary Electrochromatography. *Anal. Chem.* **2002,** 74, (8), 1819-1823.

61. Ji, J.; Rosenzweig, N.; Jones, I.; Rosenzweig, Z., Molecular Oxygen-Sensitive Fluorescent Lipobeads for Intracellular Oxygen Measurements in Murine Macrophages. *Anal. Chem.* **2001,** 73, (15), 3521-3527.

62. Lakowicz, J. R., *Principles of Fluorescence Spectroscopy, 2nd Ed.* Kluwer Academic: New York, 1999; p 9-10.

63. Goodpaster, J. V.; Harrison, J. F.; McGuffin, V. L., Ab Initio Study of Selective Fluorescence Quenching of Polycyclic Aromatic Hydrocarbons. *J. Phys. Chem. A* **2002,** 106, 10645-10654.

64. Goodpaster, J. V.; Howerton, S. B.; McGuffin, V. L., Forensic Analysis of Commercial Petroleum Products Using Selective Fluorescence Quenching. *J. Forensic. Sci.* **2001,** 46, (6), 1358-1371.

65. Goodpaster, J. V.; McGuffin, V. L., Fluorescence Quenching as an Indirect Detection Method for Nitrated Explosives. *Anal. Chem.* **2001,** 73, (9), 2004-2011.

66. Howerton, S. B.; Goodpaster, J. V.; McGuffin, V. L., Characterization of polycyclic aromatic hydrocarbons in environmental samples by selective fluorescence quenching. *Anal. Chim. Acta* **2002,** 459, 61-73.

67. Pandey, S.; Fletcher, K. A.; Powell, J. R.; McHale, M. E. R.; Kauppila, A.-S. M.; Acree, W. A.; Fetzer, J. C.; Dai, W.; Harvey, R. G., Spectrochemical investigations of fluorescence quenching agents Part 5. Effect of surfactants on the ability of nitromethane to selectively quench fluorescence emission of alternants PAHs. *Spectrochim. Acta Part A* **1997,** 53, 165-172.

68. Sawicki, E.; Stanley, T. W.; Elbert, W. C., Quenchofluorometric Analysis for Fluoranthenic Hydrocarbons in the Presence of Other Types of Aromatic Hydrocarbon. *Talanta* **1964,** 11, 1433-1441.

69. Caldwell, R. A.; Creed, D.; DeMarco, D. C.; Melton, L. A.; Ohta, H.; Wine, P. H., Charge-Transfer Quenching of Singlet Excited Complexes. *J. Am. Chem. Soc.* **1980,** 102, (7), 2369-2377.

70. Weisberg, C. A.; Ellickson, M. L., Practical modifications to U.S. EPA Method 8330 for the analysis of explosives by high performance liquid chromatography (HPLC). *Am. Lab.* **1998,** 30, (4), 32N-32V.

71. Nelson, P., Index to EPA Test Methods. In Library, U. E. N. E. R., Ed. United States Environmental Protection Agency: 2003.

72. Goodpaster, J. V.; McGuffin, V. L., Separation of Nitramine and Nitroaromatic Explosives by Capillary Liquid Chromatography. *J. Liq. Chrom.* **2001,** 24, (13), 1965-1978.

73. Method 8330: Nitroaromatics and Nitramines by High Performance Liquid Chromatography (HPLC). In EPA, U. S., Ed. 1994.

Chapter 2. Experimental Methods and Materials

Chapter 2: Experimental Methods and Materials

2.1 Time-Resolved Spectroscopy

2.1.1. Introduction

In this section, a brief overview of time-resolved spectroscopic techniques will be provided, in order to familiarize the reader with the instrumentation used throughout this thesis. For physical organic chemists, directly observing reaction intermediates *via* the use of time-resolved spectroscopy has proved invaluable in the elucidation of reaction mechanisms. The Scaiano Group's laser facility has a variety of lasers available as excitation sources, and the capacity to observe fleeting intermediates *via* their transient absorption and emission, monitored on either the nanosecond and picosecond timescale.

Table 1 lists the parameters for the three pulsed lasers used as excitation sources in this thesis.

Table 2.1. Pulsed lasers available at the Scaiano Group Laser Facility and referenced in this thesis.

Laser	Wavelength (nm)	Average Power (mJ/pulse)	Average pulse duration
Surelite Nd:YAG[a] (fourth harmonic)	266	≤ 20	~6 ns
Lumonics EX-530 Excimer	308	50-100	~8 ns
Surelite Nd:YAG[a] (third harmonic)	355	≤ 25	~6 ns

[a]YAG is Yttrium Aluminum Garnet.

2.1.2 Laser Flash Photolysis: Historical Development

Laser flash photolysis (LFP) is a spectroscopic technique used to observe transient species that have been generated following pulsed laser excitation of corresponding precursors. Put very briefly, the laser flash photolysis experiment is analogous to that of a very fast spectrophotometer.

Flash photolysis was first introduced by Norrish and Porter using a flash lamp as excitation source and they later shared the 1967 Nobel prize for their pioneering research.[1-3] While Norrish and Porter's original system operated on the microsecond to millisecond time scale, the discovery and advancement of pulsed lasers in the early 1960s quickly led to the development of flash photolysis on the nanosecond time scale (nLFP): within a few years, Porter[4, 5], Kosonocky[6], and Lindqvist[7] had all reported on the use of a pulsed laser as an excitation source. In the early days of LFP, the majority of 'home-assembled' systems used nitrogen or ruby lasers and the generated species were monitored using well-established pulse radiolysis detection systems. Subsequent advances in computer technologies led to the developments of the first computer-controlled laser flash photolysis system in the late 1970's by Scaiano and Small at the University of Notre Dame.[8-10] This system was lauded as a significant improvement with respect to data acquisition and processing and eventually became the prototype upon which many other systems were designed. Today, extensive miniaturization of the electronics and optics required for laser flash photolysis has resulted in bench-top 'mini-LFP' systems that incorporate everything required except the excitation laser in a single, 12" x 18" instrument.[11] As well, laser pulses lasting picoseconds, femtoseconds,

or even attoseconds in duration are in use by scientists in various disciplines to follow events on increasingly shorter timescales.

The fact that ever shorter laser pulses are pursued is due to an intrinsic condition for studying photochemical events occurring on short time scales. Much like the relationship between a camera's shutter speed relative to the movement of its subject, the duration of the excitation laser pulse must be shorter than the monitored process, otherwise the signal will be obscured. Furthermore, *laser* pulses are desirable because the excitation source must be sufficiently intense to generate detectable amounts of the transient species. In the case of the nanosecond lasers used in this thesis, this corresponds to a minimum time resolution of approximately 15 ns.

Again, the operation of the LFP system is, put simply, a very fast spectrophotometer coupled with a pulsed excitation source. The nanosecond systems employed in the research described in this thesis were used for the analysis of transparent solution-phase samples using both absorption and emission detection techniques. Since the entire experimental laser set-up has been explained thoroughly elsewhere,[12] the general concept is described in the following section.

2.1.3. Laser Flash Photolysis Fundamentals

Following pulsed laser excitation to generate the transient species of interest, the sample is irradiated with light from a monitoring beam; where the geometry of the excitation and monitoring light sources (*i.e.*, at 90° or ~0° with respect to each other) is dependent upon the optical density of the sample (*vide infra*). The monitoring beam incorporates a xenon lamp, allowing the acquisition of spectroscopic data from nearly

230 nm to 800 nm, though the actual window is largely determined by the detection system (*vide infra*). The original LFP systems in the Scaiano Group had monitoring beams that were pulsed in order to increase the output intensity by a factor of 5-20 for several milliseconds, thus improving the signal-to-noise ratio. Recently, however, this necessity was removed by replacing the monitoring beams with new high-intensity ceramic lamps from Luzchem Research, Inc.

After probing the sample, the monitoring beam is subsequently focused onto the entrance slit of a high-intensity monochromator that selects the wavelength of light reaching the detector, located at the exit slit of the monochromator. The detector in our system is a photomultiplier tube (PMT) operating on six dynodes. In the PMT, the optical signal generates a current that is terminated into a load resistor (typically 93 Ω depending on the signal cables) resulting in a voltage signal. The time-dependent voltage signal is captured by a Tektronix digitizing oscilliscope (equipped with pre-trigger capabilities) and the electrical signal is converted to a digital signal. The oscilloscope is interfaced to a Power MacIntosh computer that provides experimental control through in-house software programmed in the LabView 5.1 environment from National Instruments (later, a PC computer using software developed by Luzchem Research, Inc. replaced these components). Each constituent of the LFP system (laser, lamp, lamp pulser, shutters, *etc.*) is coordinated by a line synchronizer via a series of transistor-transistor linked (TTL) pulses that originate at the same point on a 60 Hz sine wave.

The timed sequence of the PMT output is illustrated schematically in Figure 2.1. Opening the monitoring beam shutter causes a sharp increase in the PMT output that is recorded as the pre-pulse baseline. The laser then fires, striking a fiber optic cable that triggers the digitizer to start collecting data. The recorded signal is shown inside the box in Figure 2.1. The intensity of the monitoring beam itself is measured on a second channel and becomes the baseline from which changes in PMT voltage levels are determined. Kinetic information is obtained from the average of a set number of laser shots (usually 4). The intensity data is plotted with respect to time in order to give a time-dependent decay trace. Transient absorption spectra are generated by compiling the kinetic data acquired at several different wavelengths and constructing a plot of intensity *vs.* wavelength. In order to compare the signals from separate acquisitions, the intensity of the monitoring beam is maintained at a constant level through the use of a programmable power supply. The PMT output is set to a desired level and maintained throughout the duration of the experiment.

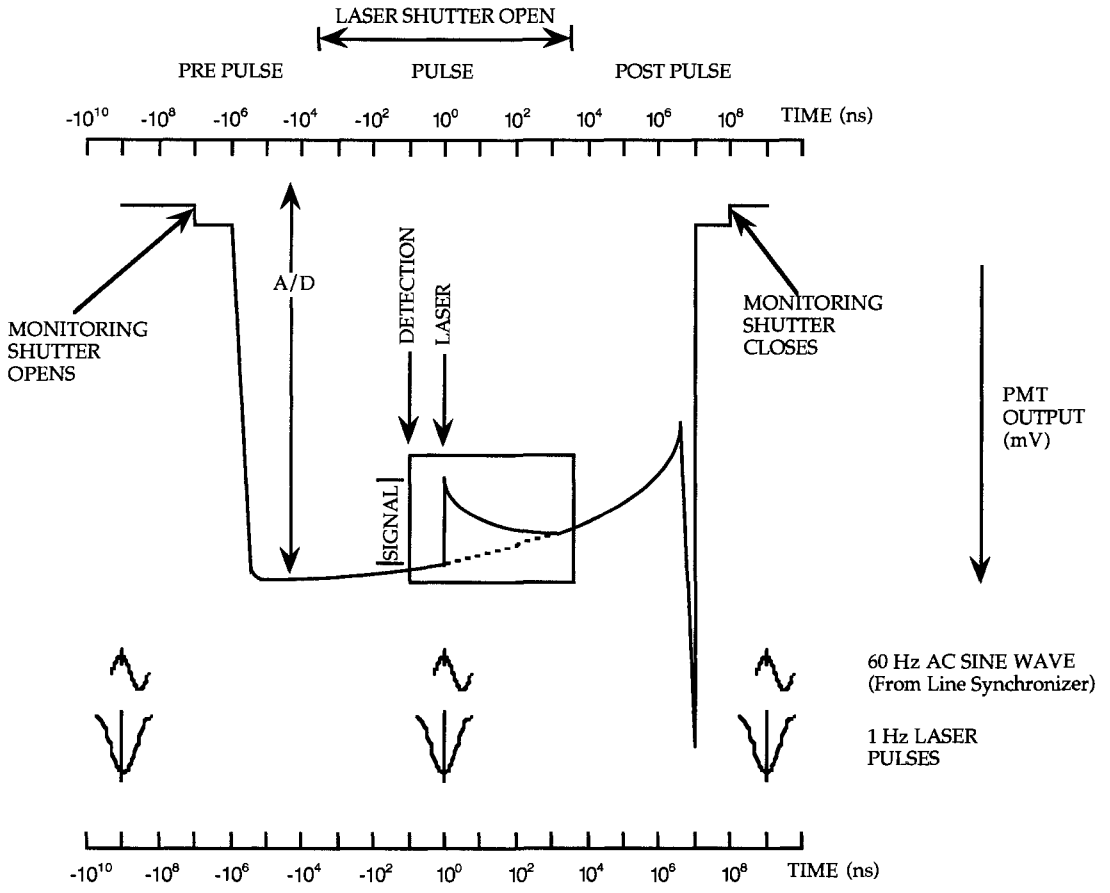

Figure 2.1. Plot of the PMT output versus time for a period before and after the laser pulse. Note: this diagram only applies to systems where the monitoring lamp is pulsed. From: Michelle N. Chrétien's Doctoral Thesis.[13]

For all of the experiments described in this thesis, the samples were transmissive, and in these cases the LFP experiment uses a detection mode based on changes in the transmission characteristics of the sample. This technique allows monitoring of both the formation of new species as well as the disappearance of 'instantaneously-formed' transients (*i.e.* species generated within the duration of the laser pulse). As mentioned previously, following laser-induced formation of the excited state or reactive intermediate, the sample is probed by light from the monitoring lamp. The experimentally measured signal is converted (see below) to the change in absorbance,

abbreviated ΔOD from the historical term "optical density". The ΔOD reflects the change in the incident monitoring beam intensity converted to absorbance units ($I_{t=0}$ or I_0), following laser excitation ($I_{t=t}$ or I_t). A schematic of the LFP system showing the experimental geometry for transient absorption spectroscopy is given in Figure 2.2.

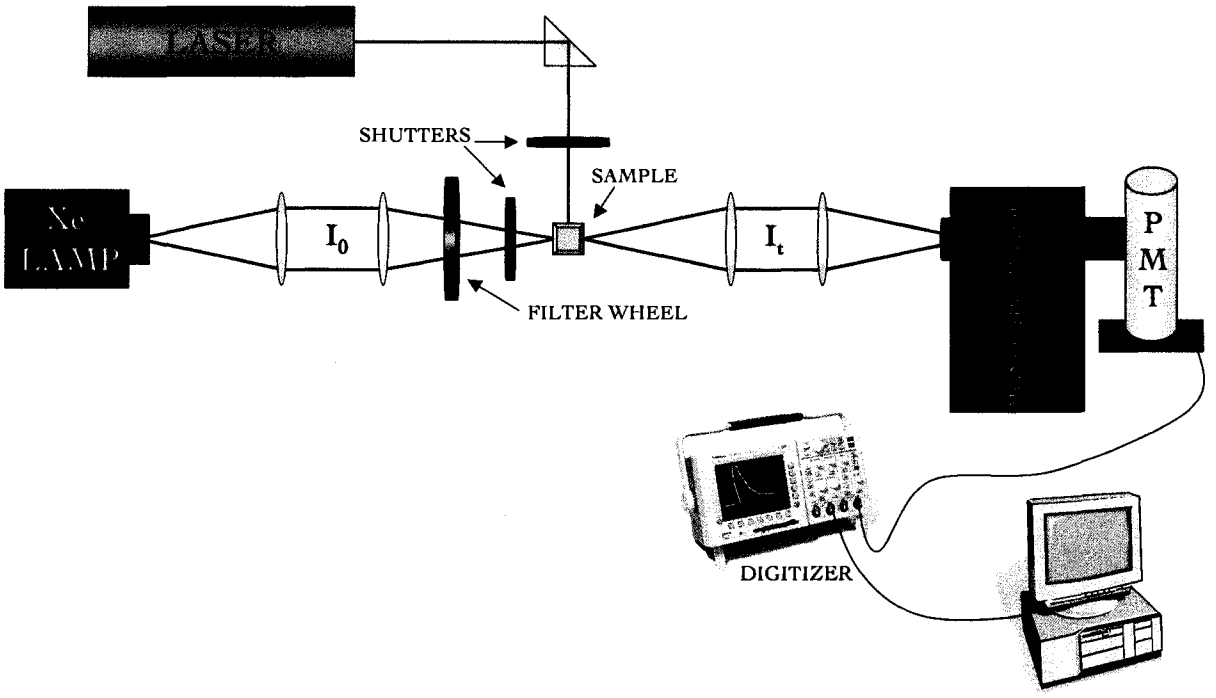

Figure 2. 2. Schematic of the laser flash photolysis system for monitoring absorption changes in a transparent sample. From: Michelle N. Chrétien's Doctoral Thesis.[13]

The monitoring beam is concentrated and focused on a small 2 mm hole in the sample holder. Transient absorption spectra are recorded on a point-by-point basis, where the time windows of data capture are preset before the acquisition, and the wavelength is changed over the course of the experiment. The resultant spectrum is called a difference spectrum (hence ΔOD), and represents the difference between the molar absorption coefficient of the ground state (ε_{GS}) and the transient (ε_T) at the probed

wavelength. This is illustrated in Equations 2.1 and 2.2 (modifications of the well-known Beer-Lambert Law for absorption),

$$OD_{t=0} = \varepsilon_{GS}\,\ell\,C_{GS} \qquad \text{Absorbance at t = 0} \qquad (2.1)$$

$$OD_{t=t} = \varepsilon_{GS}\,\ell\,(C_{GS} - C_T) + \varepsilon_T\,\ell\,C_T \qquad \text{Absorbance at t = t} \qquad (2.2)$$

where $OD_{t=0}$ and $OD_{t=t}$ are the absorbances before and after excitation respectively; C_{GS} is the ground state concentration before excitation, C_T is the transient concentration produced following excitation, and ℓ is the optical path length, for a system with 1:1 stoichiometry. The change in absorbance following laser excitation can be obtained by the combination of Equations 2.1 and 2.2 to give the expression in Equation 2.3.

$$\Delta OD_{t=t} = (\varepsilon_T - \varepsilon_{GS})\,\ell\,C_T \qquad (2.3)$$

Using the Beer-Lambert Law we can further describe the transmitted intensity of the probe beam (I_{PB}) before and after the laser excitation in terms of Equations 2.4 and 2.5, respectively.

$$I_{t=0} = I_{PB} \times 10^{(-\varepsilon_{GS}\ell C_{GS})} \qquad (2.4)$$

$$I_{t=t} = I_{PB} \times 10^{(-\varepsilon_{GS}\ell C_{GS} + (\varepsilon_T - \varepsilon_{GS})\ell C_T)} \qquad (2.5)$$

Combining the previous three equations gives 2.6;

$$\Delta OD_{t=t} = -\log\left(\frac{I_{t=t}}{I_{t=0}}\right) \qquad (2.6)$$

which is then rearranged to give ΔOD in terms of the experimentally observed quantity, the signal from the PMT.

$$\Delta OD_{t=t} = -\log\left(1 - \frac{signal_{t=t}}{I_{t=0}}\right) \qquad (2.7)$$

Clear transient absorption spectra of just the desired transient are thus only possible when $\varepsilon_{GS}=0$; *i.e.* when the ground state is transparent at the monitored wavelength. In regions of the spectrum where the ground state also absorbs, the observed signal is dependent on the absorption characteristics of the precursor; for example, if $\varepsilon_{GS} > \varepsilon_T$ the observed signal will be negative (known as bleaching), if $\varepsilon_{GS} < \varepsilon_T$ the signal will be positive, and if $\varepsilon_{GS} = \varepsilon_T$ no signal will be observed.

Using nanosecond laser flash photolysis, transients having lifetimes more than twice as long as the laser pulse duration can be easily studied. Consequently, this technique is ideally suited to the examination of a number of excited states and reactive intermediates such as excited triplet states, radicals, ions, and radical ions. In addition to providing spectral information, LFP can also be used to investigate reaction mechanisms by examining the kinetic behaviour of transients generated following laser excitation. Applying the appropriate kinetic equations allows for the determination of useful parameters such as rate constants and reaction orders.

2.1.4. Time-Resolved Luminescence Techniques

In addition to time-resolved absorption spectroscopy, the LFP system in the Scaiano Group is also capable of detecting time-resolved luminescence.

Luminescence, the radiative relaxation of an electronically excited state, is subdivided into two categories: fluorescence and phosphorescence, depending on whether or not relaxation of the excited state involves a change in multiplicity.[14] The term *fluorescence* describes the emission of a photon during the relaxation of an excited

state to a ground state of the same multiplicity; usually the transition between an excited singlet and ground singlet state. As this process is spin-allowed, it occurs very rapidly, with rate constants ranging from 10^6 s^{-1} to 10^{12} s^{-1}; thus typical fluorescence lifetimes are on the order of 10 ns. *Phosphorescence* is the emission of light accompanying the transition between states of different multiplicity, *e.g.* the emission associated with relaxation of singlet oxygen to its triplet ground state. As this process is spin-forbidden, phosphorescence lifetimes are typically in the millisecond to second range, or even longer. Phosphorescence is uncommon in the solution phase at room temperature due to the presence of numerous competing non-radiative de-activation pathways.

Time-resolved fluorescence spectroscopy has proven to be complementary to steady-state techniques, and it has distinct advantages and disadvantages. Firstly, this technique contains information that cannot be obtained from steady-state fluorescence spectra; for example, species with overlapping emission spectra can often be resolved on the basis of differences in their fluorescence lifetimes. Secondly, fluorescence techniques are extremely sensitive, since the emitted photons are recorded against a baseline of zero emission whereas transient absorption spectroscopy measures small changes in transmitted light intensity (a popular analogy used to illustrate this concept is that of lighting a match in a darkened room *vs.* a bright room). Lastly, fluorescence lifetimes can provide important information about the environment surrounding the excited-state species. For example, in a project undertaken during my undergraduate studies, we were able to use fluorescence lifetimes to determine DNA damage by

analysis of the different decay kinetics for nucleic acid dyes bound to double- *vs.* single-stranded DNA.[15] However, transient fluorescence spectroscopy does have one significant disadvantage: unlike transient absorption spectroscopy, in fluorescence we are limited to the observation of only one type transient, *i.e.* those excited singlet states that are luminescent.

The experimental magnitude measured in a time-resolved fluorescence experiment is actually the lifetime of the singlet excited-state, commonly referred to as the *fluorescence lifetime* or τ_f. It must be noted that the fluorescence lifetime differs from the *radiative lifetime,* which is an intrinsic value and is not significantly affected by changes to the sample environment. The relationship between these values is given in Equation 2.10, where k_{rad} is the inverse of the radiative lifetime and k_{nr} represents the rate of any non-radiative deactivation of the singlet state.

$$\tau_f = \Phi_f \tau_{rad} = \frac{1}{k_{rad} + \Sigma k_{nr}} \qquad (2.10)$$

The value Φ_f is known as the fluorescence quantum yield, or the fraction of the overall deactivation processes that are emissive ($\Phi_f = k_{rad}/(k_{rad}+\Sigma k_{nr})$.[16] Thus, it is important not to confuse the fluorescence lifetime (measured by this technique) with the radiative lifetime (a value which requires knowledge of Φ_f).

Determination of fluorescence lifetimes of fluorophores in solution is made possible using the LFP set-up described above by operating the system in 'emission-mode'. In this mode, the laser pulse is used as an excitation source to generate the

singlet excited state. The monitoring beam is simply switched off during the experiment, and thus the monochromator and photomultiplier are allowed to collect any incident photons emitted from the sample. The data analysis software on the computer, when set to emission-mode, then inverts the incoming digital signal captured by the oscilloscope, displaying fluorescence intensity as a function of time, rather than ΔOD. However, while switching from absorption to emission modes on the nanosecond laser flash photolysis system is a relatively simple process, it unfortunately has one severe limitation.

Recall two previous statements: 1) the duration of the excitation laser pulse must be shorter than the monitored process, otherwise the signal will be obscured; and 2) typical fluorescence lifetimes are on the order of 10 ns. Unfortunately, these two facts mean that the time-resolved fluorescence of the majority of fluorophores cannot be measured using this technique (instead, picosecond lasers with either single-photon counting or streak camera detection systems are used; these techniques are thoroughly described elsewhere).[17]

However, the main fluorophore used in the second portion of this thesis, pyrene (and its derivatives), has an unusually long lifetime (up to 475 ns in dilute solution).[18] Thus, for this particular molecule, we were able to the nLFP system to acquire time-resolved fluorescence under a variety of conditions.

2.1.5. Factors Affecting LFP Experiments

In Chapters 3, 4 and 5 the chromophores studied by LFP generally had a ground-state absorbance on the order of 0.3-0.5 at the wavelength of excitation, in order to

maximize the production of transients. This accepted value is a compromise between the improved signals obtained from high transient concentrations and the exponential reduction in monitoring beam intensity (I_0) as it passes through the sample volume as a function of the ground-state absorption. However, in the case of the pyrene emission experiments, a highly concentrated sample (3 mM) was required to generate our species of interest, the pyrene excimer. Thus, to avoid the problems associated with the high degree of ground-state absorption, a nearly parallel or "front-face" beam arrangement, contrary to the right angle configuration shown in Figure 2.2.

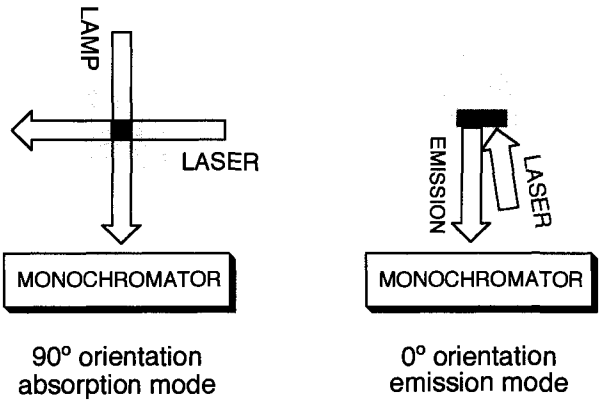

Figure 2.3. Top view of a stylized sample cell illustrating the right-angle orientation used in transient absorption measurements (left) and the front-face orientation used in transient fluorescence measurements (right).

Along with ground-state absorbance, there are several other factors that must be considered when preparing a laser flash photolysis experiment,[19] including:

- *Sample concentration.* In addition to the concerns mentioned above, highly absorbing samples can also result in the generation of "shock" or acoustic waves, creating a repetitive signal superimposed on the transient's signal. The frequency of the wave

is determined by both the size of the sample cell and the speed of sound in the solution; thus significant acoustic waves are generated when a large portion of the incident laser pulse energy is absorbed in a small volume of solution.

- *Laser power.* Generally, signal-to-noise ratios are reduced by maximizing signal intensities. Since a large signal is the result of high transient concentrations, which in turn are directly related to laser power, it might appear that the use of high laser power would be advantageous in all cases. However, this is false for several reasons. Firstly, higher concentrations of transient species may result in the introduction of unexpected transient-transient reactions and the observed chemistry may significantly differ than that observed under lower intensity irradiation. Secondly, the use of high-energy laser pulses can also result in the observation of two-photon processes where, due to the photon density, a transient formed following absorption of a photon can absorb a second photon resulting in new chemistry and different reactive intermediates; for example, photo-ejection of an electron is a common process resulting from two-photon absorption.
- *Sample cell configuration.* For LFP experiments using excitation or monitoring light sources in the UV portion of the spectrum, defect-free, high quality quartz or fused silica sample cells are essential, as the sample cell must be perfectly transparent in the spectral regions of interest and an unblemished surface is required to prevent light scattering and other secondary effects. The appropriate sample cell may be either a static container such as employed in conventional spectroscopy, or part of a 'flow-system' incorporating a reservoir where the sample solution is continually

flushed through the sample cell during data acquisition. There are advantages and disadvantages to the use of both static and flow cells. In general, a flow-system should be used when the sample is to be subjected to multiple laser shots in order to avoid substrate depletion, the accumulation of a competitively absorbing photoproduct, and interference from a photoproduct that may participate in the transient photochemistry. In the research reported in this thesis, the majority of experiments used static cells (unless otherwise noted) because all of the transients observed are highly sensitive to the presence of oxygen, and flow systems are unfortunately more difficult to maintain under anaerobic conditions as a result of their increased number of connections.

2.1.6. Concluding Remarks

It is truly remarkable that, in less than 40 years, the timescales penetrable by these methods have decreased from milliseconds to femtoseconds - over 12 orders of magnitude! It is a testament to these advances that laser flash photolysis and its various accompanying detection techniques have become some of the most powerful tools for physical organic chemists.

Since the bulk of the experimental results presented in this thesis are derived from time-resolved absorption and fluorescence using a pulsed laser as the excitation source, the preceding in-depth descriptions have been included here to help familiarize the reader with time-resolved spectroscopic techniques. In the sections that follow, however, general descriptions of the materials and methods specific to each chapter are

outlined. For further specific details, or where exceptions may be noted, please refer to the chapter text.

2.2 Materials and Methods: Chapter 3

2.2.1 Materials and Sample Preparation

Benzene was Omnisolv HPLC grade and used as received. High quality grade (>98%) reagents ethylbenzene, benzylcyanide, diphenylmethane, diphenylacetonitrile and fluorene were newly purchased from Aldrich (Oakville, Canada), and were used as received. Samples of 9-cyanofluorene were kindly provided by E. Font-Sanchis. Samples of di-*tert*-butylperoxide (from Aldrich) were filtered daily through activated, basic, Brockman I aluminum oxide (from Aldrich) before use to eliminate any traces of hydroperoxide.

The laser samples were always freshly prepared, purged with nitrogen or oxygen, where indicated, for a minimum of 15 minutes, then sealed with rubber septa (previously repetitively soaked in toluene to remove plasticizer contaminants) and parafilm to prevent leakage.

UV-vis ground-state absorption spectra were measured on a CARY-1 UV-vis spectrophotometer in 10x10 mm^2 high-quality quartz cuvettes from Hellma (Plainview, NY, USA); UV-vis transient absorption spectra and kinetic traces were measured using the previously described nLFP system in static 'home-blown' 7x7 mm^2 quartz cuvettes, (raw quartz tubing purchased from Friedrich&Dimmock, Inc; Millville, NJ, USA) .

2.2.2. Data Analysis and Computational Investigations

Transient absorption data acquired and digitized by the LFP oscilloscope and corresponding software was subsequently transferred to the Kaleidagraph data analysis program. Rate constants were extracted by fitting transient growths and decays using relevant exponential expressions; transient absorption spectra points were fitted to a smoothed curve using a cubic spline fitting.

For the computational investigations of the persistent carbon-centred radicals, all radical species were optimized in the doublet spin state. Geometries were optimized using the Gaussian03 software program using the unrestricted B3LYP density functional theory method with the 6-31G(d) basis sets. Mulliken spin distributions were also obtained using the B3LYP/6-31G(d) level of theory.

2.3. Materials and Methods: Chapter 4

2.3.1 Materials and Sample Preparation

Samples of the dimer 2,2,3,3,-tetraphenylsuccinonitrile (TPS) were kindly supplied by M. Frenette; this compound had been synthesized from its monomer, as described elsewhere.[20] Dibenzylketone (DBK), 1,1-diphenylethane (DPE), and benzophenone (BP), were obtained from Aldrich (Oakville, Ontario), and were recrystallized from ethanol before use. Spectroscopy-grade OmniSolv toluene or benzene were used as solvents. Samples of di-*tert*-butylperoxide (from Aldrich) were filtered daily through activated, basic, Brockman I aluminum oxide (from Aldrich) before use in order to eliminate any traces of hydroperoxide.

The samples were always freshly prepared, purged with nitrogen or oxygen, where indicated, for a minimum of 15 minutes, then sealed with rubber septa and parafilm to prevent leakage.

2.3.2 Steady-state *vs.* Pulsed Photolysis

Steady-state irradiations were carried out in a Luzchem photoreactor equipped with 8 or 12 low-pressure Hg UVB lamps (λ_{max} ~ 300 nm); in some experiments the cooling fan was disabled in order to allow the chamber temperature to increase to ~50°C.

Pulsed laser irradiations were carried out by fixing a static 7x7 mm^2 quartz cells contaning about 2 mL of sample about 1 m from the exit window of the laser beam. The firing of the laser was set to a frequency of 1 Hz, thus the total number of shots could be determined by the length of time the laser shutter was left open.

2.3.3. Spectroscopic Measurements and Product Studies

UV-vis ground-state absorption spectra were measured on a CARY-1 UV-vis spectrophotometer in 10x10 mm^2 high-quality quartz cuvettes from Hellma (Plainview, NY, USA); UV-vis transient absorption spectra and kinetic traces were measured using the previously described nLFP system in static 'home-blown' 7x7 mm^2 quartz cuvettes, (raw quartz tubing purchased from Friedrich&Dimmock, Inc; Millville, NJ, USA) .

Preliminary product studies (not shown) were carried out using a HPLC-MS Integrity System from Waters, Inc. (2690 Reverse-Phase Separations Module, coupled to the 996 Photodiode Array and Integrity TMD). Quantitative product studies were

carried out using a GC-MS from Agilent Technologies (6890 GC equipped with a 5973 MSD). In brief: during the photolyses (steady-state or pulsed irradiation) aliquots were removed from the sample over the course of the reaction. Then, a 1 mL of acetonitrile containing an internal standard (pyrene) was spiked with 10 uL of the aliquot, and 1 uL of this new solution was injected into the GC/MS.

^{1}H and ^{13}C NMR spectra were recorded on a Bruker-Avance-300 spectrometer at 300 and 75.4 MHz, respectively. Non-corrected melting points were determined on a Mel-Temp-II apparatus. Further details on the synthesis of 2,2,3-triphenylproprionitrile can be found in Appendix 4A.

2.3.4. Data Analysis and Computational Investigations

Identical to the description in Section 2.2.2.

2.4. Materials and Methods: Chapter 5

2.4.1 Materials and Sample Preparation

Reagents, solvents, and analytical techniques were identical to those described in Section 2.3, with a few additions:

Fenvalerate (FV) was obtained from Calbiochem (Darmstadt, Germany); benzopinacol, triphenylphosphine (TP), triphenylphosphine oxide (TPO) and *m*-phenoxyphenylacetonitrile were all newly purchased from Aldrich (Oakville, Ontario); all reagents were used as received. Samples of the 3-phenyl coumaranone dimer were kindly supplied by M. Frenette; this compound had also been synthesized from its

monomer, as described elsewhere.[20] Acetonitrile, water, and methanol were all spectroscopy-grade OmniSolv solvents and used as received.

Sample preparations were similar to those described above.

2.4.2 Steady-state Photolysis, Laser Flash Photolysis, and Product Studies

Steady-state photolyses, laser flash photolyses, and product studies were carried out as described above. Notable exception: some samples were continuously purged with air or oxygen during the photolysis to maintain a constant concentration of dissolved molecular oxygen. These exceptions are noted in the chapter text.

2.5 Material and Methods: Chapter 6

2.5.1 Materials and Sample Preparation

Pyrene (99%) was obtained from Aldrich (Oakville, Ontario) and recrystallized from methanol before use. Nitromethane (NM), nitroethane (NE), nitrobenzene (NB), *p*-dicyanobenzene (DCB), 5-nitro-*m*-xylene (5NX), trioctylamine (TOA), tribenzylamine (TBA), *N,N*-dimethylaniline (DMA), and *p*-dimethoxybenzene (DMB) were all obtained from Aldrich and recrystallized from methanol or ethanol before use. *N,N*-dimethyl-2,6-diisopropylaniline (DDA) from Carbolabs, Inc. (Bethany, Conn., USA), *m*-dinitrobenzene (mDNB) from Avocado Research Chemicals (Heysham, U.K.), and *p*-dinitrobenzene (pDNB) from Eastman Organic Chemicals (Rochester, N.Y., U.S.A.) were also recrystallized from methanol or ethanol before use.

Fluorescence of nitrogen-saturated solutions of 3 mM pyrene in 99% ethanol or spectroscopic-grade acetonitrile were measured in fused silica cuvettes from Luzchem

Research with a 10 mm or 7 mm optical path, for steady-state or time-resolved measurements, respectively. Carefully purging these samples with nitrogen was critical, since oxygen is a good excited-state quencher; oxygen concentrations above 1% of saturation (5% relative to air) can interfere with the quenching plots. Quenchers were added either as neat liquids or as solutions in ethanol or acetonitrile (also purged with nitrogen) in 5 to 10 μL increments to pyrene samples using a 10 μL Hamilton syringe.

2.5.2. Instrumentation

Steady-state fluorescence spectroscopy was carried out using a Photon Technology International luminescence spectrometer; average excitation and emission slit widths were 2 nm.

Time resolved fluorescence was recorded using the nanosecond LFP set-up in emission mode, as described above. A total of four shots were averaged when obtaining the decay traces. For fluorescence lifetimes above 50 ns, typical errors are <3% for the main emission component, while shorter lifetimes can have as much as 10% error.

2.6 Material and Methods: Chapter 7

2.6.1 Pyrene Fluoresence Quenching by Dissolved Molecular Oxygen

Pyrene (99%) was obtained from Aldrich (Oakville, Ontario) and recrystallized from methanol before use.

Samples of 3 mM pyrene in 99% ethanol were purged with mixtures of nitrogen and oxygen using a calibrated flowmeter (Air Products and Chemicals, Inc.) ranging from 0% to 100% O_2, for a minimum of 15 minutes. Steady-state fluorescence spectra of

these solutions were measured in fused silica cuvettes from Luzchem Research with a 10 mm optical path, using a Photon Technology International luminescence spectrometer; average excitation and emission slit widths were 2 nm.

Oxygen consumption measurements were carried out by monitoring the un-inhibited autoxidation of cumene to cumenehydroperoxide in chlorobenzene as initiated thermally by azobisisobutyronitrile (AIBN). Samples of cumene and chlorobenzene (from Aldrich) were passed through a column of neutral alumina daily in order to remove impurities. AIBN (from Aldrich) was recrystallized from methanol before use. The prepared 3 mL samples contained 5.35 M cumene and 3 mM pyrene in chlorobenzene, prepared under air (no purging) and placed in septa-sealed 10x10 mm^2 fused silica cuvettes.

Steady-state fluorescence measurements were carried out using the same luminescence spectrometer at 45°C (sample cell temperature controlled by a thermo-stated water bath). At the beginning of each experiment, 100 μL of a 0.42 M solution of AIBN in chlorobenzene was injected into the sample (final concentration = 8.5 mM) to initiate the autoxidation.

2.6.2. Pyrene Fluorescence Quenching in Silicone Films

Pyrene-loaded polydimethylsiloxane films were prepared as follows: 15 mg of pyrene was added to disposable test tubes. To this was added 1 g of RTV615A (GE Silicones, Waterford, NY) followed by 1 g of spectroscopic-grade hexane (Fischer Scientific, dried with molecular sieves). After sonication for 3 hours, 100 mg of the cross-linking agent RTV615B (GE Silicones, Waterford, NY) was added. The samples

were sonicated for another 20 minutes and 0.1 mL of the slightly viscous solution was cast dropwise onto glass microscope slides, and left in an oven at 60°C overnight. The resulting pyrene-loaded silicone films were generally used within 7 days of preparation, to avoid ageing effects. Typically, film thicknesses averaged less than 1 mm and had pyrene loadings of less than 15% (w/w). All films are air-saturated.

Steady-state fluorescence spectra of the films were taken on a Perkin-Elmer LS-50 fluorimeter. Prior to measurement, the films would be placed in a sealed jar containing a 2x2 cm^2 wadded tissue that had been soaked in (neat) liquid quencher; exposure times were measured with a stopwatch.

2.6.3. Pyrene Fluorescence Quenching in Zeolite Y

Dimethylaniline (DMA) and 5-nitro-*m*-xylene (5NX) were purchased from Aldrich and used as received. In general, Py@Y materials were prepared as follows: 3 g of NaY was activated at 480°C overnight. In spectroscopic-grade hexane, the sample of NaY was stirred for 1 hour along with 450 mg of pyrene. The solid was removed by suction filtration, then stirred a further 30 minutes in fresh hexane. Following a second filtration, the solid was divided into two parts: one half was placed in a vacuum-sealed desiccator and left aside to "age" undisturbed until further used. The other half was then subdivided in two: each part was then stirred in fresh hexane, either with or without the presence of quencher. The solid was removed from these two samples, and each was further subdivided into 3 parts and treated in one of three ways: placed under vacuum for 2 hours, placed under vacuum for 2 hours and then flushed with nitrogen, or placed under vacuum and flushed with gaseous NO•.

The filtrates removed from the solid zeolite were collected and combined to determine the loadings of pyrene and quencher: for example, by measuring the ground-state absorption spectra, the amount of pyrene not incorporated into the cavities of NaY can be calculated by the molar extinction coefficent (ε_{338} = 65 000 $M^{-1}cm^{-1}$).

Steady-state fluorescence spectroscopy of the solid-state samples was carried out with a Perkin-Elmer LS-50 fluorimeter. Time resolved fluorescence was recorded using the nanosecond LFP set-up in diffuse-reflectance mode (for a full description of this technique, consult reference 13). A total of four shots were averaged when obtaining the decay traces. For fluorescence lifetimes above 50 ns, typical errors are <3% for the main emission component, while shorter lifetimes can have as much as 10% error.

2.6 References

1. Norrish, R. G. W.; Porter, G., Chemical reactions produced by very high light intensities. *Nature* **1949,** 164, 658.

2. Scaiano, J. C., Early History of Laser Flash Photolysis. *Acc. Chem. Res.* **1983,** 16, 234.

3. Porter, G., The absorption spectroscopy of substances of short life. *Discuss. Faraday Soc.* **1950,** 60, (69).

4. Porter, G.; Steinfeld, J. I., Giant-pulse-laser flash photolysis of phthalocyanine vapor. *J. Chem. Phys.* **1966,** 45, (3456).

5. Porter, G.; Topp, M. R., Nanosecond laser flash photolysis and the absorption spectra of excited singlet states. *Nature* **1968,** 220, 1228.

6. Kosonocky, W. F., Observations of the triplet state in phthalocyanines. *J. Chem. Phys.* **1965,** 43, 831.

7. Lindqvist, L., Utilization of a laser with pulsed ultraviolet emission in flash photolysis. Triplet state of acridine. *Hebd. Seances Acad. Sci. Ser. C* **1966,** 263, 852.

8. Small, R. D.; Scaiano, J. C., Reaction of type II biradicals with paraquat ions. Measurement of biradical lifetimes. *J. Phys. Chem.* **1977,** 81, 828.

9. Small, R. D.; Scaiano, J. C., Photochemistry of phenyl alkyl ketones. The lifetime of the intermediate biradicals. *J. Phys. Chem.* **1977,** 81, 2126.

10. Small, R. D.; Scaiano, J. C., The absolute rate constants of hydrogen abstraction by tert-butoxy radicals. *J. Am. Chem. Soc.* **1978,** 100, 296.

11. Scaiano, J. C. www.luzchem.com/products/lfp.php.

12. Berinstain, A. Development of Laser Techniques for Applications in Biomolecules and Cellular Systems. Doctoral thesis, University of Ottawa, Ottawa, 1997.

13. Chrétien, M. N. Photochemical, Photophysical, and Photobiological Studies of Zeolite Guest-Host Complexes. Doctoral Thesis, University of Ottawa, Ottawa, 2005.

14. Lakowicz, J. R., *Principles of Fluorescence Spectroscopy, 2nd Ed.* Kluwer Academic: New York, 1999; p 9-10.

15. Cosa, G.; Focsaneanu, K.-S.; McLean, J. R. N.; Scaiano, J. C., Direct determination of single to double stranded DNA ratio in solution applying time-resolved fluorescence measurements of dye-DNA complexes. *Chem. Commun.* **2000,** 689.

16. Turro, N. J., *Modern Molecular Photochemistry.* University Science Books: Sausalito, 1991.

17. Mikelsons, L. Experimental and Computational Studies of the Interactions of Cyanine Dyes with DNA. Doctoral Thesis, University of Ottawa, Ottawa, 2007.

18. Birks, J. B., *Photophysics of Aromatic Molecules*. Wiley-Interscience: New York, 1970.

19. Hadel, L. M., Laser Flash Photolysis. In *Handbook of Organic Photochemistry, Volume II*, Scaiano, J. C., Ed. CRC Press: Boca Raton, 1989.

20. Frenette, M.; Aliaga, C.; Font-Sanchis, E.; Scaiano, J. C., Bond Dissociation Energies for Radical Dimers Derived from Highly Stabilized Carbon-Centered Radicals. *Org. Lett.* **2004,** 6, (15), 2579-2582.

Chapter 3. Persistent Carbon-Centred Radicals

Chapter 3. Persistent Carbon-Centred Radicals

3.1 Introduction

The study of carbon-centred radicals is largely a study of fleeting intermediates, requiring time-resolved techniques for their observation. Although some examples of long-lived carbon centred radicals are well-known, in general, carbon-centered radicals are considered to be transient species, reacting readily with each other, with solvents, or with molecular oxygen with rates approaching diffusion-control.[1-3] However, research carried out in the Scaiano Group revealed that a family of lactone molecules displayed significant persistent character and an attenuated reactivity towards oxygen;[4-6] these molecules were thus investigated for their antioxidant potential.

Chain breaking antioxidants are molecules that react with peroxyl radicals by hydrogen transfer processes stopping oxidative chains and generating stabilized radicals unreactive toward oxygen.[7] Thus, phenols are good antioxidants because they meet these criteria. However, most carbon-centred radicals are highly reactive towards oxygen, and as a result hydrogen atom donors bearing labile C–H bonds cannot be considered as antioxidants. In addition, while hydrogen abstraction reactions from benzylic C-H versus phenolic O-H bonds have nearly identical enthalpic changes, phenolic-based antioxidants make preferable hydrogen donors because the abstraction occurs through a proton-coupled electron transfer mechanism (PCET) with faster rate constants. Therefore, despite being moderately efficient hydrogen donors, molecules such as 1,4-cyclohexadiene are *not* antioxidants.[8]

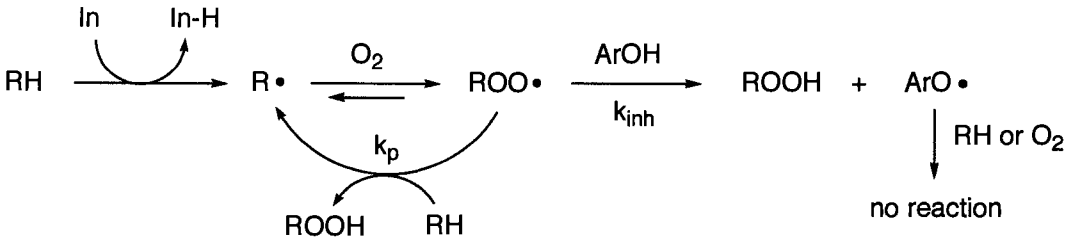

Scheme 3.1. The autoxidation chain reaction; inhibition mechanism shown in blue with a phenol-based antioxidant.

However, members of the Scaiano Group had identified the antioxidant properties of several coumaranone derivatives, in particular HP-136, sold commercially by CIBA Specialty Chemicals as a stabilizing agent for high-temperature polymer processing. As mentioned in Section 1.1.2., careful examination of this molecule and its derivatives led to a list of five parameters to explain their diminished reactivity towards oxygen: (a) benzylic resonance stabilization; (b) favourable stereoelectronic effects; (c) unpaired spin delocalization on heteroatoms; (d) electron withdrawing and/or donating effects, and (e) steric effects.[4]

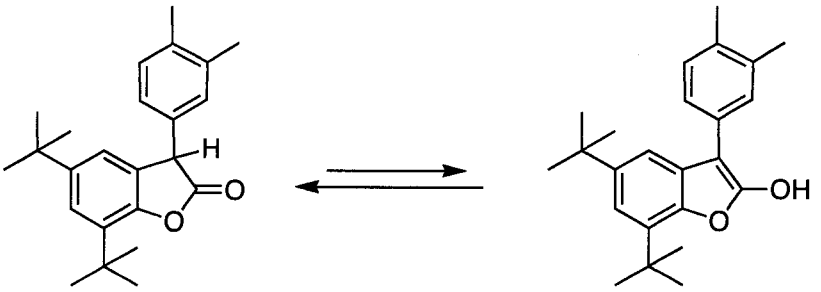

Scheme 3.2. Keto-enol tautomerization of the antioxidant HP-136. Research in the Scaiano Group revealed that, in fact, the enol form is the hydrogen donor.

The elucidation of this list soon led us to identify other functionalities responsible for free radical persistence. For example, while investigating the photodecomposition of the pesticide fenvalerate,[9] we noted that one of the resulting radical intermediates was remarkably long lived.

Direct UV irradiation of fenvalerate in aqueous solution leads to the Norrish Type I homolytic CO-CH(*i*-Pr) bond cleavage, followed by rapid decarboxylation of the primary carbonyloxyl radical, generating two carbon-centred benzylic radicals: the α-cyano-*m*-phenoxylbenzyl radical **2** and the 1-(4-chlorophenyl)-2-methyl-1-propyl radical 3. Subsequent recombination of these radicals leads to the decarboxylated product 1 with little or no memory effect leading to a complete loss of the configuration of the starting FV (Scheme 3.2). Thus, even if the starting material consists of a single FV diastereoisomer, a mixture of the two diastereoisomers of 1 is formed. Under non-UV photolysis (λ>350 nm), no conversion takes place, and all of the starting material is recovered. This photochemical behavior is in agreement with the general photoreactivity of arylacetic acids and derivatives.[2,3]

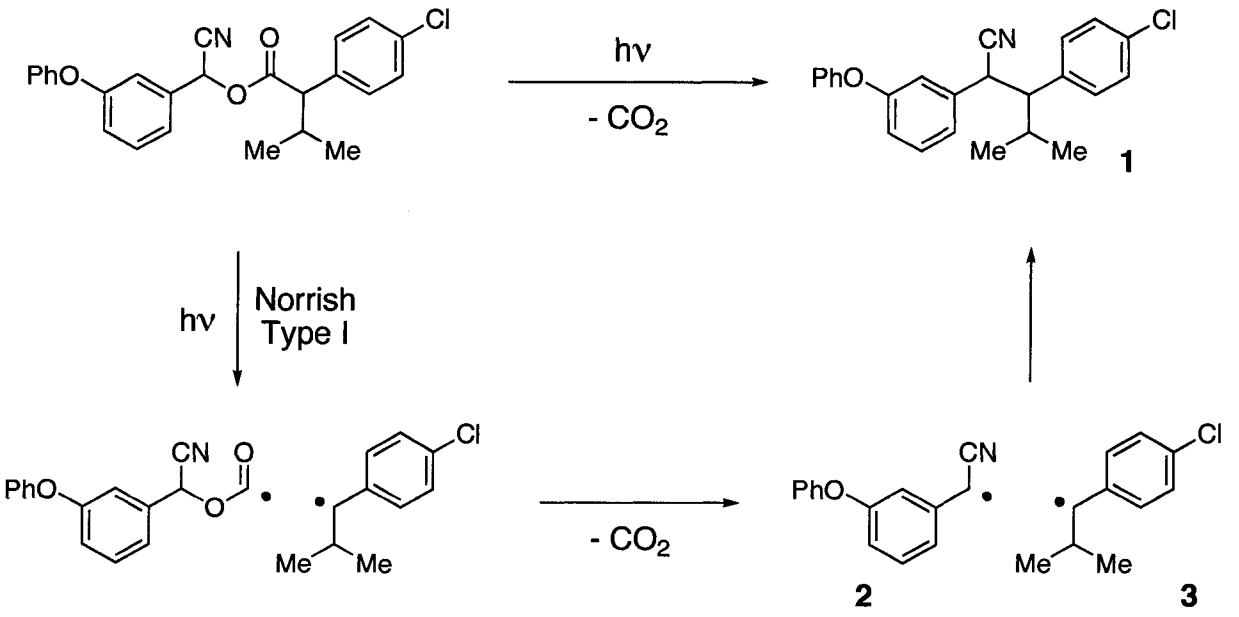

Scheme 3.3. Photodecomposition of the pesticide fenvalerate.

Laser flash photolysis studies revealed the cyano-substituted radical **2** to be reasonably long-lived and unreactive towards oxygen; remarkable for a secondary benzylic radical. Since the other benzylic radical **3** displayed expected transient behaviour, we concluded that the persistent free radical effect was responsible for the formation of the cross-product **1** as the overall dominant photodecomposition product.

In order to gain further insight into the operation of the persistent free radical effect in this photodecomposition, we examined the behaviour of other nitrile-derived carbon-centred radicals.[10] This chapter describes the research that led to the discovery of their persistent nature and greatly attenuated reactivity toward oxygen.

It should be noted that, in the context of these applications (and in this thesis), the reactivity toward oxygen is based on laser flash photolysis studies where "unreactive radicals" are those with oxygen quenching rate constants $\leq 5 \times 10^3$ $M^{-1}s^{-1}$.

This represents an attenuation by at least six orders of magnitude by comparison with typical carbon-centred radical reactivities.[8]

3.2. Laser Flash Photolysis Studies 1: Reactivity towards alkoxyl radicals

Of the five factors listed above, steric hindrance is the characteristic most often used to explain the persistence and lack of reactivity towards molecular oxygen of carbon-centred radicals.[11] Thus, the nitrile-derived molecules of Scheme 3.4 were examined in an attempt to address the issue where only criteria (a) to (d) are present. As part of this investigation, we also observed the reactivity of these derivatives towards alkoxyl radicals.

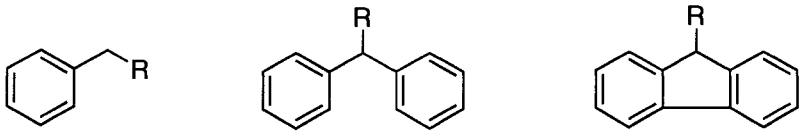

1a R = CH_3
1b R = CN

2a R = H
2b R = CN

3a R = H
3b R = CN

Scheme 3.4. Nitrile compounds and their hydrocarbon counterparts studied.

The reactivity towards alkoxyl radicals was determined by studying their reaction with *tert*-butoxyl radicals using laser flash photolysis techniques.[12] The radicals produced in these reactions have significant absorptions in the UV region that can be used to monitor their formation directly. Thus, the *tert*-butoxyl radicals were produced by 355 nm laser excitation of a de-aerated solution of the peroxide in benzene (50/50 v/v%) (Scheme 3.5).

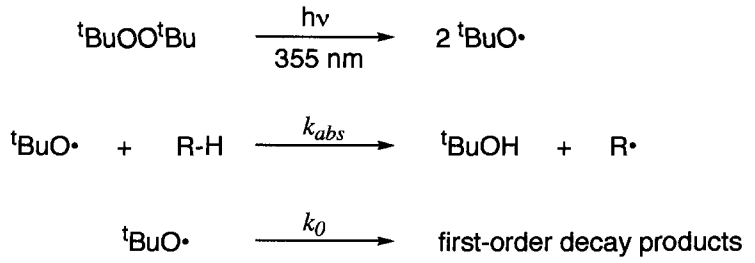

Scheme 3.5. Independent photochemical generation of benzylic radicals using hydrogen abstraction by *tert*-butoxyl radicals.

The growth of the radical signal reflects the hydrogen abstraction (k_{abs}) and other first-order forms of decay of the *tert*-butoxyl radical (k_0), such as reaction with the solvent and β-cleavage. Therefore, the experimental rate constant for the growth is a combination of these processes, given by Equation 3.1.

$$k_{obs} = k_0 + k_{abs}[R-H] \tag{3.1}$$

Plotting the observed rate constant for the growth of the corresponding radical as a function of [R-H] thus yields the hydrogen abstraction rate constants; a representative growth trace and resulting plot are shown in Figure 3.1 for phenylacetonitrile (**1b**).

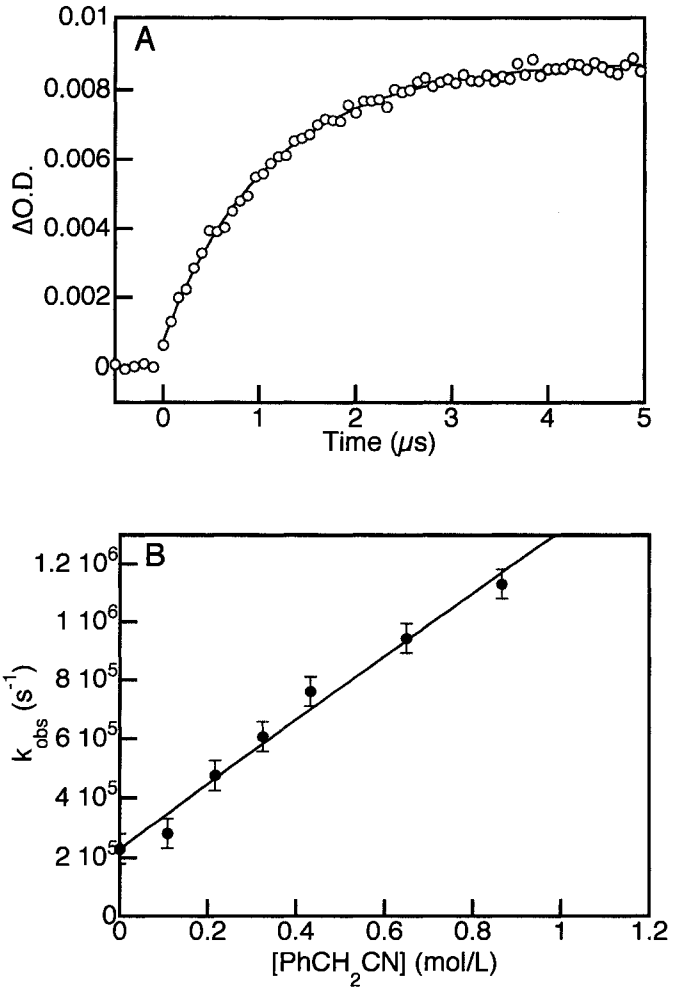

Figure 3.1. (A) Sample growth trace at 470 nm for the α-cyanobenzyl radical, generated from 0.65 M $PhCH_2CN$ in 50:50 benzene: di-*tert*-butylperoxide solvent under nitrogen after 355 nm laser excitation. (B) Observed rate constants for hydrogen abstraction from $PhCH_2CN$ by *tert*-butoxyl radical.

The rate constants determined from plots of k_{obs} *vs.* [RH] are given in Table 3.1. The rate constants for the hydrogen abstraction of nitrile compounds are enhanced relative to their unsubstituted counterparts, with differences ranging from slight (for phenylacetonitrile) to a factor of four (for 9-cyanofluorene). This is remarkable, since *tert*-butoxyl is a very electrophillic radical and under normal conditions α-cyano

substitution would be expected to decrease the reactivity.[12-15] The fact that it does not suggests that delocalization onto the cyano group contributes to benzyl radical stabilization.

Table 3.1. Rate constants for the reactions of *tert*-butoxyl radicals with hydrogen donors, transient absorption maxima, and resulting radical reactivity towards oxygen.

Radical from:	k_{abs} (10^6 $M^{-1}s^{-1}$)	λ_{max} for the radical (nm)	Approx. $t_{1/2}$ (μs)	Radical reacts with O_2?[a]
HP-136	12.4	340	375	No
1a[12]	1.05	309	10	Yes
1b	1.08	470	30	No
2a[16]	0.91	340	20	Yes
2b	4.21	510	130	No
3a	6.2	500	45	Yes
3b	26.9	540	270	No

[a]Based on laser flash photolysis conditions, on the μs timescale. Typical errors are <5%.

Table 3.1 also contains the approximate half-lives of the radical species in organic solution. In the cases of secondary benzylic radicals **2a** and **3a**, addition of a cyano group results in a 6-fold increase in half-lives. For **1a**, replacing the methyl group with a nitrile group results in a 3-fold increase (unlike the other two species, this is a substitution to make another secondary benzylic radical, not an addition to make a tertiary benzylic radical).

This significant enhancement in the observed half-lives in solution indicates that the radicals generated from the nitrile derivatives experience attenuated self-reactions and side-reactions with the starting material or solvent.[17, 18] As Ingold and Griller had outlined in 1976, these factors, along with reduced reactivity towards molecular oxygen,

are the main criteria for persistent radicals.[11] Therefore, we subsequently investigated the possible persistent nature of these species by examining their reactivity towards O_2 under the conditions of laser flash photolysis.

3.3. Laser Flash Photolysis Studies 2: Reactivity towards molecular oxygen

Laser flash photolysis studies of di-*tert*-butylperoxide at 355 nm in the presence of the substrates were carried out in order to generate the corresponding radicals and to study their reactivity with oxygen (absorption maxima are also shown in Table 3.1).

From the transient absorption spectra, it is clear that addition of an α-cyano group results in the appearance of bands in the visible region of the spectrum for **1b** and **2b** while the visible band in the fluorenyl radical spectrum is red-shifted from 500 nm to 540 nm. (Fig. 3.2 C). As well, the visible bands are more intense than in the case of the benzyl radical; this enhancement has been attributed to the presence of heteroatoms.[1]

The comparison of nitrogen- and oxygen-saturated samples showed that both radical growth and decay were not affected by oxygen for all of the cyano-substituted radicals; decays for these radicals under nitrogen and oxygen are shown in Figure 3.3. However, in oxygen-saturated samples, the radicals from **1a**, **2a**, and **3a** were totally quenched, with barely a fast spike indicating their presence in the early stages following the laser pulse.

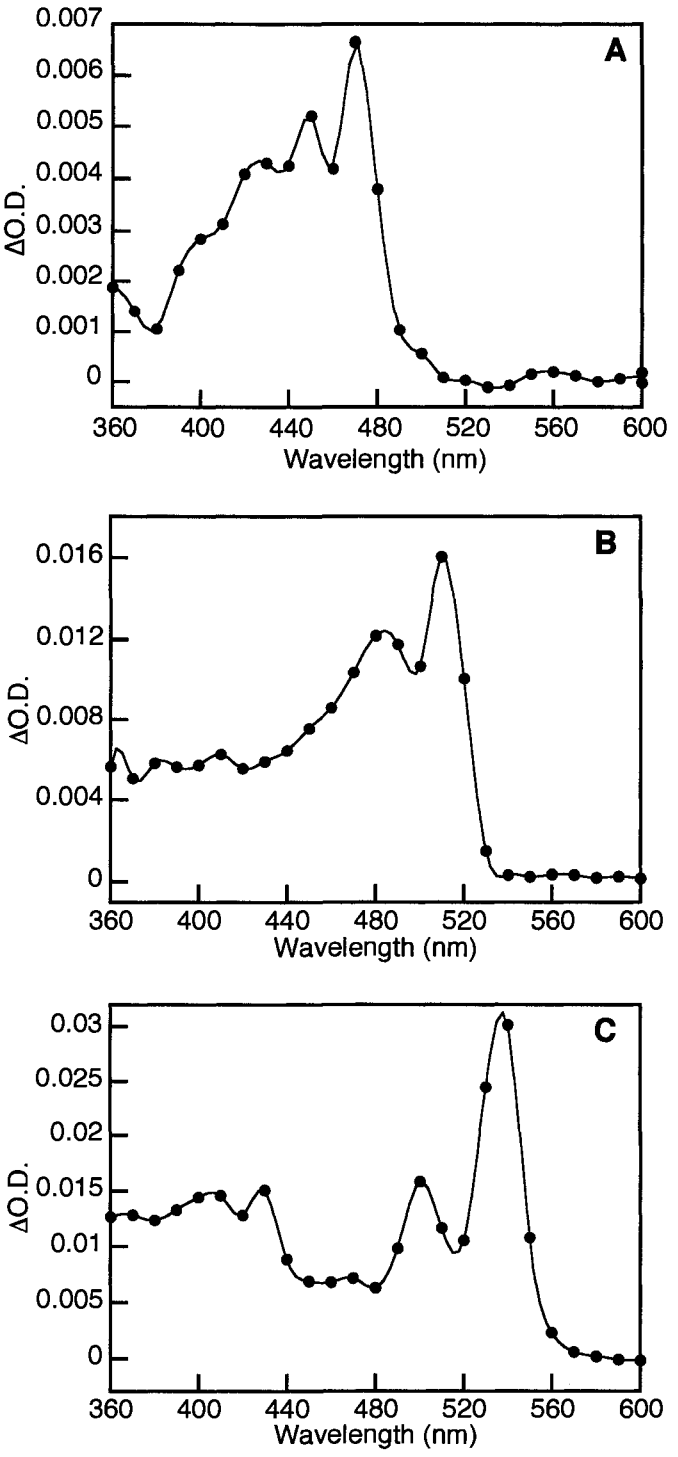

Figure 3.2. Transient visible absorption spectra of nitriles in 50:50 benzene: di-*tert*-butylperoxide solvent under nitrogen after 355 nm laser excitation (A) 0.6 M phenylacetonitrile, 2.64 μs after the laser pulse; (B) 0.184 M diphenylacetonitrile, 3.48 μs after the laser pulse; (C) 0.01 M 9-cyanofluorene, 8.40 μs after the laser pulse.

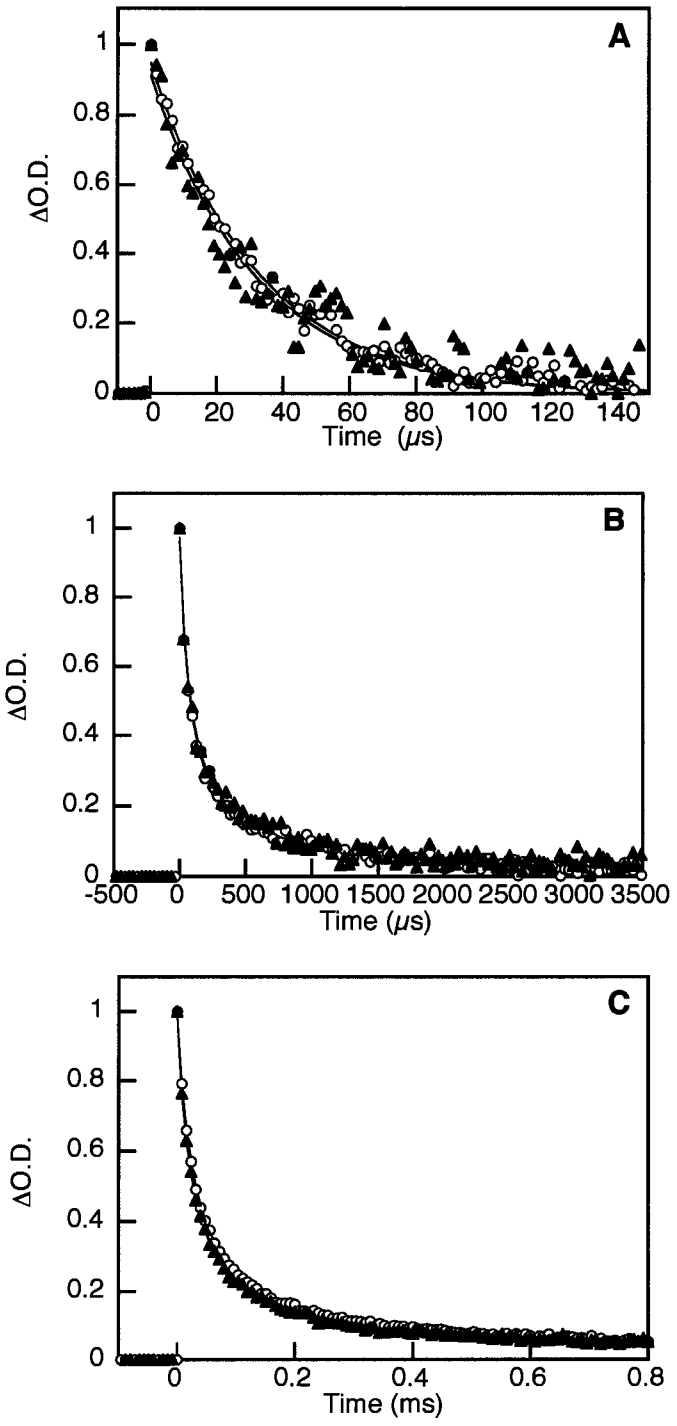

Figure 3.3. Transient decay traces for α-cyano carbon-centred radicals in 50:50 benzene: di-*tert*-butylperoxide solvent under N_2 (O) or O_2 (▲) after 355 nm laser excitation. (A) 0.6 M phenylacetonitrile, monitored at 470 nm; (B) 0.184 M diphenylacetonitrile, monitored at 510 nm; (C) 0.01 M 9-cyanofluorene, monitored at 540 nm.

Laser flash photolysis studies clearly demonstrated that the simple addition of a nitrile group dramatically enhances the longevities of carbon-centred radicals, as well as rendering them unreactive to molecular oxygen on the microsecond and millisecond timescales. Thus, in addition to the coumaranone derivatives, we concluded that, on the timescales of laser flash photolysis, α-cyano substituted carbon-centred radicals can also display antioxidant potential and that these species are not only *resonance-stabilized*, but can also be considered to be *persistent* radicals.

3.4. The α-cyano Group: Computational investigations

In general, radicals with multiple possible resonance structures are 'stabilized' radicals, where increased delocalization of the unpaired electron over multiple atoms contributes to the observed stability. As well, the presence of electron withdrawing groups such as nitrile moieties is often used to rationalize radical stability.[19-21] However, do resonance effects and electron-withdrawing groups affect radical persistence?

Radicals with multiple nitrile groups are known to prefer radical-radical reactions such as disproportionation and dimerization over reactions with molecules such as hydrogen abstractions and addition to π systems. In 1976, Ingold and Kaba investigated the effect of α-cyano groups on carbon-centred radical decay kinetics; specifically the tricyanomethyl radical.[21] With three highly electronegative groups attached, the authors suspected it might be a non-planar radical, like $\bullet CF_3$ or $\bullet CCl_3$, with similar diffusion-controlled self-reaction decay kinetics.

Instead, they observed the remarkable persistence of this radical, and concluded that its planar geometry and p-π delocalization are largely responsible for its longevity.

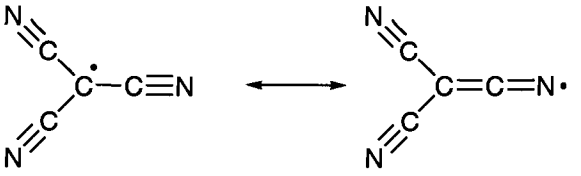

Scheme 3.6. Resonance forms of the tricyanomethyl radical.

A considerable activation energy is required for the recombination of tricyanomethyl radicals: to dimerize, one or both of the radicals must be distorted from the strongly preferred planar geometry. Consequently, the dimerization is unfavourable and observed decay rate constants are lowered. These results were surprising to the authors, who had contended earlier that persistence was primarily due to steric effects. Clearly, the authors conceded, electronic and stereoelectronic factors must also be considered. To this end, we investigated the effect of the nitrile group on radical stability and persistence *via* computational studies.

The molecular geometries of the radicals obtained from **1-3a** and **1-3b** were optimized and Mulliken spin distributions determined using the Gaussian03 software program (for full details, see Chapter 2; for full results, see Appendix 3A).[22] For radicals **1a**, **1b**, **3a**, and **3b**, the carbon radical centres are co-planar with the adjacent aromatic rings, indicating delocalization of the unpaired electron through the aromatic π system; *i.e.* the p orbitals of the π system and the unhybridized p orbital on the radical centre are of proper orientation. However, in radicals **2a** and **2b** the carbon centres are not planar: in **2a**, C5-C4-C12-H13 and C16-C14-C12-H13 (see Appendix 3A for atom designations) have a dihedral angles of 162°; in other words, the phenyl rings are twisted out of the plane by about 18° -- a configuration that is expected due to steric interactions between

phenyl hydrogens H10 and H20. Radical **2b** is also non-planar: it has comparative dihedral angles of 153°, corresponding to an out-of-plane twist of 27° for each phenyl ring. That the α-cyanodiphenylmethyl radical displays a lesser degree of planarity than its unsubstituted analogue is not surprising, given the increased spin delocalization on the nitrogen atom accompanied by decreased delocalization in the aryl moieties (see below). This finding follows Hartzler's 1966 hypothesis that "the diphenylcyanomethyl radicals would not be planar...[t]he aryldicyanomethyl radicals, however, probably are planar and enjoy stabilization by conjugation with all three substituents".[23]

As stated previously, resonance delocalization into the aromatic π system at the *para* and *ortho* positions is responsible for the 'stability' of the unsubstituted benzylic radicals. This resonance, however, does not render these radicals persistent nor unreactive with oxygen. Thus, it seems that the contribution of the resonance from centered on nitrogen is decisive to explain the behaviour of **1–3b** radicals.

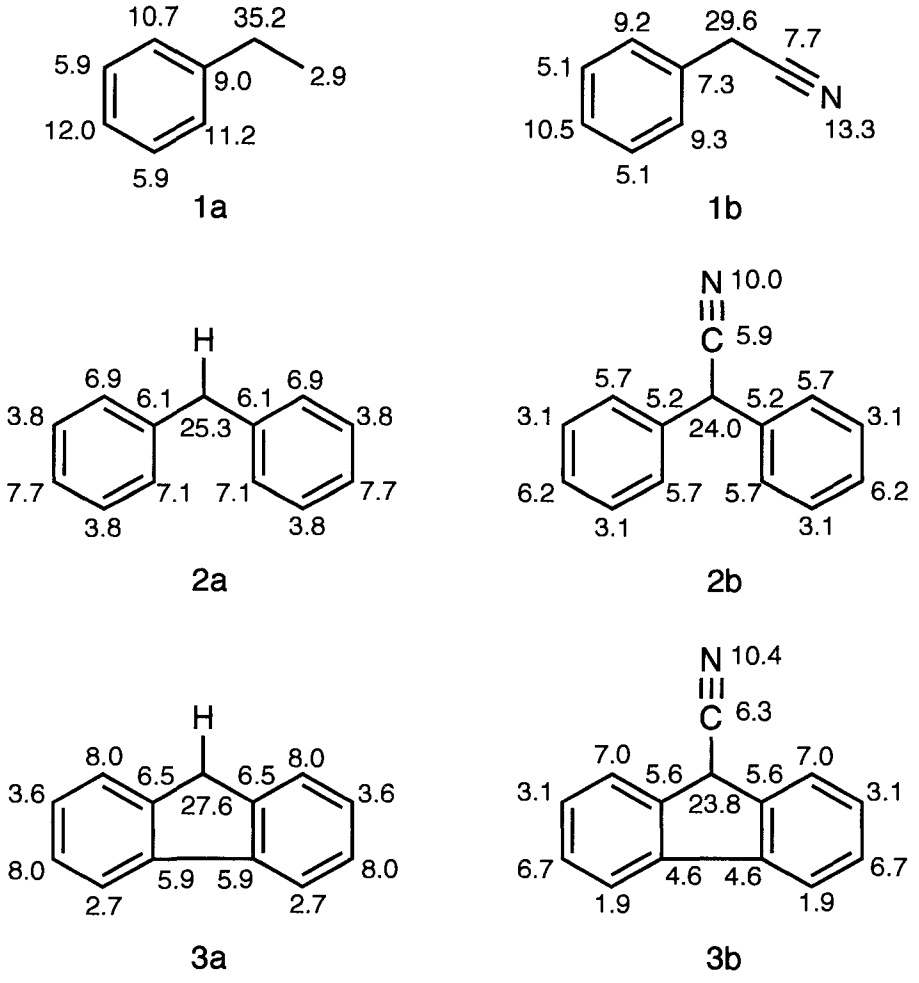

Scheme 3.7. Unpaired electron spin distribution (in % total spin) for the carbon skeleton of radicals studied.

Spin density calculation data for the unsubstituted benzylic radicals **1-3a** show that about 25-35% of the unpaired electron is located on the benzylic carbon atom (see Table 2 and Scheme 7). However, radicals generated from nitrile compounds show a 10-13% contribution of the unpaired electron on the nitrogen atom of the cyano group due to resonance delocalization, (*e.g.*, 13.3% for **1b**) a phenomenon that was previously reported for oxygen atoms.[4]

What is remarkable is the fact that the increased spin distribution on the heteroatom does not necessarily come at the expense of the contribution at the carbon radical centre. For example, in the case of the fluorenyl radical, addition of an α-cyano group resulted in a decrease of only ~3.8% on the benzylic carbon. Instead, it appears the increased density on the nitrogen atom is due to a significant decrease in the total spin density on the aromatic rings: at least 10% in all three cases.

Table 3. 2. Selected spin distributions for radicals studied.

Radical	C (% total spin)[b]	N (% total spin)[b]	Total aromatic contribution (% total spin)[b]
1a	35.2		54.7
1b	29.6	13.3	43.5
2a	25.3		70.8
2b	24.0	10.0	60.0
3a	27.6		69.4
3b	23.8	10.4	57.8

[b]Percent total spin calculated as follows: obtained Mulliken spin distributions for each atom were converted to absolute values and summed. The values reported in this table are thus the atom's contributing fraction to the total overall distribution; *i.e.*

$$\%\ total\ spin = \frac{|s|}{\sum |s|} \times 100\%$$

This resonance effect has profound consequences on the bond lengths and bond orders in the corresponding radicals. For example, Scheme 8 shows the values for radicals from **1a** and **1b**: for the α-cyanobenzyl radical **1b**, the carbon-carbon bond length is shortened from 1.46 Å in acetonitrile[24] to 1.398 Å, though it is not quite as short

as a normal carbon-carbon double bond (1.34 Å)[24]. As well, the carbon-nitrogen bond is slightly elongated, from 1.16 Å to 1.178 Å, as shown in Scheme 8 below.

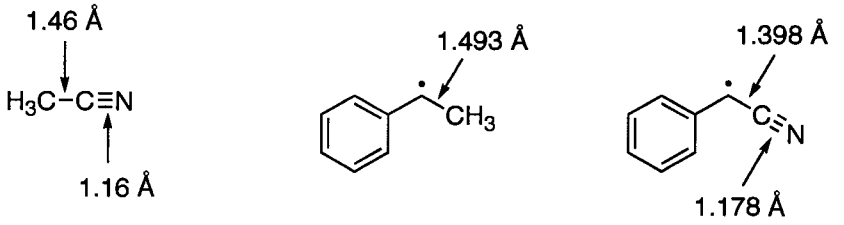

Scheme 3.8. Selected bond lengths (values for acetonitrile from Reference 24, all others obtained from the geometry optimization calculations).

Therefore, the carbon-carbon bond can be accurately described as having partial double-bond character. This, combined with the significant decrease in the total spin density on the aromatic rings suggests that the resonance forms corresponding to delocalization of the unpaired electron in the aromatic π system have become less significant in favour of increased contribution from the nitrogen atom.

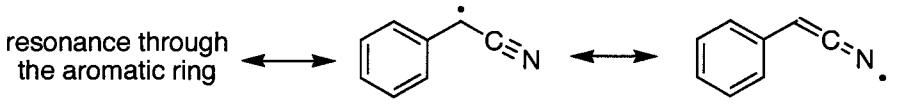

Scheme 3.9. Resonance forms of the α-cyanobenzyl radical.

However, atomic charge distributions computed using the CHELPG method[25] were also intriguing: the carbon radical centres in the nitrile derivatives are much more electropositive than their unsubstituted counterparts (*ca.* -0.22 *versus ca.* -0.45). Since the attack by molecular oxygen is electrophillic, this increased positive partial charge at the

carbon centres could be another contributing factor to the attenuated reactivity towards oxygen of these radical species.

The combination of this increased electropositivity and unpaired electron spin delocalization on the nitrogen atom (along with other favourable stereoelectronic effects) thus leads to a *stabilized and persistent* benzylic radical.

3.5 Conclusions

The lack of reactivity towards oxygen of radicals generated from nitrile compounds is surprising, particularly for radicals derived from **1b** and **2b**. On the other hand, it is clear that a high spin delocalization on the cyano group, as it has been demonstrated by spin density calculations, contributes to the stability of these radicals. Finally, the reactivity enhancements toward alkoxyl radicals caused by nitrile substitution are even more remarkable when one considers that alkoxyl radicals are electrophilic. The dramatic effect of -CN on radical reactivity toward oxygen, while unexpected, can be rationalized on the basis of the same five parameters as for other radicals, with spin density on nitrogen and electron withdrawing effects adding to stabilization achieved by benzylic delocalization.

3.6 References

1. Chatgilialoglu, C., Electronic Absorption Spectra of Free Radicals. In *Handbook of Organic Photochemistry*, Scaiano, J. C., Ed. CRC Press: Boca Raton, Florida, 1989; Vol. II, pp 3-11.

2. Gilbert, A.; Baggott, J., *Essentials of Molecular Photochemistry*. Blackwell: Oxford, 1991.

3. Turro, N. J., *Modern Molecular Photochemistry*. University Science Books: Sausalito, 1991.

4. Bejan, E. V.; Font-Sanchis, E.; Scaiano, J. C., Lactone-derived Carbon-centered Radicals: Formation and reactivity with Oxygen. *Org. Lett.* **2001,** 3, (25), 4059-4062.

5. Scaiano, J. C.; Martin, A.; Yap, G. P. A.; Ingold, K. U., A Carbon Centered Radical Unreactive Towards Oxygen: Unusual Radical Stabilization by a Lactone Ring. *Org. Lett.* **2000,** 2, (7), 899-901.

6. Aliaga, C.; Stuart, D. R.; Aspée, A.; Scaiano, J. C., Solvent Effects on Hydrogen Abstraction Reaction from Lactones with Antioxidant Properties. *Org. Lett.* **2005,** 7, 3665.

7. Denisov, E. T., *Oxidation and antioxidants in organic chemistry and biology*. Taylor & Francis: Boca Raton, 2005.

8. Maillard, B.; Ingold, K. U.; Scaiano, J. C., Rate constants for the reactions of free radicals with oxygen in solution. *J. Am. Chem. Soc.* **1983,** 105, 5095.

9. Sanjuán, A.; Aguirre, G.; Alvaro, M.; García, H.; Scaiano, J. C.; Chrétien, M. C.; Focsaneanu, K.-S., Product studies and laser flash photolysis of direct and 2,4,6-triphenylpyrylium-zeolite Y photocatalyzed degradation of fenvalerate. *Photochem. Photobiol. Sci.* **2002,** 1, 955-959.

10. Font-Sanchis, E.; Aliaga, C.; Focsaneanu, K.-S.; Scaiano, J. C., Greatly Attenuated Reactivity of Nitrile-Derived Carbon-centered Radicals toward Oxygen. *Chem. Commun.* **2002,** (15), 1576-1577.

11. Griller, D.; Ingold, K. U., Persistent Carbon-Centered Radicals. *Acc. Chem. Res.* **1976,** 9, 13-18.

12. Paul, H.; Small Jr., R. D.; Scaiano, J. C., Hydrogen Abstraction by tert-butoxy radicals. A laser flash photolysis and electron spin resonance study. *J. Am. Chem. Soc.* **1978,** 100, 4520.

13. Baignee, A.; Howard, J. A.; Scaiano, J. C.; Stewart, L. C., Absolute rate constants for reactions of cumyloxy in solution. *J. Am. Chem. Soc.* **1983,** 105, 6120.

14. Das, P. K.; Encinas, M. V.; Steenken, S.; Scaiano, J. C., Reaction of tert-butoxy radicals with phenols. Comparison with the reactions of carbonyl triplets. *J. Am. Chem. Soc.* **1981,** 103, 4162.

15. Wong, P. C.; Griller, D.; Scaiano, J. C., A kinetic study of the reactions of tert-butoxyl with alkenes: hydrogen abstraction vs. addition. *J. Am. Chem. Soc.* **1982,** 104, 5106.

16. Arends, I. W. C. E.; Mulder, P.; Clark, K. B.; Wayner, D. D. M., Rate constants for termination and TEMPO trapping of some resonance stabilized hydroaromatic radicals in the liquid phase. *J. Phys. Chem.* **1995,** 99, (8182).

17. Gostowski, R. C.; Bailey, T.; Bonner, S. D.; Emrich, E. E.; Steelman, S. L., Steric hindrance on bimolecular coupling rate constants of carbon-centered radicals. *J. Phys. Org. Chem.* **2000,** 13, 735.

18. Korth, H. G.; Lommes, P.; Sicking, W.; Sustmann, R., Rate constants for the bimolecular self-reaction of cyano-substituted alkyl radicals in solution. *Int. J. Chem. Kin.* **1983,** 15, 267.

19. Renaud, P.; Sibi, M. P., *Radicals in Organic Synthesis, Vol. 1 and* 2. Wiley-VCH: New York, 2001.

20. Zard, S. Z., *Radical Reactions in Organic Synthesis.* Oxford University Press: Oxford, 2003.

21. Kaba, R. A.; Ingold, K. U., Kinetic applications of electron paramagnetic resonance spectroscopy. XXIII Cyanomethyl radicals. *J. Am. Chem. Soc.* **1976,** 98, 523.

22. Frisch, M. J.; Trucks, G. W.; Schlegel, H. B.; Scuseria, G. E.; Robb, M. A.; Cheeseman, J. R.; Montgomery, J., J. A.; Vreven, T.; Kudin, K. N.; Burant, J. C.; Millam, J. M.; Iyengar, S. S.; Tomasi, J.; Barone, V.; Mennucci, B.; Cossi, M.; Scalmani, G.; Rega, N.; Petersson, G. A.; Nakatsuji, H.; Hada, M.; Ehara, M.; Toyota, K.; Fukuda, R.; Hasegawa, J.; Ishida, M.; Nakajima, T.; Honda, Y.; Kitao, O.; Nakai, H.; Klene, M.; Li, X.; Knox, J. E.; Hratchian, H. P.; Cross, J. B.; Adamo, C.; Jaramillo, J.; Gomperts, R.; Stratmann, R. E.; Yazyev, O.; Austin, A. J.; Cammi, R.; Pomelli, C.; Ochterski, J. W.; Ayala, P. Y.; Morokuma, K.; Voth, G. A.; Salvador, P.; Dannenberg, J. J.; Zakrzewski, V. G.; Dapprich, S.; Daniels, A. D.;

Strain, M. C.; Farkas, O.; Malick, D. K.; Rabuck, A. D.; Raghavachari, K.; Foresman, J. B.; Ortiz, J. V.; Cui, Q.; Baboul, A. G.; Clifford, S.; Cioslowski, J.; Stefanov, B. B.; Liu, G.; Liashenko, A.; Piskorz, P.; Komaromi, I.; Martin, R. L.; Fox, D. J.; Keith, T.; Al-Laham, M. A.; Peng, C. Y.; Nanayakkara, A.; Challacombe, M.; Gill, P. M. W.; Johnson, B.; Chen, W.; Wong, M. W.; Gonzalez, C.; Pople, J. A. *Gaussian 03, Revision B.04*, Gaussian, Inc.: Pittsburgh, PA, 2003.

23. Hartzler, H. D., Polycyano Radicals. *J. Org. Chem.* **1966,** 31, 2654.

24. Solomons, T. W. G., *Organic Chemistry*. 6th Ed. ed.; John Wiley & Sons, Inc.: New York, 1996.

25. Breneman, C. M.; Wiberg, K. B., Determining atom-centered monopoles from molecular electrostatic potentials. The need for high sampling density in formamide conformational analysis. *J. Comp. Chem.* **1990,** 11, 361.

Appendix 3A. Computational Studies Data

Table 3. Spin Distribution for the α-methylbenzyl radical (**1a**)

Atom No.	Atom	Mulliken atomic spin density	Absolute atomic spin density	% total spin[c]
1	C	0.262757	0.262757	12.0
2	C	-0.128034	0.128034	5.9
3	C	0.232887	0.232887	10.7
4	C	-0.196482	0.196482	9.0
5	C	0.244916	0.244916	11.2
6	C	-0.129613	0.129613	5.9
7	H	-0.012805	0.012805	0.6
8	H	0.004906	0.004906	0.2
9	H	-0.010732	0.010732	0.5
10	H	-0.011434	0.011434	0.5
11	H	0.004966	0.004966	0.2
12	C	0.768154	0.768154	35.2
13	C	-0.063455	0.063455	2.9
14	H	-0.038342	0.038342	1.8
15	H	0.001308	0.001308	0.1
16	H	0.035538	0.035538	1.6
17	H	0.035465	0.035465	1.6
SUM		1.000000	2.181794	100.0

[c] $\%\ total\ spin = \frac{|s|}{\sum |s|} \times 100\%$

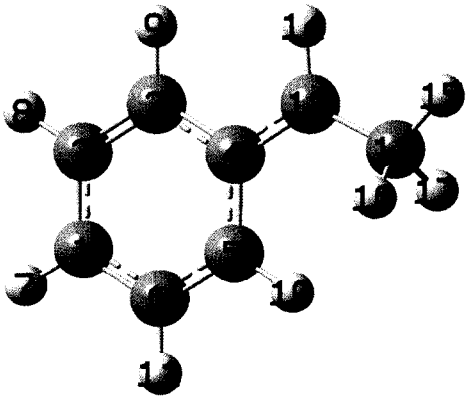

Table 4. Spin Distribution for the α-cyanobenzyl radical (**1b**)

Atom No.	Atom	Mulliken atomic spin density	Absolute atomic spin density	% total spin[c]
1	C	0.237155	0.237155	10.5
2	C	-0.115089	0.115089	5.1
3	C	0.206791	0.206791	9.2
4	C	-0.163855	0.163855	7.3
5	C	0.209473	0.209473	9.3
6	C	-0.114961	0.114961	5.1
7	H	-0.011241	0.011241	0.5
8	H	0.004279	0.004279	0.2
9	H	-0.009377	0.009377	0.4
10	H	-0.009267	0.009267	0.4
11	H	0.004291	0.004291	0.2
12	C	0.667415	0.667415	29.6
13	H	-0.031046	0.031046	1.4
14	C	-0.174025	0.174025	7.7
15	N	0.299458	0.299458	13.3
SUM		1.000000	2.257723	100.0

[c] $\%\ total\ spin = \frac{|s|}{\sum |s|} \times 100\%$

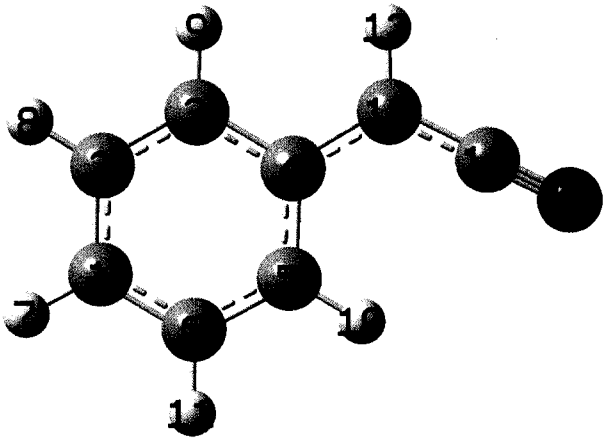

Table 5. Spin Distribution for the diphenylmethyl radical (**2a**)

Atom No.	Atom	Mulliken atomic spin density	Absolute atomic spin density	% total spin[c]
1	C	0.198860	0.198860	7.7
2	C	-0.097880	0.097880	3.8
3	C	0.178245	0.178245	6.9
4	C	-0.158934	0.158934	6.1
5	C	0.184986	0.184986	7.1
6	C	-0.098926	0.098926	3.8
7	H	-0.009610	0.009610	0.4
8	H	0.003848	0.003848	0.1
9	H	-0.007861	0.007861	0.3
10	H	-0.008273	0.008273	0.3
11	H	0.003989	0.003989	0.2
12	C	0.654748	0.654748	25.3
13	H	-0.031635	0.031635	1.2
14	C	-0.158933	0.158933	6.1
15	C	0.178243	0.178243	6.9
16	C	0.184984	0.184984	7.1
17	C	-0.097879	0.097879	3.8
18	H	-0.007860	0.007860	0.3
19	C	-0.098925	0.098925	3.8
20	H	-0.008273	0.008273	0.3
21	C	0.198858	0.198858	7.7
22	H	0.003848	0.003848	0.1
23	H	0.003989	0.003989	0.2
24	H	-0.009610	0.009610	0.4
SUM		1.000000	2.589197	100.0

[c] $\%\ total\ spin = \frac{|s|}{\sum|s|} \times 100\%$

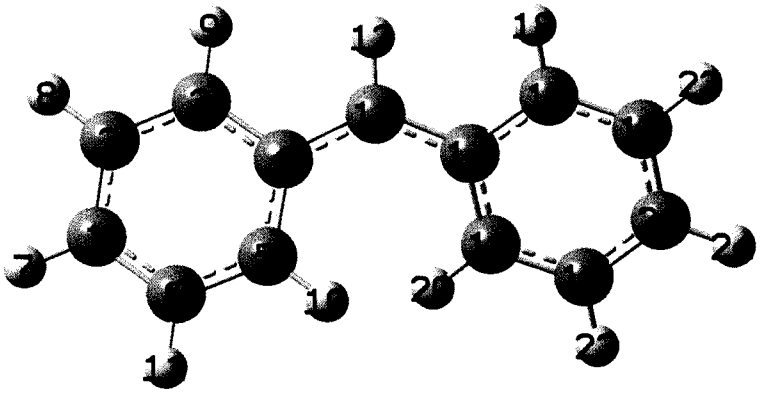

Table 6. Spin Distribution for the α-cyanodiphenylmethyl radical (**2b**)

Atom No.	Atom	Mulliken atomic spin density	Absolute atomic spin density	% total spin[c]
1	C	0.156718	0.156718	6.2
2	C	-0.077869	0.077869	3.1
3	C	0.144437	0.144437	5.7
4	C	-0.129892	0.129892	5.2
5	C	0.143844	0.143844	5.7
6	C	-0.078197	0.078197	3.1
7	H	-0.007435	0.007435	0.3
8	H	0.003100	0.003100	0.1
9	H	-0.006475	0.006475	0.3
10	H	-0.006419	0.006419	0.3
11	H	0.003291	0.003291	0.1
12	C	0.606246	0.606246	24.0
13	C	-0.129881	0.129881	5.2
14	C	0.144417	0.144417	5.7
15	C	0.143823	0.143823	5.7
16	C	-0.077857	0.077857	3.1
17	H	-0.006475	0.006475	0.3
18	C	-0.078185	0.078185	3.1
19	H	-0.006418	0.006418	0.3
20	C	0.156693	0.156693	6.2
21	H	0.003099	0.003099	0.1
22	H	0.003290	0.003290	0.1
23	H	-0.007434	0.007434	0.3
24	C	-0.148221	0.148221	5.9
25	N	0.251799	0.251799	10.0
SUM		1.000000	2.521515	100.0

[c] $\%\ total\ spin = \frac{|s|}{\sum|s|} \times 100\%$

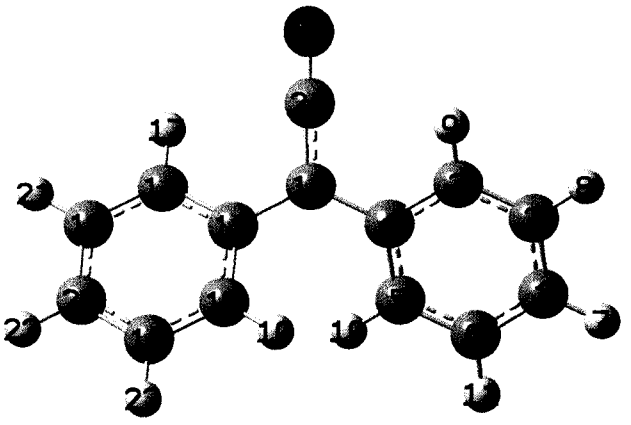

Table 7. Spin Distribution for the fluorenyl radical (**3a**)

Atom No.	Atom	Mulliken atomic spin density	Absolute atomic spin density	% total spin[c]
1	C	0.182589	0.182589	6.2
2	C	-0.081107	0.081107	3.1
3	C	0.183336	0.183336	5.7
4	C	-0.147983	0.147983	5.2
5	C	0.134200	0.134200	5.7
6	C	-0.061223	0.061223	3.1
7	H	-0.008923	0.008923	0.3
8	H	0.002836	0.002836	0.1
9	H	-0.008224	0.008224	0.3
10	H	0.002256	0.002256	0.3
11	C	0.631461	0.631461	0.1
12	H	-0.026977	0.026977	24.0
13	C	-0.147983	0.147983	5.2
14	C	0.183336	0.183336	5.7
15	C	-0.081107	0.081107	5.7
16	C	0.182589	0.182589	3.1
17	C	-0.061223	0.061223	0.3
18	C	0.134200	0.134200	3.1
19	H	-0.008224	0.008224	0.3
20	H	0.002836	0.002836	6.2
21	H	-0.008923	0.008923	0.1
22	H	0.002256	0.002256	0.1
SUM		1.000000	2.283792	100.0

[c] $\%\ total\ spin = \frac{|s|}{\sum |s|} \times 100\%$

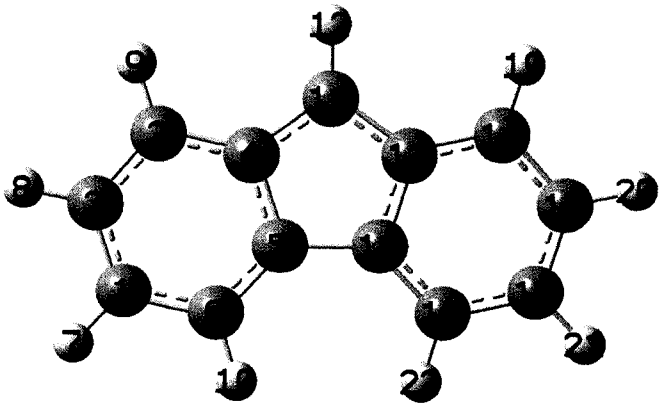

Table 8. Spin Distribution for the α-cyanofluorenyl radical (**3b**)

Atom No.	Atom	Mulliken atomic spin density	Absolute atomic spin density	% total spin[c]
1	C	0.158636	0.158636	6.7
2	C	-0.074048	0.074048	3.1
3	C	0.165867	0.165867	7.0
4	C	-0.133363	0.133363	5.6
5	C	0.107956	0.107956	4.6
6	C	-0.045297	0.045297	1.9
7	H	-0.007641	0.007641	0.3
8	H	0.002564	0.002564	0.1
9	H	-0.007145	0.007145	0.3
10	H	0.001633	0.001633	0.1
11	C	0.564639	0.564639	23.8
12	C	-0.133363	0.133363	5.6
13	C	0.165867	0.165867	7.0
14	C	-0.074048	0.074048	3.1
15	C	0.158636	0.158636	6.7
16	C	-0.045297	0.045297	1.9
17	C	0.107956	0.107956	4.6
18	H	-0.007145	0.007145	0.3
19	H	0.002564	0.002564	0.1
20	H	-0.007641	0.007641	0.3
21	H	0.001633	0.001633	0.1
22	C	-0.150562	0.150562	6.3
23	N	0.247598	0.247598	10.4
SUM		1.000000	2.371099	100.0

[c] $\%\ total\ spin = \frac{|s|}{\sum |s|} \times 100\%$

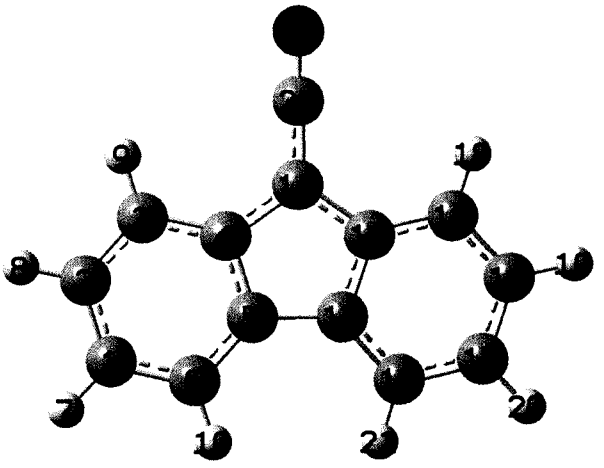

Chapter 4. Organic Synthesis Using the Persistent Free Radical Effect

Chapter 4. Organic Synthesis Using the Persistent Free Radical Effect

4.1 Introduction

Encouraged by the discovery of persistent carbon-centred radicals,[1] we were interested in investigating possible applications of these novel intermediates in addition to their use as peroxyl radical-scavenging antioxidants. As part of these studies, dimers of these radicals were prepared from their corresponding monomers by M. Frenette, introduced in Chapter 1.[2] Recall that, in toluene solution, these diamagnetic molecules are in thermal equilibrium with the radical species. For example, solutions of the dimer formed from the α-cyanodiphenylmethyl radical (1, 1, 2, 2-tetraphenyl succinonitrile, TPS) are stable at room temperature; we used the term *dynamic stability* to describe the attenuation of these persistent radicals towards possible side-reactions with the solvent.

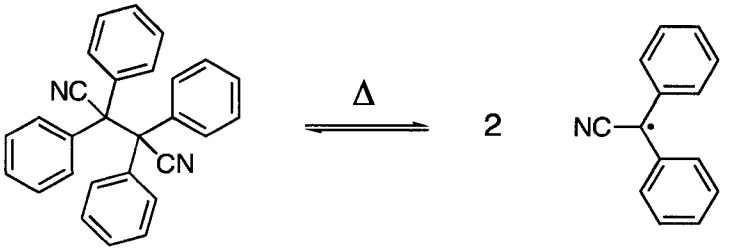

Scheme 4.1. TPS is in thermal equilibrium with the α-cyanodiphenylmethyl radical.

Thus, the usual fate of these radicals is to recombine to reform TPS. If a new species, capable of reacting with the radicals, is introduced in the system, one can anticipate reactions with the α-cyanodiphenylmethyl leading to new products. We considered

exploiting this characteristic buffer-like behavior *via* the Fischer-Ingold Persistent Free Radical Effect (PFRE).[3,4]

Inspired by the operation of this effect, a novel synthetic method was devised: produce persistent radicals thermally from their corresponding dimers, while generating transient radicals *in situ* photochemically. The persistent radicals-dimer equilibrium behaves as an effective "radical buffer", with the former trapping the transient radicals to form the cross-reaction product, while the dimer, through the equilibrium of Scheme 4.1 keeps the supply of radicals available. The radicals used here are not as entirely persistent as, say, the 2,2,6,6-tetramethylpiperidine-1-oxyl (TEMPO) radical,[5] since they *do* react to form the dimer. However, their recombination is effectively 'incomplete' as a result of the radicals ⇆ dimer equilibrium. As a consequence, the introduction of a second radical species will cause the TPS to appear to have lost its stability, when in reality it is not directly involved in any new reactions.

As part of these proof-of-concept studies, we chose dibenzylketone (DBK) as the source of photochemically-generated transient radicals. Under steady-state photolysis in toluene using UVB lamps DBK undergoes Norrish Type I cleavage and fast decarbonylation (on the sub-nanosecond timescale) to yield benzyl radicals. In the absence of other substrates, the benzyl radicals recombine to form 1, 2-diphenylethane (DPE) as the only significant product.[6,7]

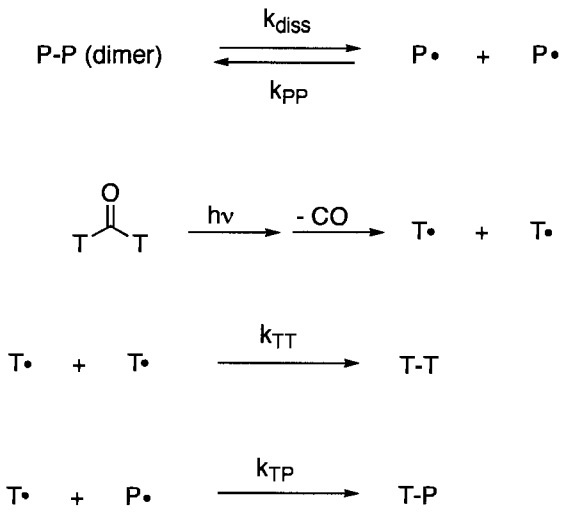

Scheme 4.2. Modified reaction steps in the operation of the Persistent Free Radical Effect.

Therefore, by combining the photoreaction of DBK and the thermal equilibrium of TPS, we obtain a simple, yet effective one-pot synthesis of 2, 2, 3-triphenyl-propionitrile, TPP. This is illustrated in Scheme 4.2, where the individual modified reaction steps are shown as they would operate in the Persistent Free Radical Effect.

The first direct application of the PFRE to organic synthesis was reported by Studer *et al.* in 2000.[8] In his system, Studer used the reversible dissociation of alkoxyamines for the generation of cyclic compounds in an attempt to avoid the use of organotin derivatives normally employed in such transformations. Since then, other examples of synthesis employing the PFRE have been described in the literature.[4, 9-16] However, we believe this method to be the first to involve C-C bond formation through independent control of persistent and transient radicals.

4.2 Stability *vs.* Persistence: Comparison of the two radical intermediates

Chapter 3 discussed the many factors influencing persistence and lack of reactivity towards molecular oxygen for certain carbon-centred radicals. In the system examined here, we aimed for novel organic synthesis through the recombination of two benzylic radicals. This section outlines the time-resolved behaviour of each of these intermediates and their expected roles in the operation of the Persistent Free Radical Effect.

Figure 4.1 shows the transient absorption spectra and corresponding decay traces for the benzyl and α-cyanodiphenylmethyl radicals, generated independently of each other using 308 nm laser flash photolysis (see Figure caption text for details). The benzyl radical itself is one of the most examined conjugated π radicals.[17, 18] The well-established absorptions in the ultraviolet and visible regions of the spectrum can be assigned to specific electronic transitions in the radical species. For example, Figure 4.1A displays the characteristic sharp absorption of a primary benzyl radicals at 317 nm, corresponding to the $\nu_{0,0}$ band (with an extinction coefficient of ~8,800 $M^{-1}cm^{-1}$).[17] For the tertiary α-cyanodiphenylmethyl radical, addition of the nitrile group causes an enhancement and broadening of this UV band. A second, previously undetectable band ($\varepsilon \sim 130$ $M^{-1}cm^{-1}$ in the benzyl radical spectrum), decaying with identical kinetics, appears in the visible region of the spectrum, centred around 510 nm. As mentioned previously, the broadening and enhancements of these transitions have been attributed to the presence of the nitrogen atom.[17] Most importantly, what must be noted is that these radical intermediates decay on timescales differing by over a factor of 16: the

benzyl radical displays a half-life of about 8 μs, while the α-cyanodiphenylmethyl decays with a half-life of nearly 130 μs under similar conditions.

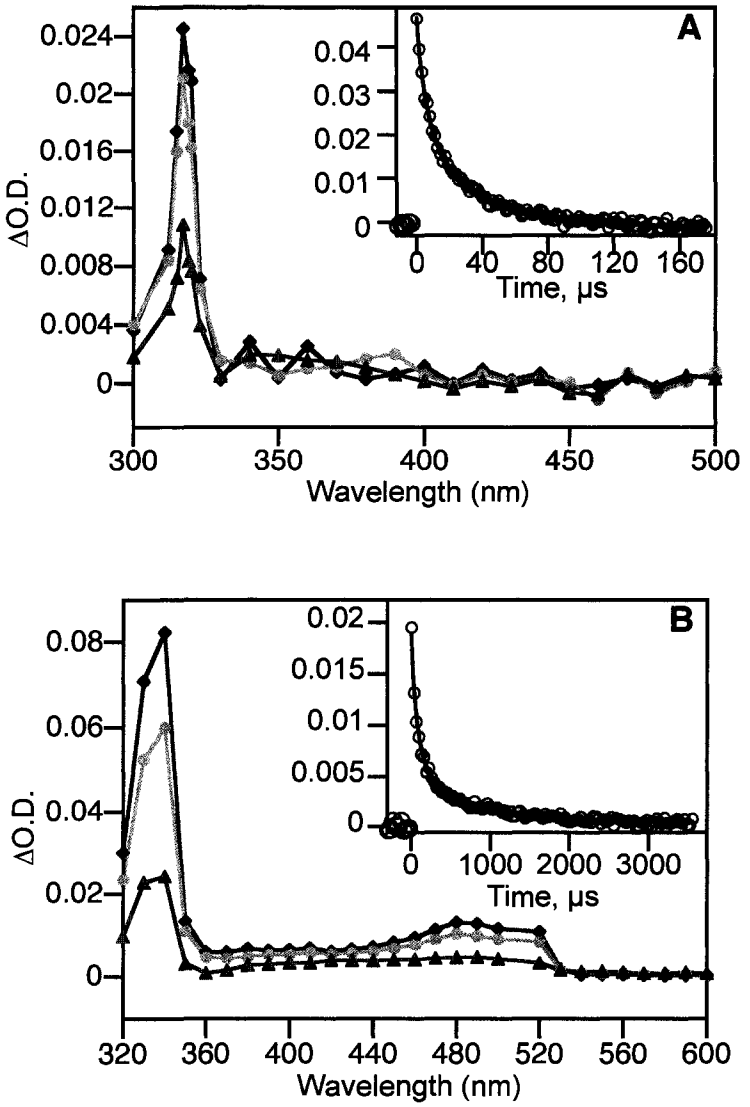

Figure 4.1. (A) Transient absorption spectrum of the benzyl radical, generated *via* 308 nm LFP of 2 mM DBK in N_2-purged benzene; (◆) 0.64 μs (●) 4.16 μs and (▲) 33.1 μs after the laser pulse. Inset: decay trace taken at 317 nm. (B) Transient absorption spectrum of the α-cyanodiphenylmethyl radical, generated *via* 355 nm LFP of 0.184 M diphenylacetonitrile in N_2-purged 50:50 benzene: di-*tert*-butylperoxide (◆) 3.48 μs (●) 70.3 μs and (▲) 515 μs after the laser pulse. Inset: decay trace taken at 510 nm.

Thus, the benzyl radical, while widely recognized as a highly resonance-stabilized radical, cannot be considered to be a persistent species. Rather, it displays second-order decay kinetics in toluene solution, indicating that the primary decay pathway is recombination to form DPE. Meanwhile, the α-cyanodiphenylmethyl radical also displays second-order decay kinetics; its main decay pathway is also recombination to form the head-to-head dimer (as confirmed by M. Frenette). Thus, while the benzyl radicals likely undergo hydrogen-abstractions with the solvent (toluene), these are identity reactions and so are not reflected in the overall decay order. If the α-cyanodiphenylmethyl radicals were undergoing hydrogen abstractions or other such reactions with the solvent, then it would introduce a first-order component to the observed decay. Since this is not the case, it is clear that the fate of the radicals is to simply recombine to reform the dimer; what we described as *dynamic stability*.

Recall that Ingold and Griller had established attenuated self-reaction as one of the criteria for a persistent radical.[19] A 16-fold reduction in the rate of recombination of these radicals would therefore represent such a required attenuation, and thus these species, while not as infinitely long-lived as TEMPO radicals, can be considered to be persistent on short timescales, relative to benzyl radicals.

According to the kinetic requirements for the operation of the PFRE, then, we anticipated that introduction of the transient benzyl radical in the presence of the somewhat persistent α-cyanodiphenylmethyl radical will lead to formation of the cross-reaction product, 2, 2, 3-triphenyl-propionitrile, as the main product. We designed this system to have the α-cyanodiphenylmethyl radicals generated thermally from their

dimers; however, we investigated the effect of producing the benzyl radicals photochemically *via* steady-state (lamp) *versus* pulsed (laser flash) irradiation sources.

4.3 Lamp Photolysis Results

Once we had confirmed that the two radical species we had chosen for our proof-of-concept studies had sufficiently differing lifetimes, we proceeded with both steady-state and pulsed photolysis of solutions containing DBK and TPS at various temperatures (Scheme 4.3).

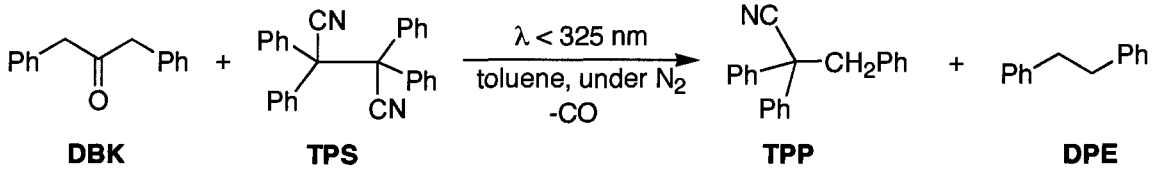

Scheme 4.3. Synthesis of TPP (with DPE by-product) using the PFRE.

UVB irradiation may be continuous or pulsed.

After several preliminary studies, it was found that formation of the cross-reaction product was optimal using an excess of TPS starting material (in order to increase the starting concentration of persistent radicals). Continuous lamp irradiation of a nitrogen-purged toluene solution containing 1.8 mM TPS and 0.98 mM DBK at ~27°C (measured inside the photoreactor with the cooling fans on) led to ~45% conversion of DBK to TPP, with a considerable amount of DPE (Figure 4.2).

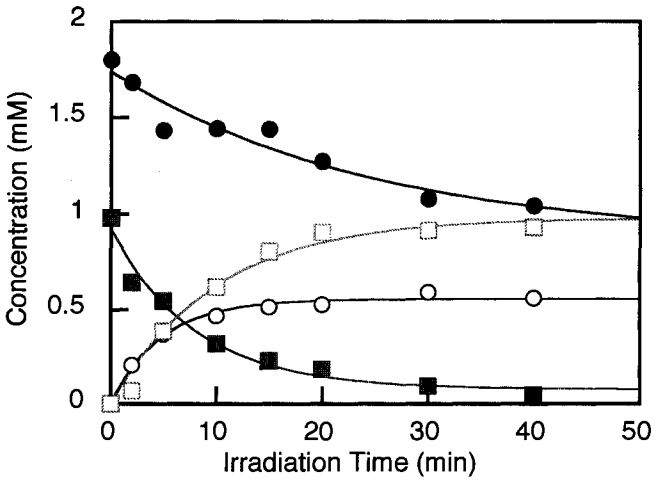

Figure 4.2. UVB lamp photolysis of 1.8 mM TPS and 0.98 mM DBK in nitrogen-purged toluene at ~27°C and followed by GC-MS: TPS (●), DBK (■), DPE (○), TPP (□).

If the cooling fans within the photoreactor are switched off, the temperature inside the instrument reaches a plateau of about 50°C within 20 minutes. When the steady-state irradiation of a similar toluene solution was carried out under these conditions, the amount of DPE was significantly reduced (Figure 4.3). After 40 min of UVB irradiation, ~75% of the DBK was converted to TPP, with the remainder being DPE, formed initially in the reaction.

This is consistent with the more efficient trapping of benzyl radical by α-cyanodiphenylmethyl radical as the steady state concentration of the latter increases when the equilibrium of Scheme 4.1 is displaced at higher temperatures. Recall that the bond dissociation energy for the central carbon-carbon bond in the TPS dimer is ~26 kcal/mol:[2] thus, increasing the temperature from 25°C to 50°C would provide sufficient energy to shift the equilibrium to the radical species (for a discussion on approximate concentrations, *vide infra*).

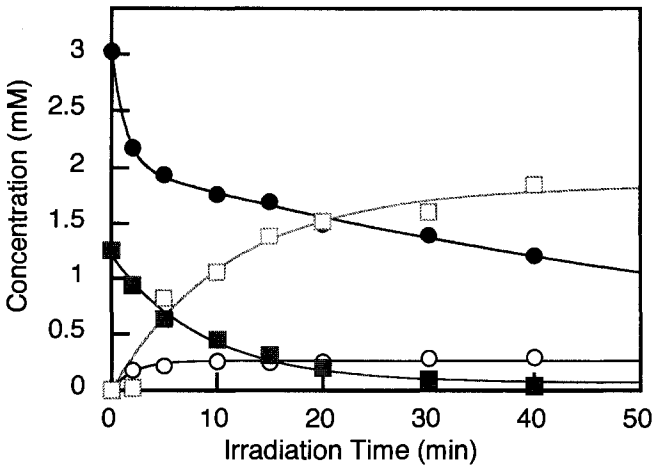

Figure 4.3. UVB lamp photolysis of 3.0 mM TPS and 1.2 mM DBK in nitrogen-purged toluene at ~50°C and followed by GC-MS: TPS (●), DBK (■), DPE (○), TPP (□).

In both cases, it must be emphasized that TPP and DPE were the only observed products: none of the possible side-products (such as from hydrogen abstraction or disproportionation reactions) were formed during the photolysis. Considering the reputation radical-radical recombination reactions have for generating complex product mixtures, we were truly pleased at the remarkably clean results. As well, our results suggested that something other than the geometric mean rule[20-22] was controlling product formation in this system.

Subsequently, a large-scale photolysis for proof-of-concept purposes was carried out using 300 mg DBK and 500 mg TPS in 250 mL deaerated toluene in a 300 mL quartz Erlenmeyer flask. Following 20 hours of UVB irradiation at ~50°C, 0.36 g of TPP was isolated, corresponding to a conversion of 53% (see Appendix 4A for details). Therefore, although this technique appears time-consuming, it nevertheless represents an extremely simple, clean, and effective one-pot synthesis of TPP.

We also examined the product, TPP for thermal and photochemical stability. We found that, unlike the alkoxyamines used as initiators for living free radical polymerization (Scheme 4.4),[23, 24] the product formed from this T•/P• combination was highly stable: prolonged heating and/or irradiation in nitrogen-purged toluene solution showed no decomposition of the starting material, any potential radical intermediates were not observable by steady-state or time-resolved spectroscopy.

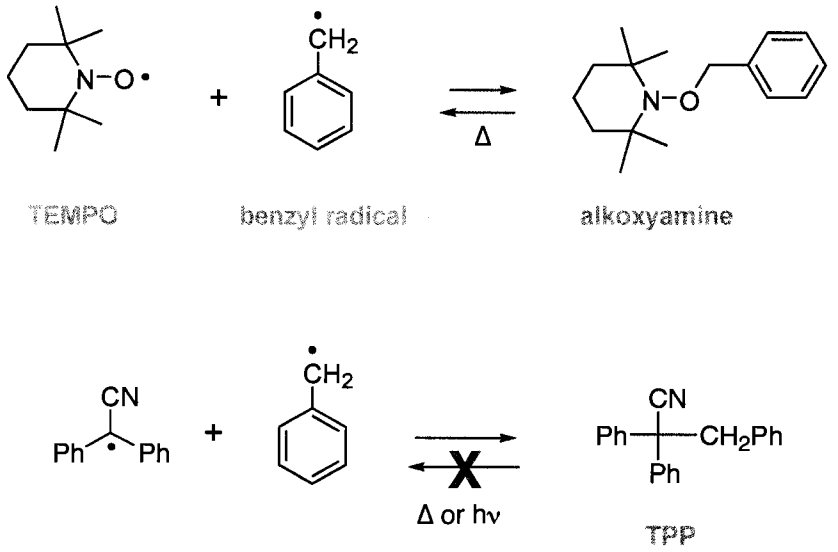

Scheme 4.4. Unlike alkoxyamines, formed though the coupling of persistent TEMPO radicals with transient radicals, the carbon-carbon bond formed in this system is thermally and photochemically stable at moderate temperatures and light intensities.

4.4 Laser Flash Photolysis Results

Following the dramatic effect of temperature on the supply of α-cyanodiphenylmethyl radicals, and hence on the relative yields of cross-reaction and self-reaction products during steady-state irradiation, we investigated the effect of

producing the benzyl radicals photochemically *via* a pulsed irradiation source, *i.e.* laser flash photolysis.

Interestingly, under 308 nm laser pulse excitation of a nitrogen-purged toluene solution of 2.0 mM TPS and 2.0 mM DBK, the observed reaction product mixture was the inverse of that obtained under steady-state irradiation conditions: the dominant product was DPE (~65% conversion), with only small amounts of TPP formed (Figure 4.4).

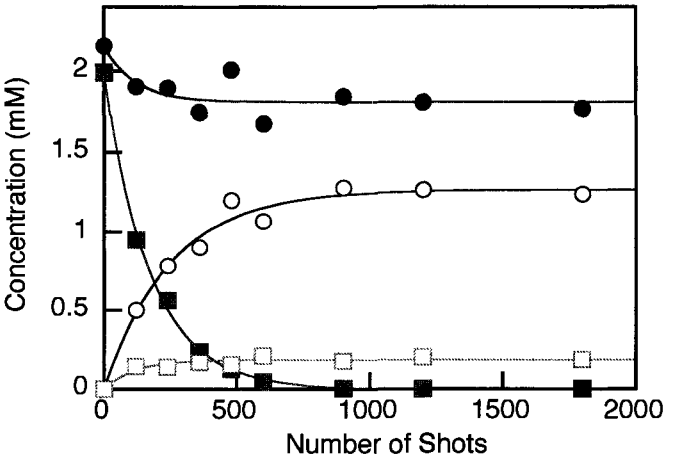

Figure 4.4. 308 nm laser pulse photolysis of 2.0 mM TPS and 2.0 mM DBK in nitrogen-purged toluene at room temperature and followed by GC-MS: TPS (●), DBK (■), DPE (○), TPP (□).

This clearly suggests that pulsed irradiation conditions favour recombination of the transient benzyl radical, in spite of the presence of the equilibrium concentration of α-cyanodiphenylmethyl radical.

It is interesting to compare the results from laser and lamp irradiation, where the ratio of self-reaction product (DPE) to cross-reaction product (TPP) reflects the thermal and light intensity dependence of the supply of the two radical intermediates.

In general, we expect $k_{TT} \approx \frac{1}{2} k_{TP} \approx \frac{1}{4} k_{diff}$. Therefore, cross-reaction can only dominate if the condition of Equation 4.1 is fulfilled.

$$\begin{aligned} & k_{TP}[T\bullet][P\bullet] >> k_{TT}[T\bullet]^2 \\ i.e.: \quad & k_{TP}[P\bullet] >> k_{TT}[T\bullet] \end{aligned} \tag{4.1}$$

As the rate constants for the self-reaction and cross-reactions are both near diffusion-control, we may further approximate Equation 4.1 by equating $k_{TT} \approx k_{TP}$. In this case, the expression is reduced to simply [P•]>>[T•], *i.e.* the single most important criterion for the persistent free radical effect.[3]

Since radical concentrations generated by pulsed lasers can easily be four orders of magnitude higher than those achieved under lamp illumination, the latter case provides an effective means to meet this criterion. Intrigued, we thus examined the factors controlling product formation in the former case.

At 25°C, the benzyl radical decay is virtually insensitive to the presence of TPS (Figure 4.5): the decay still follows clean second order kinetics, indicating that recombination to give DPE is the only important reaction path. Only after ~90% of the radicals have decayed does the second order fit of the data [$(signal)^{-1}$ vs. time] show some deviations from linearity, suggesting minor involvement of another mode of decay in a mode that only takes over at low concentrations of benzyl radical; this mode is presumably the cross combination of Scheme 4.2 leading to TPP.

In fact, this observation would represent another minor example of the Persistent Free Radical Effect: immediately following the laser pulse, the local concentration of benzyl radical is relatively high (typically 10^{-4} to 10^{-5} M). As a result, self-reaction to form DPE is favoured:

$$\textit{Rate of self-reaction of benzyl radicals} = k_{TT}[T\bullet]^2 \qquad (4.2)$$

However, after approximately 45 μs, the concentration of this radical is depleted to roughly 10%, and therefore is of similar or lesser magnitude than equilibrium concentration of the α-cyanodiphenylmethyl radical also present (≤ 10^{-6} M at room temperature). As a result, the conditions required for the operation of the PFRE are met and the cross-reaction forming TPP becomes the dominant pathway:

$$\textit{Rate of cross-reaction} = k_{TP}[T\bullet][P\bullet] \qquad (4.3)$$

This produces a pseudo-first-order component in the observed decay of the benzyl radical species, as evidenced by the upward-curving deviation in Figure 4.5B.

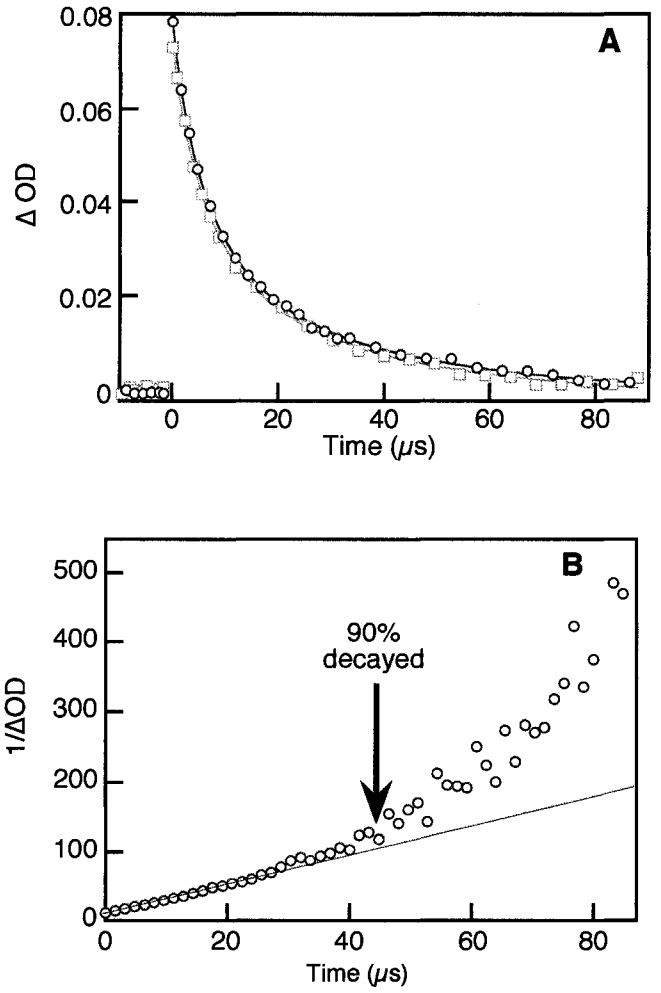

Figure 4.5. (A) Decay trace taken at 317 nm of a nitrogen-purged toluene solution of 2.7 mM DBK with (O) and without (□) the presence of 3.2 mM TPS, following 308 nm laser excitation at 25°C, fitted with 2nd-order expressions. (B) DBK and TPS in toluene, $(signal)^{-1}$ vs. time.

We anticipated that this effect could also be observed by influencing the supply of α-cyanodiphenylmethyl radicals *via* the thermal equilibrium of Scheme 4.1. Thus, in contrast with the 25°C results, at higher temperatures the difference between the decay traces in the presence and absence of TPS is quite clear, as shown in Figure 4.6. In a nitrogen-purged toluene solution of DBK and TPS, as the temperature increases, the

decay of benzyl radicals accelerates, incorporating a first-order component to the observed kinetics (Figure 4.6A). The graph in Figure 4.6B shows that this result is not an artifact of DBK itself.

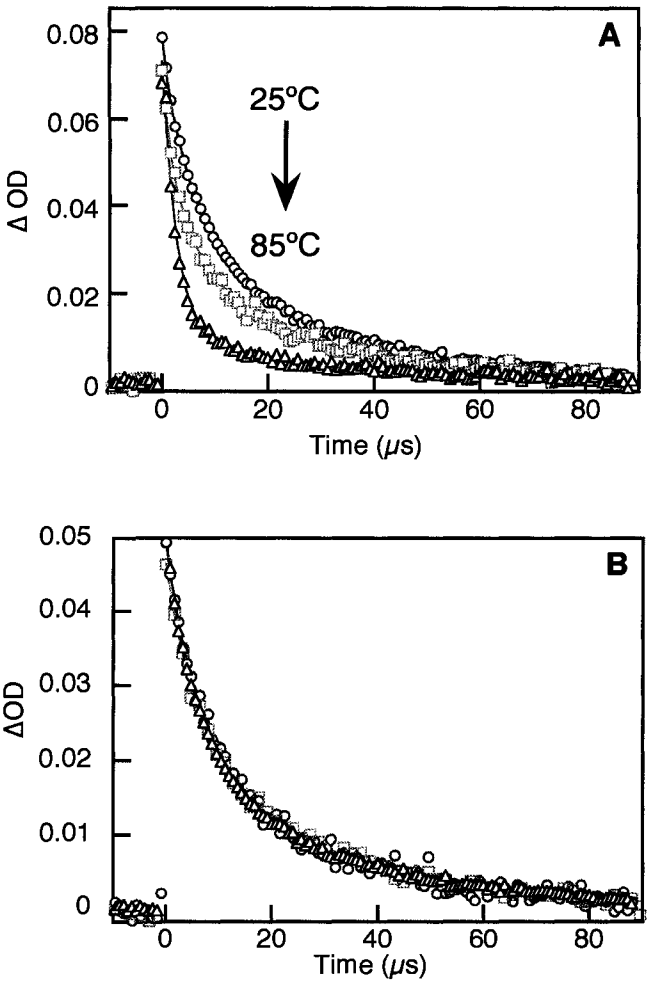

Figure 4.6. (A) Decay traces of a nitrogen-purged toluene solution of 2.7 mM DBK and 3.2 mM TPS after 308 nm laser excitation, monitored at 317 nm and fitted with 2nd-order or 1st+2nd- order expressions at ~25 °C (O), ~55 °C (□), and ~85 °C(Δ). (B) Decay traces of a nitrogen-purged toluene solution of 2.7 mM DBK, fitted with 2nd-order kinetics at ~25 °C (O), ~55 °C (□), and ~75 °C (Δ).

This effect is reflected in the product distribution if an identical laser flash photolysis is carried out at an elevated temperature: 308 nm laser pulse excitation of a nitrogen-purged toluene solution of 2.0 mM TPS and 2.0 mM DBK at ~45°C results in a slightly increased proportion of cross-reaction product TPP at the expense of the self-reaction product DPE (compare Figure 4.7 with Figure 4.4).

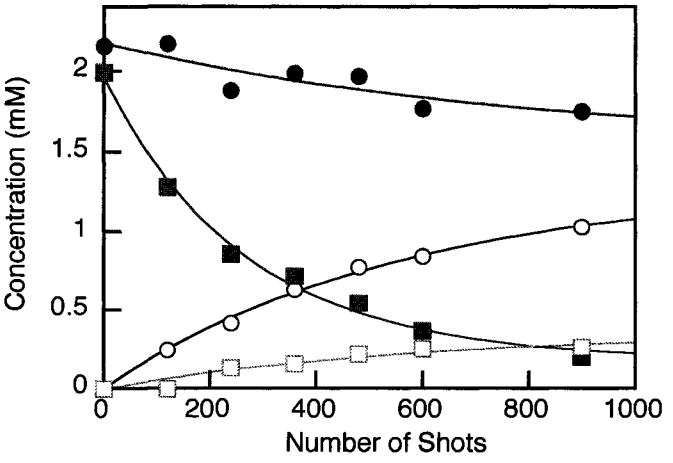

Figure 4.7. 308 nm laser pulse photolysis of 2.0 mM TPS and 2.0 mM DBK in nitrogen-purged toluene at ~45°C temperature and followed by GC-MS: TPS (●), DBK (■), DPE (○), TPP (□).

Thus, even a small increase in the temperature of the solution results in more efficient trapping of the benzyl radical by the α-cyanodiphenylmethyl radical.

Therefore, meeting the criterion of Equation 4.1 under conditions of laser excitation is easier at higher temperatures, since the concentration of P• will follow a van't Hoff dependence with temperature, controlled by the central carbon-carbon bond dissociation energy for the dimer (~26 kcal/mol). Although the exact concentration of

the persistent radical in this system is unknown, we can get a very rough approximation using the thermodynamic values associated with another dimer, the head-to-head HP-136 dimer. synthesized by M. Frenette. For this starting material, the BDE of the central carbon-carbon bond is slightly weaker: 23 kcal/mol. With an estimated value of +120±5 kcal/mol for the ΔS[1], using the van't Hoff expression and the equilibrium constant,

$$\ln K_{eq} = \frac{\Delta S}{R} - \frac{\Delta H}{RT} \tag{4.4}$$

$$K_{eq} = \frac{[P\bullet]^2}{[\text{dimer}]} \tag{4.5}$$

a 3 mM solution of HP-136 dimer at 50°C would contain on the order of nearly 10^{-5} to 10^{-6} M radical species.[25] Since the BDE in the dimer used in these experiments has a somewhat stronger bond, we must consider these values to be an upper limit to the actual radical concentration.

The traces of Figure 4.6 and the product distribution of Figure 4.7 confirm these ideas; consistently with this, the yield of cross-combination products under conditions of laser excitation improves at high temperature. In light of these findings, we concluded that the kinetics controlling the mechanism of operation of the PFRE were also responsible for the observed products in the recombination reactions of benzyl and α-cyanodiphenylmethyl radicals.

[1] This value can be determined either from the y-axis intercept of a van't Hoff plot (see reference 2) or may be approximated using statistical mechanical formulae appropriate to the dissociation of a diatomic.

Therefore, by combining the photoreaction of DBK and the thermal equilibrium of TPS, we were successful in obtaining a simple, yet effective one-pot synthesis of 2, 2, 3-triphenyl-propionitrile, TPP. This is illustrated in Scheme 4.2, where the individual modified reaction steps are shown adjacent to their corresponding analogues as operating in the Persistent Free Radical Effect.

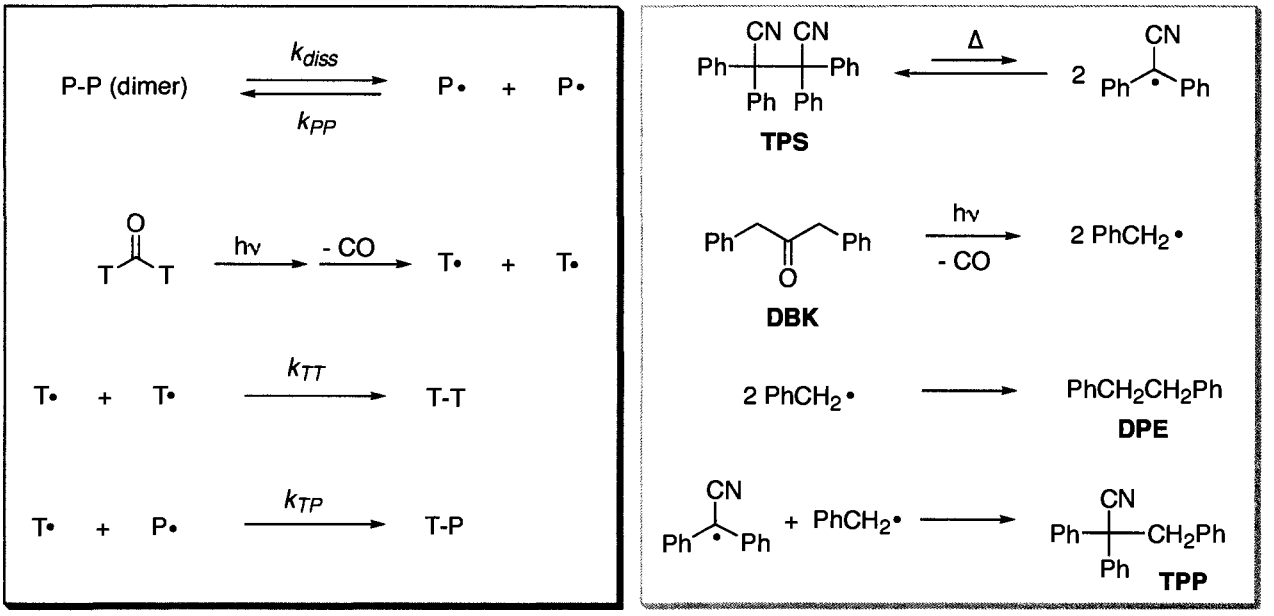

Scheme 4. 5. Reaction steps in the synthesis of 2,2,3-triphenyl-proprionitrile and their respective analogues in the operation of the Persistent Free Radical Effect.

In typical reported examples of the PFRE, k_{PP} is near zero and the radical P• is truly 'persistent' (*e.g.* TEMPO); however, this is not a strict requirement, as long as $k_{PP} << k_{TT}$. In the traditional interpretation of the PFRE, the maximum product selectivity occurs when the rates of production of transient and persistent radicals are identical. The example in this chapter is somewhat different from the case originally

described by Fischer, in that the two radicals are not formed from a single precursor, nor are they produced in a stoichiometric ratio (a synopsis of Fischer's mathematical description is provided in Appendix 4B).

As well, the conventional mechanism of the PFRE has been described as 'self-adjusting';[4] in fact, the modified mechanism of Scheme 4.5 also has this characteristic, except that the origin of the concentration adjustment is different. In Scheme 4.5, the concentration of persistent radical is supplied by the dissociation equilibrium for the dimer P-P. Thus, if P• is consumed by reaction with T•, the equilibrium will maintain the persistent radical concentration, effectively acting as a 'radical buffer'. In contrast with Equation 1.2 and Scheme 1.7, the mechanism of Scheme 4.5 does not allow the concentration of P• to grow to any arbitrary value, but rather it is capped by the equilibrium constant. In effect, P-P is a 'dormant' source of radical P•; however, it is possible to adjust the concentration by changing the temperature.

Most interestingly, the combination of a thermal and a photochemical source for the two radicals allows virtually independent control of the supply of the two radicals, since photochemical reactions tend to show low temperature dependence, but their rate can be adjusted by changing the light intensity. We anticipate that while similar syntheses could be performed using only thermal sources for both T• and P•, it is clear that in this case one would lose the independent control of the two sources that is achieved by using a combination of thermal and photochemical sources.

What again must be emphasized is the remarkable 'cleanliness' of the obtained product mixture: in all cases of either lamp or laser irradation, TPP and DPE were the

only observed products. Therefore, we reasoned that carbon-carbon bond formation is made possible by careful selection of the persistent and transient radical species.

4.5 Computational Investigations

In order to help us rationalize the results obtained, we expanded some of our earlier calculations of spin distribution mentioned in Chapter 3. Recall that the spin density distribution on the α-cyanodiphenylmethyl radical shows that about 24% of the unpaired electron is located on the benzylic carbon atom, and a 10% contribution of this density is found on the nitrogen atom of the cyano group (Scheme 3.7); this resonance delocalization increases the C-C(N) double bond character, reducing the bond length from 1.458Å in 1, 1, 2, 2-tetraphenyl succinonitrile to 1.418Å for radical species. We concluded that the combination of this delocalization with other favourable stereoelectronic effects resulted in a *stabilized and persistent* benzylic radical.

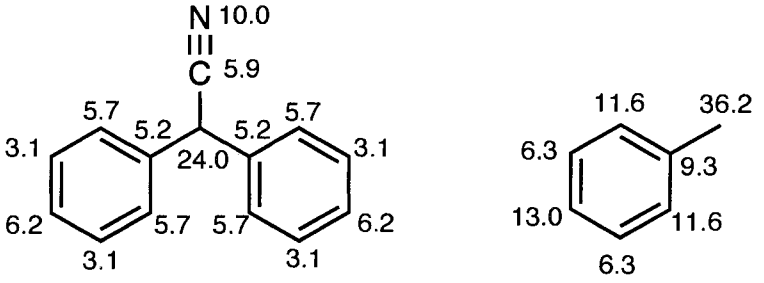

Figure 4.8. Unpaired electron spin distribution (in % total spin) for the carbon skeleton of the α-cyanodiphenylmethyl radical (left) and benzyl radical (right).

On the other hand, the benzyl radical itself has a much higher spin density at the carbon centre (~36%) and does not enjoy the same attributes that lead to persistence and a lack of reactivity towards molecular oxygen; thus it is considered to be a *stabilized but transient* radical.

Intriguingly, charge distributions computed using the CHELPG method assigns to the carbon radical center in the α-cyanodiphenylmethyl radical a value that is noticeably more positive (-0.225) in comparison to the value assigned to the carbon centre in the benzyl radical (-0.451). Thus, with respect to each other, the α-cyanodiphenylmethyl radical displays greater electrophilic character and is activated towards nucleophilic attack from the benzyl radical. Therefore, the resulting product distribution can also be interpreted in terms of charge control: the significant difference between the charges favours cross-reaction between the two radicals.[26, 27]

4.6 Conclusions

Free radical reactions, and in particular those involving radical coupling, have a reputation for yielding complex mixtures of products. However, we can circumvent this issue if we require the radical intermediates to be *disciplined;*[28] that is, rigorous control of the kinetic parameters defining the radical-radical or radical-molecule reactions. It is clear that reactions involving radicals with different persistent character can actually result in high-yield, clean synthetic procedures whenever a convenient source of the more persistent radical can be identified, as with the α-cyanodiphenylmethyl radical and a variety of similarly labile radical dimers.

In the system described in this chapter, the dimer effectively behaves as a radical buffer, maintaining an adequate concentration of radicals. While this approach follows the same reactivity patterns normally identified with the persistent free radical effect, it is the first example to allow for complete independent control of the supply of the two radicals that is achieved by using a combination of thermal and photochemical sources; it is also the first to involve head-to-head carbon-carbon bond formation between two separately generated radical species.

4.7 References

1. Font-Sanchis, E.; Aliaga, C.; Focsaneanu, K.-S.; Scaiano, J. C., Greatly Attenuated Reactivity of Nitrile-Derived Carbon-centered Radicals toward Oxygen. *Chem. Commun.* 2002, (15), 1576-1577.

2. Frenette, M.; Aliaga, C.; Font-Sanchis, E.; Scaiano, J. C., Bond Dissociation Energies for Radical Dimers Derived from Highly Stabilized Carbon-Centered Radicals. *Org. Lett.* 2004, 6, (15), 2579-2582.

3. Fischer, H., Unusual Selectivities of Radical Reactions by Internal Suppression of Fast Modes. *J. Am. Chem. Soc.* 1986, 108, (14), 3925-3927.

4. Fischer, H., The Persistent Radical Effect: A Principle for Selective Radical Reactions and Living Radical Polymerizations. *Chem. Rev.* 2001, 101, 3585-3610.

5. Lebelev, O. L.; Kazarnovsky, S. N., *Zhur. Obshch. Khim.* 1960, 30, 1631.

6. Engel, P. S., Photochemistry of Dibenzyl Ketone. *J. Am. Chem. Soc.* 1970, 92, 6074-6076.

7. Lunazzi, L.; Ingold, K. U.; Scaiano, J. C., Absolute Rate Constants for the Decarbonylation of the Phenylacetyl Radical. *J.Phys.Chem.* 1983, 87, 529-530.

8. Studer, A., Tin-free cyclization reactions using the persistent radical effect. *Angew. Chem. Int. Ed.* 2000, 39, 1108.

9. Alajarin, M.; Vidal, A.; Ortin, M.-M.; Bautista, D., Persistent radical effect in the intramolecular addition of benzylic radical onto ketenimines: selective cross-coupling of α-(indol-2-yl)-benzyl radicals with the 1-cyano-1-methylethyl radical. *New. J. Chem.* 2004, 28, 570-577.

10. Magnus, P.; Venable, J. D.; Shen, L.; Lynch, V., Some reactions of persistent benzofuranone radicals related to the 'old' diazonamide structure. *Tet. Lett.* 2005, 46, 707-710.

11. Renaud, P.; Sibi, M. P., *Radicals in Organic Synthesis, Vol. 1 and 2.* Wiley-VCH: New York, 2001.

12. Sanjuán, A.; Aguirre, G.; Alvaro, M.; García, H.; Scaiano, J. C.; Chrétien, M. N.; Focsaneanu, K.-S., Product studies and laser flash photolysis of the direct and 2,4,6-triphenylpyrylium-zeolite Y photocatalyzed degradation of fenvalerate. *Photochem. Photobiol. Sci* 2002, 1, 955-959.

13. Studer, A., The Persistent Radical Effect in Organic Synthesis. *Chem. Eur. J.* 2001, 7, 1159-1164.

14. Studer, A., Tin-free radical chemistry using the persistent radical effect: alkoxyamine isomerization, addition reactions, and polymerizations. *Chem. Soc. Rev.* 2004, 33, 267-273.

15. Wetter, C.; Studer, A., Microwave-assisted free radical chemistry using the persistent radical effect. *Chem. Commun.* 2004, 174-175.

16. Zard, S. Z., *Radical Reactions in Organic Synthesis.* Oxford University Press: Oxford, 2003.

17. Chatgilialoglu, C., Electronic Absorption Spectra of Free Radicals. In *Handbook of Organic Photochemistry,* Scaiano, J. C., Ed. CRC Press: Boca Raton, Florida, 1989; Vol. II, pp 3-11.

18. Claridge, R. F. C.; Fischer, H., Self-termination and electronic spectra of substituted benzyl radicals in solution. *J. Phys. Chem.* 1983, 87, 1960.

19. Griller, D.; Ingold, K. U., Persistent Carbon-Centered Radicals. *Acc. Chem. Res.* 1976, 9, 13-18.

20. Bachmann, W. E.; Wiselogle, F. Y., The relative stability of pentaarylethanes. III. The reversible dissociation of pentaarylethanes. *J. Org. Chem.* 1936, 1, 354.

21. Blake, H. R.; Henderson, J. F.; Kutschke, K. O., The reaction between methyl radicals and isobutane. *Can. J. Chem.* 1961, 39, 1920.

22. Kerr, J. A.; Trotman-Dickenson, A. F., The reactions of alkyl radicals. In *Prog. React. Kinet.*, Porter, G., Ed. 1961; Vol. 1, p 105.

23. Fischer, H., The Persistent Radical Effect in "living" Radical Polymerization. *Macromolecules* 1997, 30, (19), 5666-5672.

24. Garcia Ballesteros, O.; Maretti, L.; Sastre, R.; Scaiano, J. C., Kintetics of Cap Separation in Nitroxide-regulated "Living" free radicla Polymerization: Application of a Novel Methodology Involving a prefluorescent Probe Nitroxide Switch. *Macromolecules* 2001, 34, 6184-6187.

25. Frenette, M., Private Communication. In 2007.

26. Gilbert, A.; Baggott, J., *Essentials of Molecular Photochemistry.* Blackwell: Oxford, 1991.

27. Turro, N. J., *Modern Molecular Photochemistry.* University Science Books: Sausalito, 1991.

28. Chatgilialoglu, C., Basic Concepts of Carbon-Carbon Bond Formation. In *Radicals in Organic Synthesis*, Renaud, P.; Sibi, M. P., Eds. Wiley-VCH: New York, 2001; Vol. Volume 1: Basic Principles, p 31.

29. Pletnev, A. A.; Larock, R. C., Carbopalladation of Nitriles: Synthesis of Benzocyclic Ketones and Cyclopentenones via Pd-Catalyzed Cyclization of alpha-(2-Iodoaryl)alkanenitriles and Related Compounds. *J. Org. Chem.* 2002, 67, (26), 9428-9438.

Appendix 4A. Syntheses of 2,2,3-triphenylproprionitrile (TPP)

i) Independent Synthesis of TPP.

An authentic sample of TPP was prepared from diphenyacetonitrile and benzyl bromide using a procedure analogous to that described by Pletnev and Larock[29]. In brief: 0.12 g of NaH (0.005 mol) in 1 mL benzene and 2 mL DMF (dried with molecular sieves) was placed in a 50 mL round-bottom flask, in an ice bath. Then, 0.97 g of diphenylacetonitrile (0.005 mol) in 2 mL DMF was added dropwise, and the resulting yellow solution was left stirring at ~4°C for 30 min. The yellowish colour disappeared upon addition of 1.03 g of benzylbromide (0.006 mol) in 1 mL DMF. The solution was allowed to warm up to room temperature, then added to distilled water, extracted three times with CH_2Cl_2, dried with $MgSO_4$. Solvent was removed *via* rotary evaporation, and the white solid was recrystallized in ethyl acetate. Yield = 1.18 g, 84%; mp = 123-125°C. GC-MS (EI) *m/z* = 283 $[M]^+$(10%), 193 (70%), 165 (73%) 91 (100%). ^1H NMR ($CDCl_3$, 500 MHz): δ 7.33-7.28 (m, 10H), 7.17-7.14 (m, 3H), 6.86 (dd, 2H, *J* = 7.3, 1.6 Hz), 3.65 (s, 2H) ppm. ^{13}C NMR ($CDCl_3$, 75.4 MHz): δ 140.38, 134.97, 130.92, 129.08, 128.35, 128.29, 127.79, 127.66, 122.19, 53.30, 45.65 ppm.

Figure 4A. 1. ^{1}H NMR ($CDCl_3$, 500 MHz) of TPP

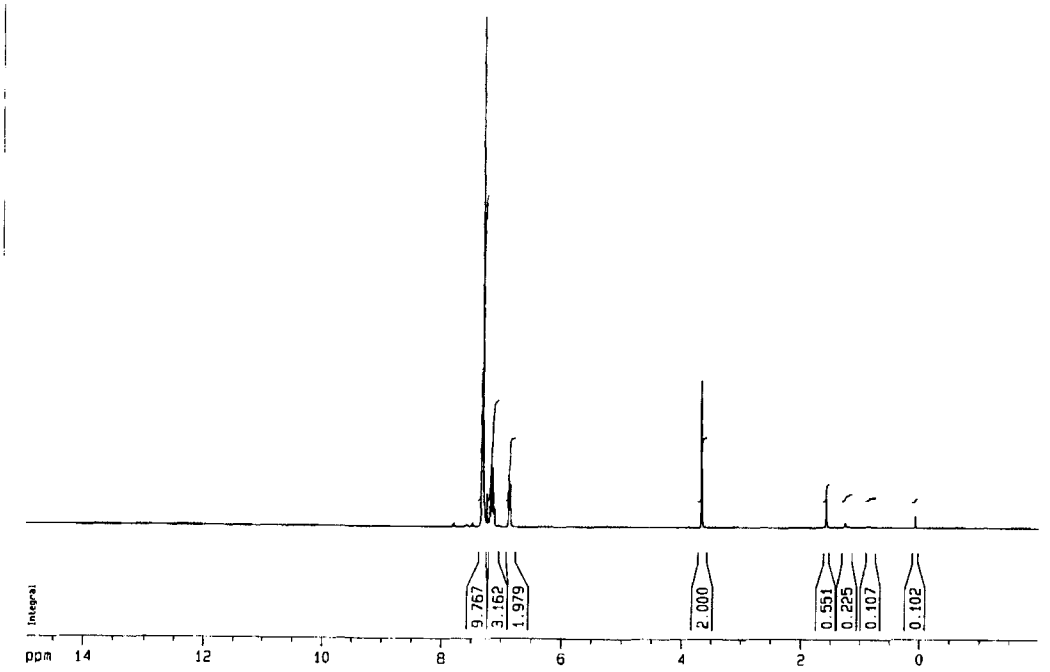

Figure 4A. 2. ^{14}C NMR ($CDCl_3$, 75.4 MHz) of TPP

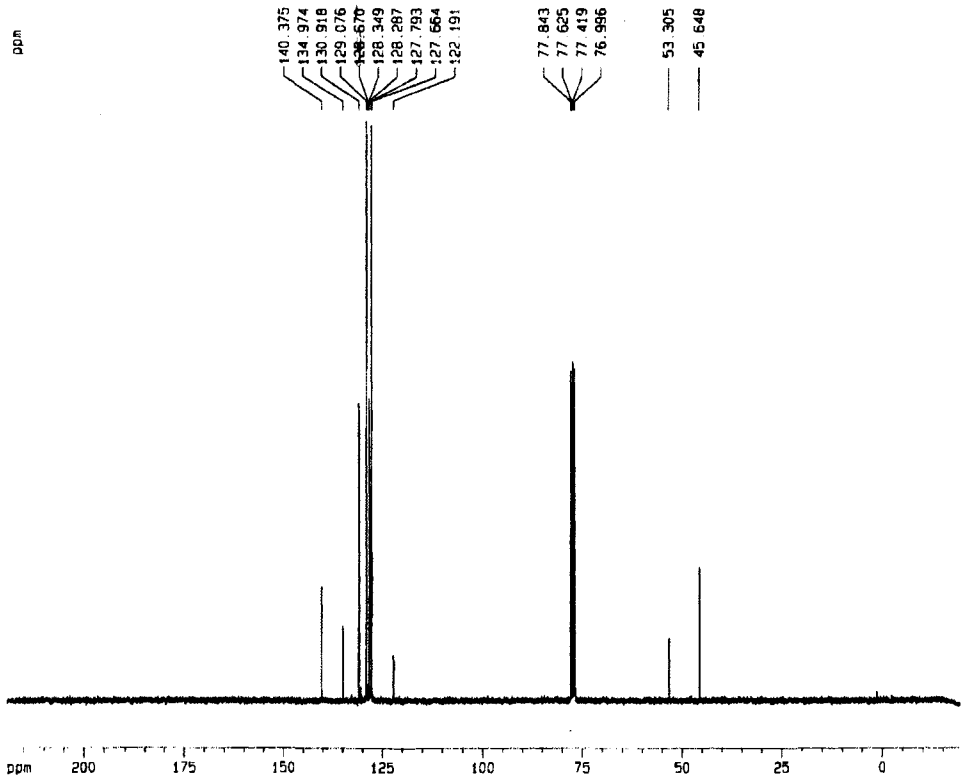

Figure 4A.3. EI-MS of TPP

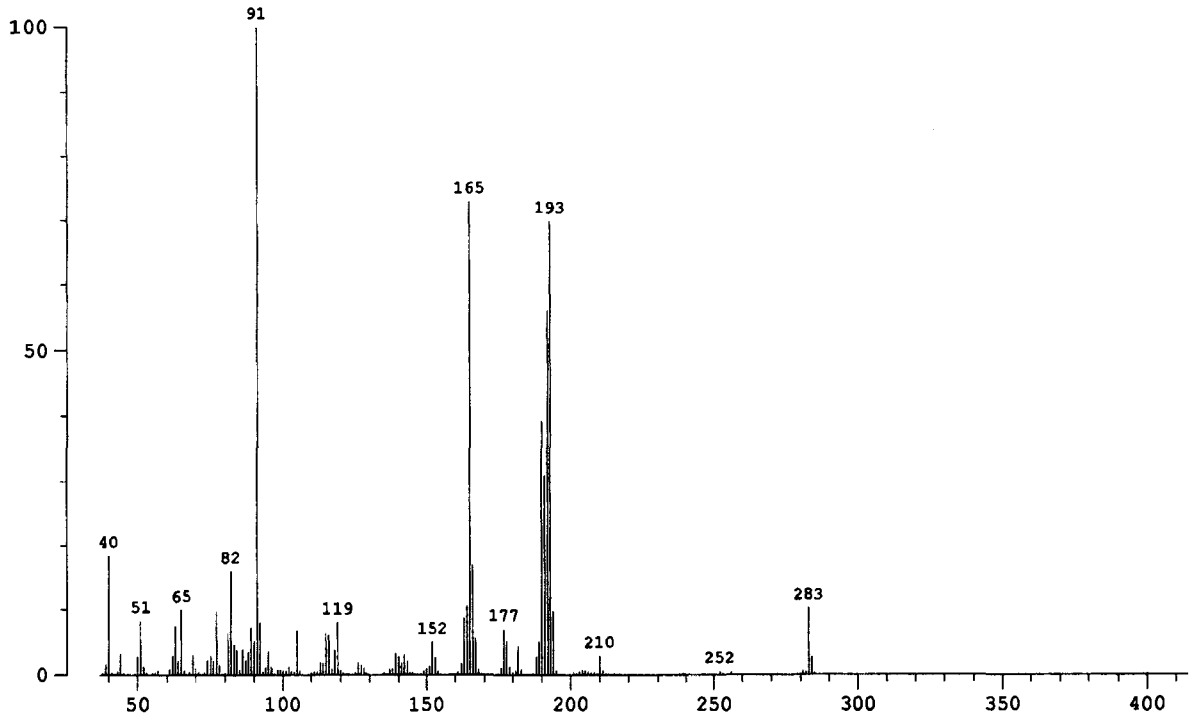

ii) Large Scale Steady State Photolysis of DBK and TPS.

In a 150 mL quartz Erlenmeyer flask, 0.285 g DBK (0.00136 mol) and 0.470 g TPS (0.00122 mol) were added to 130 mL of HPLC-grade toluene. The solution was stirred and purged with nitrogen until all of the solid was dissolved (~ 30 min). The flask was sealed and placed in the photoreactor, equipped with 12 UVB lamps, with the cooling fan left off (temperature inside the photoreactor reached a maximum of ~50°C). Periodic aliquots were taken to monitor the course of the reaction, which was irradiated for a total of 20 hours. Yield = 0.36 g, 53%; mp = 122-125°C. GC-MS (retention time and mass spectrum), ^{1}H NMR and ^{13}C NMR were identical to that of the authentic sample of TPP.

Appendix 4B. Theoretical Description of the Persistent Free Radical Effect.

Although the qualitative description of the Persistent Free Radical Effect is sufficient to rationalize the observations reported and discussed in this chapter, it is prudent to present a quantitative description as well. Thus, this Appendix will serve to outline the analysis of the kinetics directing the mechanism of this effect. It must be noted that this applies to the conventional interpretation of the PFRE, and not the radical buffer system described in this chapter.

Scheme 4B.1 summarizes the steps involved in the PFRE: T• and P• represent the transient and persistent radical species, respectively, and r and k are used to denote the rates of radical generation and bimolecular rate constants, respectively.

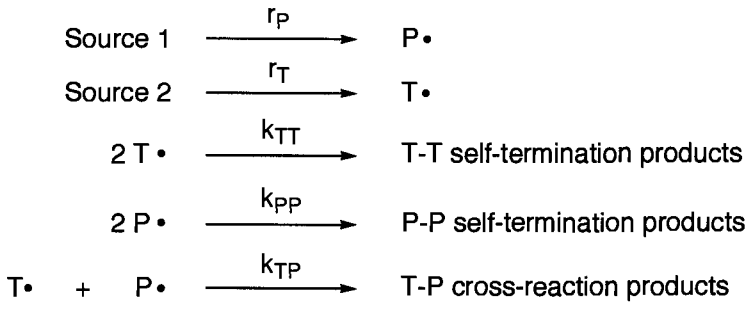

Scheme 4B.1. Steps in the Persistent Free Radical Effect.

At time $t = 0$, $[T\bullet]_0 = [P\bullet]_0 = 0$. When the reaction begins, the total concentration of generated radicals increases linearly, and at time $t = t$, $[T\bullet] = r_T t$ and $[P\bullet] = r_P t$ (assuming no radical recombinations have occurred yet). We can write the following expressions for the rate of change in concentrations of the transient and persistent radical species:

$$\frac{d[T\bullet]}{dt} = r_T - k_{TP}[T\bullet][P\bullet] - k_{TT}[T\bullet]^2 \qquad (4B.1)$$

$$\frac{d[P\bullet]}{dt} = r_p - k_{TP}[T\bullet][P\bullet] - k_{PP}[P\bullet]^2 \qquad (4B.2)$$

The system thus reaches a stationary state, when these concentrations are constant, or:

$$\frac{d[T\bullet]}{dt} = \frac{d[P\bullet]}{dt} = 0 \qquad (4B.3)$$

Now, selectivity for the formation of the cross-reaction product, T-P is represented by:

$$Selectivity(s) = \frac{k_{TP}[T\bullet][P\bullet]}{\tfrac{1}{2}k_{TT}[T\bullet]^2 + \tfrac{1}{2}k_{PP}[P\bullet]^2} = \frac{2(k_{TP}/k_{TT})([P\bullet]/[T\bullet])}{1+(k_{PP}/k_{TT})([P\bullet]/[T\bullet])^2} \qquad (4B.4)$$

Differentiating the above expression for the variable [P•]/[T•] yields a maximum for the selectivity:

$$\frac{ds}{d([P\bullet]/[T\bullet])} = 0 \quad when \quad [P\bullet]/[T\bullet] = \left(\frac{k_{TT}}{k_{PP}}\right)^{1/2} \quad i.e. \quad [P\bullet] = [T\bullet] \times \left(\frac{k_{TT}}{k_{PP}}\right)^{1/2} \qquad (4B.5)$$

Substituting this result into the stationary state expressions (4B.1) and (4B.2) gives:

$$\frac{d[T\bullet]}{dt} = r_T - k_{TP}\left(\frac{k_{TT}}{k_{PP}}\right)^{1/2}[T\bullet]^2 - k_{TT}[T\bullet]^2 \qquad (4B.6)$$

$$\frac{d[P\bullet]}{dt} = r_p - k_{TP}\left(\frac{k_{TT}}{k_{PP}}\right)^{1/2}[T\bullet]^2 - k_{TT}[T\bullet]^2 \qquad (4B.7)$$

Thus, the condition for establishing a stationary state is:

$$\frac{d[T\bullet]}{dt} = \frac{d[P\bullet]}{dt} = 0 \quad when \quad r_T = r_P \qquad (4B.8)$$

Therefore, the maximum selectivity will occur when the rates of production of transient and persistent radicals are identical. Substituting the result from Equation 4B.5 into the expression for selectivity (Equation 4B.4) yields

$$s_{\max} = \frac{k_{TP}}{(k_{TT}k_{PP})^{1/2}} \tag{4B.9}$$

If P• is not, in fact, persistent, *i.e.* if the rate constants are of similar magnitudes ($k_{TT} \approx k_{TP} \approx k_{PP}$) then $s_{\max}$ is equal to one, and the observed product distribution reflects simple statistics (TT:TP:PP = 1:2:1).

However, for typical "semi-persistent" radicals, self-termination rate constants are on the order of ~10^3 $M^{-1}s^{-1}$; the values for self-termination of transient radicals and the cross-reaction between typical T• and P• radicals are generally close to diffusion control, *i.e.* $k_{TT} \approx k_{TP} \approx k_{diff} \approx 10^9$ $M^{-1}s^{-1}$ in non-viscous liquids. Using these approximate values, we obtain $s_{\max} \sim 1000$, meaning a selectivity for the cross-reaction product T-P of 99.9%!

Therefore, while the selectivity increases with decreasing self-termination rate constant of P•, this species need not be infinitely long-lived in order to establish the Persistent Free Radical Effect. Moreover, note that Equation 4B.9 implies that [P•]>>[T•] for $k_{TT} >> k_{PP}$; a significant excess of persistent radical accumulating in the system, intuitive from a qualitative description of the PFRE, is thus supported by a thorough kinetic analysis. Also, using $k_{TT} \approx k_{TP} >> k_{PP}$ in either stationary state expression (1) or (2) indicates the existence of a dynamic equilibrium

$$r_T = r_P = k_{TP}[T\bullet][P\bullet] \tag{4B.10}$$

i.e. the cross-reaction becomes the dominant decay pathway for both radical species. It is this observation that is the crux of the PFRE.

Appendix 4C. Computational Studies Data

Table 4C.1. Spin Distribution for the benzyl radical

Atom No.	Atom	Mulliken atomic spin density	Absolute atomic spin density	% total spin[c]
1	C	0.284255	0.284255	13.0
2	C	-0.138784	0.138784	6.3
3	C	0.253426	0.253426	11.6
4	C	-0.202779	0.202779	9.3
5	C	0.253465	0.253465	11.6
6	C	-0.138790	0.13879	6.3
7	H	-0.013776	0.013776	0.6
8	H	0.005318	0.005318	0.2
9	H	-0.011715	0.011715	0.5
10	H	-0.011717	0.011717	0.5
11	H	0.005318	0.005318	0.2
12	C	0.792373	0.792373	36.2
13	H	-0.038296	0.038296	1.8
14	H	-0.038296	0.038296	1.8
SUM		1.000000	2.188308	100.0

[c] $\%\ total\ spin = \frac{|s|}{\sum |s|} \times 100\%$

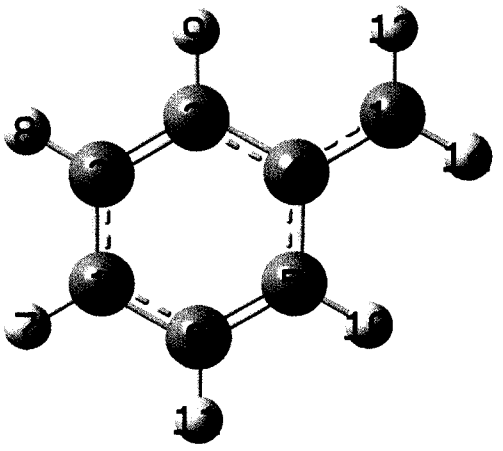

Chapter 5. Other Applications of Persistent Carbon-Centred Radicals

Chapter 5: Other Applications of Persistent Carbon-Centred Radicals

5.1 Introduction

While we were originally examining persistent carbon-centred radicals for their antioxidant potential, we soon discovered other practical uses for these intermediates. For example, Chapter 4 described a convenient application of carbon-carbon bond formation using dimers made from persistent carbon-centred radicals in a system controlled by the Persistent Free Radical Effect.

In this chapter, a few of the many other possible examples of applications of these species will be outlined, including a further description of the photodecomposition of fenvalerate, and the formation of asymmetric peroxides and hydroperoxides using the aforementioned dimers.

5.2 Photodecomposition of Fenvalerate

As mentioned briefly in Chapter 3, another interesting example of the Persistent Free Radical Effect arose when we were examining the photodecomposition of the pesticide fenvalerate. This was my first encounter with this effect, which was the subject of my fourth year Honours thesis in the University of Ottawa's undergraduate program in chemistry. While much of the product studies and some preliminary laser flash photolysis experiments performed were included in that thesis, I present here solely the follow-up LFP studies necessary to complete the understanding of the photodecomposition mechanism. These experiments were carried out at the beginning of my graduate studies, and the results were subsequently prepared for publication.[1] In

fact, it was this very project that was the impetus for our ensuing research efforts into persistent carbon-centred radicals, as described in Chapter 3.

Fenvalerate (FV, Scheme 5.1) is a molecule that finds ample use in agriculture as a potent insecticide.[2]

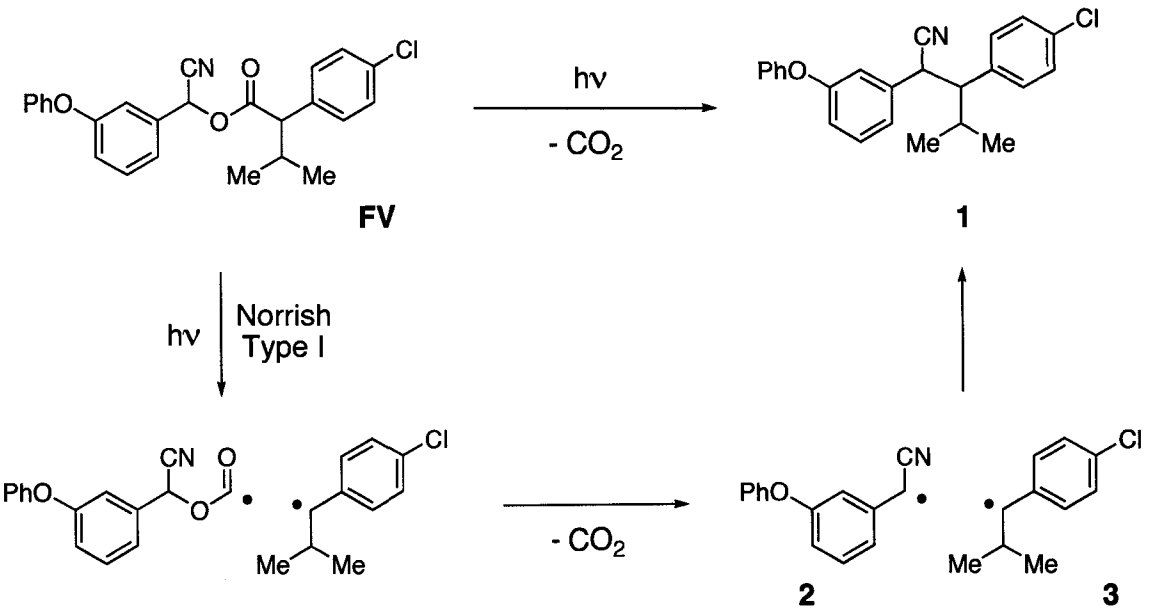

Scheme 5.1. Photodecomposition mechanism of the pesticide fenvalerate (FV).

Steady-state UVC photolysis of solutions of FV (4×10^{-3} M) in acetonitrile or water (with 8% methanol, v/v) gave rise to the decarboxylation product **1** as a mixture of two diastereomers, with trace amounts of other decomposition products.

The product distribution in aqueous solution was explained by the homolytic Norrish Type I bond breaking of the CO—CH(*i*-Pr) followed by rapid decarboxylation of the primary carbonyloxyl radical.[3] In this fashion, two carbon-centred benzylic radicals are generated as a consequence of the same bond breaking event.

Recombination of this radical-pair yielded the decarboxylation compounds **1** with little or no memory effect, leading to a complete loss of the configuration of the starting FV.

Since the benzylic radical intermediates were detectable by nanosecond laser flash photolysis, we could presume that a significant fraction, if not all, of the radical recombination occurs following the separation of the initial radical pair, as solvent cage events are too fast to be detected with nanosecond techniques.[4] Therefore, something other than geminate radical recombination was controlling product formation.

Direct detection of the proposed benzylic radicals **2** and **3** was possible by time-resolved spectroscopic techniques. Figure 5.1 shows the transient absorption spectrum recorded for FV in deaerated acetonitrile after 266 nm laser excitation, conducted under dynamic flow to avoid interference from the photogenerated products.

The spectrum shown in Figure 5.1 contains at least two different transients. The peak at 350 nm displays second-order kinetics with a half-life on the order of less than one microsecond. This absorption can be attributed to 1-(4-chlorophenyl)-2-methyl-1-propyl radical (**3**), given previous knowledge regarding UVA transitions by alkyl-substituted secondary benzylic radicals.[5]

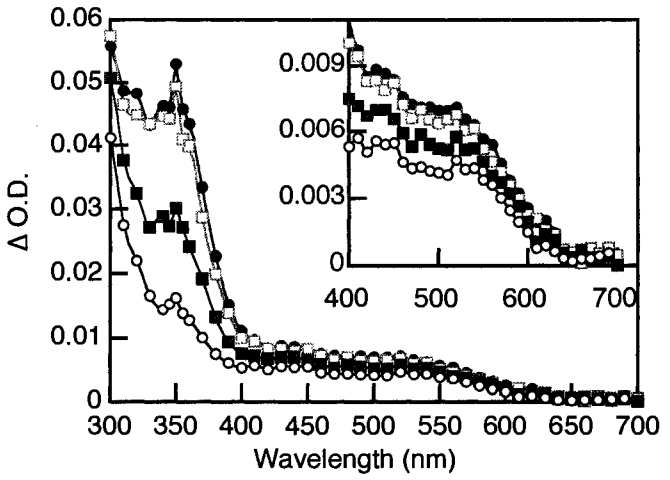

Figure 5.1. Transient absorption spectra of a nitrogen-purged solution of 3mM FV in acetonitrile following 266 nm laser excitation; 0.012 μs (●), 0.15 μs (□), 0.63 μs (■), and 1.5 μs (O) after the laser pulse; Inset: Enlarged view of the region between 400 and 700 nm.

The second intermediate at 440 nm was assigned to the radical α-cyano-m-phenoxylbenzyl radical (2). This assignment was confirmed by independent generation of the radical species via hydrogen abstraction from *m*-phenoxyphenylacetonitrile (mPPA) by *tert*-butoxyl radical (as described more thoroughly in Chapter 3). Thus, 355 nm laser flash photolysis of a sample containing 0.6 M mPPA in 50:50 (v/v) benzene:di-*tert*-butyl peroxide solvent resulted in a coincident transient absorption spectrum (a broad peak centred around 450 nm) with similar decay kinetics.

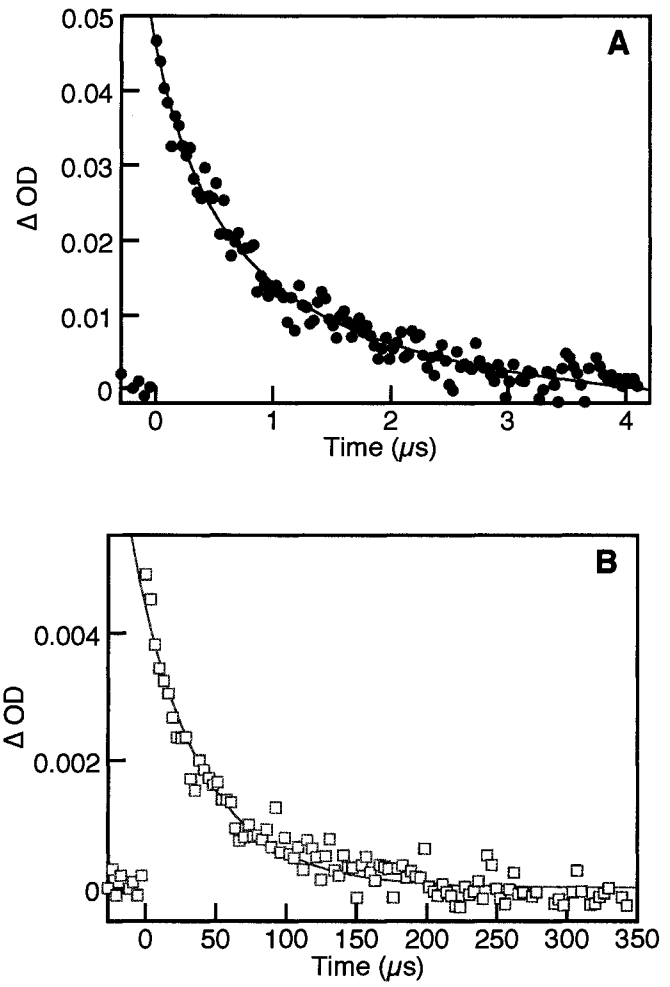

Figure 5.2: Transient decay traces of a nitrogen-purged solution of 3mM FV in acetonitrile following 266 nm laser excitation, monitored at 350 nm (A) and 440 nm (B). Note the difference in timescales.

Like the persistent carbon-centered radicals discussed previously, radical **2** was observed to be much longer-lived, decaying with a lifetime of ~37 μs, suggesting that recombination of **2** is particularly slow for a secondary benzylic radical. Furthermore, on the timescale of laser flash photolysis (tens of microseconds) **2** was found to also be unreactive toward oxygen (recall that typical reactive radicals have lifetimes of less than 100 ns in an oxygen atmosphere). Thus, we are able to consider the α-cyano-*m*-

phenoxylbenzyl radical as a *stabilized and persistent* radical. Again, it should be noted that the chapters in this thesis are not necessarily in chronological order: the observations described in this section actually preceded the discovery of the persistent nature of α-cyanobenzyl radicals; thus, it was the α-cyano-*m*-phenoxylbenzyl radical that precipitated the investigation of the family of nitrile-substituted persistent radicals described in Chapter 3.[6]

Therefore, the properties of **2** provide the ideal conditions for product-control by the conventional, Fischer-described operation of the Persistent Free Radical Effect:[7, 8] during steady state irradiation of FV, radicals **2** and **3** are generated at the same rate. Of course, since **2** undergoes attenuated recombination, it accumulates at the rate of two radicals per self-termination event of radical **3.** As a result, the cross-reaction between **2** and **3** soon takes over as the dominant reaction path for radical **3**, leading to the selective formation of **1** as the primary product.

We found it particularly remarkable that the simple kinetic phenomenon of the Persistent Free Radical Effect was responsible for the initial photoproduct in the photodecomposition of fenvalerate, and surmised that this effect may, in fact, unrecognizedly be directing product formation in many other such photoreactions!

5.3 Formation of Unsymmetric Peroxides Using Dimers of Persistent Carbon-Centred Radicals

Inspired by our proof-of-concept results with the synthesis of 1, 1, 2-triphenylproprionitrile (TPP) from dibenzylketone (DBK) and 1, 1, 2, 2-tetraphenylsuccinonitrile (TPS)[9], we wished to repeat our experiments under an air- or oxygen-saturated atmosphere in the anticipation of forming an analogous unsymmetric peroxide as an intermediate to other oxidation products (Scheme 5.2).

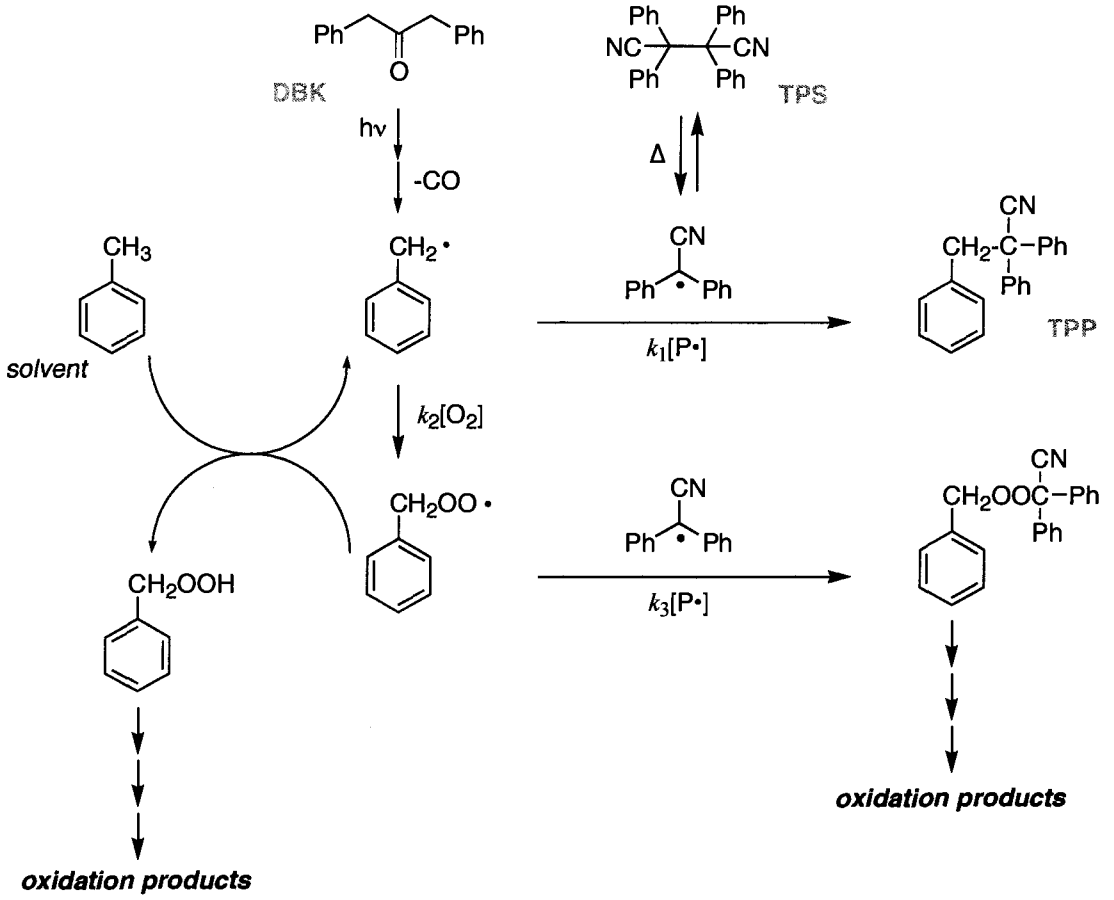

Scheme 5. 2. Formation of oxidation products via an asymmetric peroxide intermediate, using DBK and TPS as starting materials.

In this expected mechanism, benzyl radicals are produced (as in Chapter 4) *via* UVB irradiation of DBK. As these are *stabilized yet transient* radicals, under an air- or oxygen-saturated atmosphere, they will readily react with molecular oxygen (with rates approaching diffusion-control in solution) to form benzylperoxyl radicals.[10, 11] Thus, the radical buffer established *via* the dimer ⇆ radicals thermal equilibrium can result in the trapping of either benzyl or benzylperoxyl radicals, to form TPS or the unsymmetric peroxide, respectively. However, if the solvent has a labile C-H bond (*e.g.* toluene, the solvent in which TPS is somewhat soluble) then abstraction by the peroxyl radical is also feasible, forming benzyl hydroperoxide. As this reaction is equivalent to the first step in the autoxidation chain reaction[12], any trapping of peroxyl (or, indeed benzyl) radicals by the persistent α-cyanodiphenylmethyl radicals can be considered to be *antioxidant* in nature.

UVB steady-state irradiation of a toluene solution of 3.0 mM TPS and 2.0 mM under air for 60 minutes at approximately 50°C led to TPP, benzophenone, and benzaldehyde as the major products, along with small yet significant amounts of 1,2-diphenylethane (DPE) and its isomers, biphenyl, phenol, and benzyl alcohol (as monitored by GC/MS). Benzophenone is a known oxidation product of the dimer starting material,[13] and its presence represents the proportion of α-cyanodiphenylmethyl radicals which have successfully trapped transient radicals to form the peroxide intermediate. This peroxide then decomposes in the GC/MS injector to yield benzophenone and benzaldehyde *via* a thermal Kornblum-DeLaMare-type rearrangement (Scheme 5.3).[14]

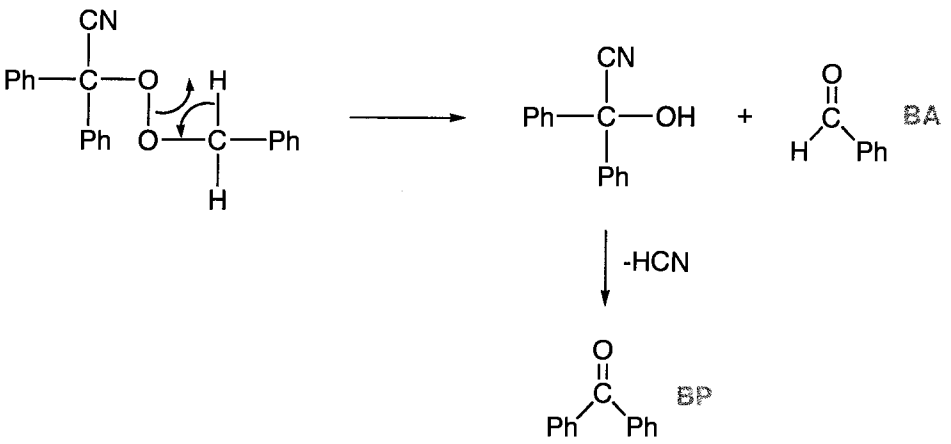

Scheme 5.3. Thermal decomposition of the peroxide intermediate yields benzophenone (BP) and benzaldehyde (BA).

However, the presence of TPP is particularly interesting: its formation indicates that the rate of trapping of benzyl radical is competitive with its addition to molecular oxygen (k_1[P•] and k_2[O_2], respectively). In toluene at ~50°C, we can expect both k_1 and k_2 to be near diffusion control (~10^9 $M^{-1}s^{-1}$) and the concentration of dissolved molecular oxygen to be on the order of 10^{-3} to 10^{-4} M;[15] thus, for the TPS dimer, the concentration of persistent radical must be at least 10^{-5} M for the radical-radical recombination of P• and benzyl radical to compete with the reaction of benzyl radical with O_2. Otherwise, the reaction of benzyl radical with O_2 and/or the recombination of P• and benzylperoxyl would have to be reversible in order to observe significant amounts of TPP.

When the photoreaction is carried out in chlorobenzene (instead of toluene) the first step in the autoxidation cycle to form benzyl hydroperoxide may be removed, since the solvent no longer has abstractable hydrogen atoms. Thus, continuous lamp

irradiation of an air-purged chlorobenzene solution containing 3.0 mM TPS and 2.0 mM DBK at ~50°C (photoreactor cooling fans off) led to ~85% consumption of DBK within 40 minutes (Figure 5.3).

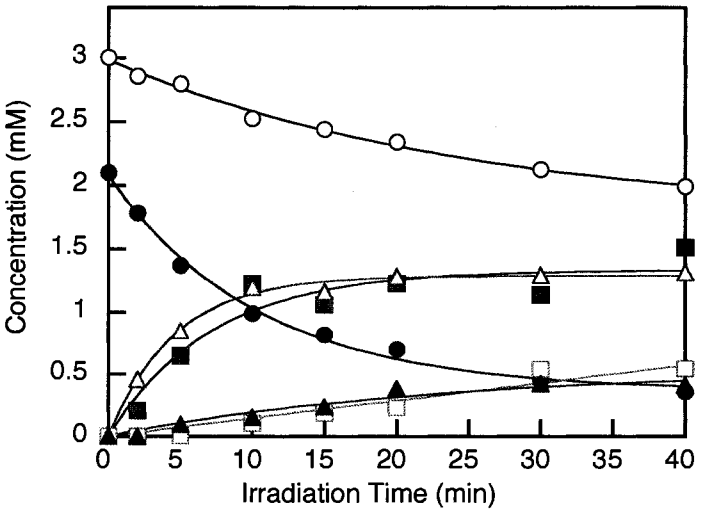

Figure 5.3. UVB lamp photolysis of 3.0 mM TPS and 2.0 mM DBK in air-purged chlorobenzene at ~50°C and followed by GC-MS: TPS (○), DBK (●), BP (■), TPP (□), DPE (▲), BA (△).

Of this portion, roughly 18% formed the direct cross-reaction product TPP, 23% the self-reaction product DPE, and 38% was converted to benzaldehyde, *via* the peroxide intermediate (the remaining ~21% of benzyl radicals formed various minor products, as mentioned above). Interestingly, the formation of BP and BA reaches a maximum after about 15 minutes of irradiation: this suggests that the dissolved oxygen in the sealed sample has been totally consumed, corresponding to a value of $[O_2]_i \sim 1.5$ mM (the solubility of oxygen in *benzene* at *25°C* is 1.9 mM)[16], while afterwards the concentrations of TPP and DPE continue to rise.

It is interesting to compare results from identical photolyses under varying conditions: chlorobenzene *versus* toluene solvent, air- *versus* oxygen-saturated solutions (all samples were purged continuously during irradiation to keep relatively constant dissolved oxygen concentration). Figure 5.4 shows the product distribution for these four samples following 40 minutes of UVB steady-state irradiation.

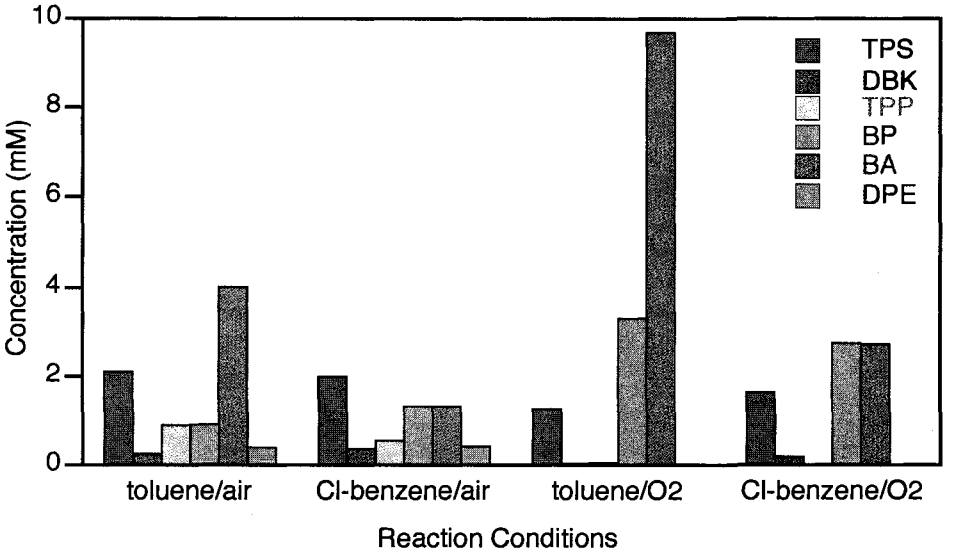

Figure 5. 4. Reactant and product distributions following 40 minutes of steady-state UVB photolyses at ~50°C of solutions containing 3.0 mM TPS and 2.0 mM DBK initially, as monitored by GC/MS. Compounds with concentrations greater than 0.1 mM shown for clarity.

A few particular results should be noted: Firstly, in toluene solvent under air, the amounts of TPS and DBK consumed are approximately equal to those in chlorobenzene under air. While the fractions of TPP, DPE, and BP produced are also similar, in toluene, the amount of benzaldehyde (BA) has been dramatically enhanced. This is

expected, as the labile benzylic hydrogen atoms on toluene (BDE ~88 kcal/mol) can be abstracted by a benzylperoxyl radical (ROO-H BDE~90 kcal/mol, k_{abs} ~ 0.08 $M^{-1}s^{-1}$ at 303 K)[10, 17], thus propagating the autoxidation chain reaction.

This effect is even greater for the samples purged with pure oxygen: essentially no TPP or DPE were observable under these conditions; instead, all of the TPS and DBK consumed were converted to BP and BA, with an enormous excess of BA.

Comparing the chlorobenzene/air and chlorobenzene/O_2 results reveals a similar trend: under oxygen, the formation of TPP and DPE has been suppressed while formation of the peroxide is favoured, as suggested by the equivalent amounts of BP and BA product.

In both cases of oxygen-saturated solutions, it is hardly surprising that oxygenated products are heavily favoured, as the concentration of dissolved molecular oxygen under a pure oxygen atmosphere is nearly five times greater than under air, for toluene and chlorobenzene solvents.[16] Hence, the rate of reaction with O_2 accelerates ($k_2[O_2]$), reducing the likelihood of trapping of benzyl radicals by α-cyanodiphenylmethyl radicals.

Most importantly, unlike the remarkably clean results obtained from the photolyses carried out under a nitrogen atmosphere in Chapter 4, the complex product mixtures obtained and the thermal instability of the desired peroxide limit this system's potential for useful organic synthesis. Fortunately, others have been successful in

applying the Persistent Free Radical Effect to the synthesis of mixed peroxides, albeit from reactions of hydroperoxides with simple phenols and alkenes.[18]

However, we were pleased with the evident peroxyl radical trapping potential of persistent carbon-centred radicals generated thermally from their dimers. Frenette *et al.* have recently extended the investigation into the peroxyl-radical trapping abilities of the dimers in the autoxidation of cumene or styrene, and achieved similar remarkable results, even at temperatures as low as 30°C.[19] Therefore, we concluded that while the oxygenated system is interesting from a mechanistic point of view, this method proved not to be a practical synthetic route to unsymmetric organic peroxides.

5.4 Formation of Hydroperoxides Using Dimers of Persistent Carbon-Centred Radicals

While we were pleased with the fact that the persistent carbon-centred radicals generated thermally from their dimer displayed antioxidant behaviour towards benzylperoxyl radicals, we were curious whether these species could also trap hydroperoxyl radicals. To investigate this possibility, we used a different dimer as our starting material: the 3-phenyl-coumaranone dimer, as shown in Scheme 5.4.

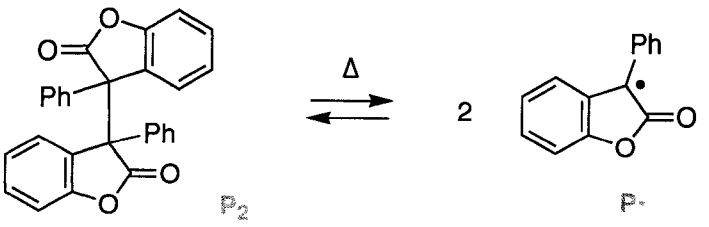

Scheme 5.4. Thermal equilibrium between the 3-phenyl-coumaranone dimer and the persistent carbon-centred radical species.

This dimer has a central carbon-carbon bond length of approximately 1.6Å, with a bond dissociation energy of nearly 24 kcal/mol (slightly weaker than the α-cyanodiphenylmethyl dimer).[20] This dimer also has greater solubility in the solvent used in the system to generate hydroperoxyl radical (acetonitrile).

The hydroperoxyl radical, HOO•, is the protonated form of superoxide, $O_2^{\bullet -}$. Superoxide is produced *in vivo* by multiple mechanisms, such as from the enzyme xanthine oxidase and as a by-product in the mitochondrial respiration cycle.[21] Hydroperoxyl radical has been implicated as one of the radical species involved in the ageing process;[22, 23] thus this species is often included along with peroxyl radicals and other reactive oxygen species when investigating systems for antioxidant potential.

In our system, we generated hydroperoxyl radical from benzopinacol. The photochemistry of benzopinacol is well-established:[24] when irradiated with UVC light (*i.e.* $\lambda < 280$ nm) in aqueous buffered solution, the central carbon-carbon bond cleaves homolytically to yield two α-hydroxydiphenylmethyl radicals, more commonly referred to as *ketyl* radicals. In the presence of dissolved molecular oxygen, ketyl radicals undergo a hydrogen atom transfer to yield the hydroperoxyl radical and a

ketone (k_5 = 3.9 x 10^9 $M^{-1}s^{-1}$),[25] in this case, benzophenone; the driving force for this reaction is the formation of the carbon-oxygen double bond (Scheme 5.5).[26] In non-aqueous solution, this process most likely occurs *via* stepwise electron and proton transfer reactions to form superoxide and hydroperoxyl radical, respectively.

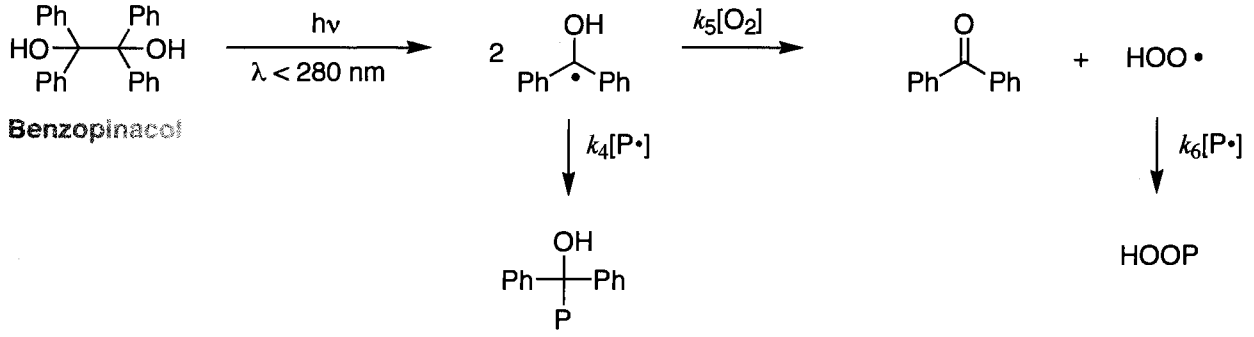

Scheme 5.5. Formation and trapping of hydroperoxyl radical.

According to Scheme 5.5 then, the persistent 3-phenyl-coumaranone radical, as produced thermally *via* the equilibrium of Scheme 5.4, may trap the ketyl radical to form a tertiary alcohol (k_4[P•]) or the hydroperoxyl radical to form the hydroperoxide "HOOP" (k_6[P•]), disregarding any knowledge of rate of reaction with molecular oxygen ((k_4[P•]). However, in this case, the choice of dimer should favour the formation of the hydroperoxide: the tertiary alcohol generated by the head-to-head recombination of the 3-phenylcoumaranone and α-hydroxydiphenylmethyl radicals would be highly sterically hindered. Thus, the bimolecular rate constant for the coupling of these two radicals must be limited, or some form of head-to-tail coupling must take place.

To investigate these possibilities, we performed a series of UVC irradiations of 13 samples, as outlined in Table 5.1. These were acetonitrile solutions, containing either 2.0

mM benzopinacol or 0.1 mM 3-phenyl-coumaranone dimer or both, continuously purged with either pure oxygen or pure nitrogen, and irradiated at various lengths using 12 UVC lamps. As the use of very short wavelength lamps can result in the formation of ozone inside the photoreactor,[27] it was necessary to turn the cooling fans on intermittently to flush out the interior. As such, the temperature measured inside the instrument over the course of the experiments averaged ~42°C.

Table 5.1. Experimental conditions for the prepared samples.

Sample No.	2 mM benzopinacol?	0.1 mM dimer?	Atm.	Irradiation Time (min.)
1	Yes	Yes	O_2	0
2	Yes	Yes	N_2	30
3	Yes	Yes	O_2	30
4	Yes	Yes	N_2	60
5	Yes	Yes	O_2	60
6	Yes	Yes	N_2	90
7	Yes	Yes	O_2	90
8	No	Yes	N_2	120
9	No	Yes	O_2	120
10	Yes	No	N_2	120
11	Yes	No	O_2	120
12	Yes	Yes	N_2	120
13	Yes	Yes	O_2	120

The results were then analyzed using GC/MS; however, in this technique, during the volatilization process the benzopinacol starting material is completely converted to benzophenone (with a trace of benzhydrol) and hydroperoxides are oxidized to aldehydes. Therefore, to monitor the possible formation of a hydroperoxide, the samples were treated with an excess of triphenylphosphine (TP, final concentration 0.3 mM) prior to injection, thus forming the corresponding alcohol and

triphenylphosphine oxide (TPO)[28], which can then more easily be monitored by GC/MS.

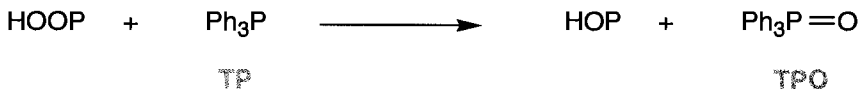

Scheme 5.6. Hydroperoxides are converted to alcohols when treated with triphenylphosphine.

After 120 minutes of irradiation, samples no. 8 and 9 showed only the dimer starting material (which appears in the chromatograph as the monomer). Samples no. 10 and 11 (benzopinacol only, under N_2 or O_2) could not be differentiated, as in both cases, the starting material is converted to benzophenone, either during the irradiation, or during GC analysis. The samples containing both benzopinacol and dimer under nitrogen (samples no. 2, 4, 6, and 12, for 30, 60, 90, and 120 minutes, respectively) showed similar, expected results: the benzopinacol appeared as benzophenone, while the dimer was largely intact.

Thus, the most intriguing results came from samples no. 1, 3, 5, 7, and 13: the system under oxygen. By GC/MS, the disappearance of dimer and triphenylphosphine was very clear; however, the tertiary alcohol HOP was not directly detectable. Instead, a variety of side-products were observed, including biphenyl and phenyl-substituted benzophenones; no clear accumulation could be determined from these compounds. However, the formation of triphenylphosphine oxide was easily monitored, and is concurrent with the consumption of starting materials. According to the conversion of

TP to TPO, in this steady-state photolysis, roughly ~35% of the dimer was used to generate the hydroperoxide HOOP.

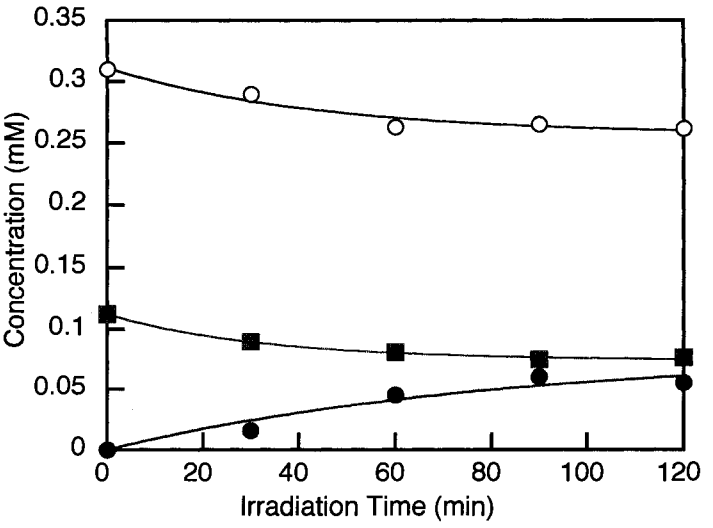

Figure 5.5. UVC lamp photolysis of 2.0 mM benzopinacol and 0.1 mM 3-phenyl-coumaranone dimer in oxygen-purged acetonitrile at ~42°C, treated with triphenylphosphine (0.3 mM) and followed by GC-MS: TP (O), dimer (■), TPO (●).

However, this analysis is solely based on the disappearance of TP and rise of TPO: it does not indicate the amount of persistent 4-phenyl-coumaranone radicals that may have trapped the intermediate ketyl radicals, perhaps through some head-to-tail coupling reactions. However, such recombinations would yield bulky alcohols which would likely fall apart in the GC/MS injector (as per the 'HOP' alcohol), and thus could not be monitored. Therefore, while the growth of TPO indicates that a hydroperoxide is indeed being formed in this system, it is possible that pre-emptive trapping of the α-hydroxydiphenylmethyl radical ($k_4[P\bullet]$) is competitive with its reaction with oxygen ($k_5[O_2]$). Let us consider the criteria needed for this to occur: under an atmosphere of pure oxygen, the concentration of dissolved oxygen in acetonitrile is approximately 9

mM; assuming a value of ~10^9 $M^{-1}s^{-1}$ for k_5 gives $k_5[O_2] \approx 10^7$ s^{-1}. Let us then assume that k_4 is near the diffusion-controlled limit if the coupling is to be competitive: likely for most radical-radical termination reactions, but maybe not so for the recombination of two bulky species (for comparison, the absolute rate constant for the coupling of triphenylmethyl ($Ph_3C\bullet$) with triphenylmethylperoxyl ($Ph_3COO\bullet$) radicals is $1.5x10^8$ $M^{-1}s^{-1}$)[29]. Therefore, in order for trapping of the ketyl radical to compete with reaction with oxygen, (*i.e.* $k_4[P\bullet] > 10^6$ s^{-1}) the concentration of persistent radical must be on the order of 10^{-3} M – clearly impossible for a 0.1 mM solution of dimer! Thus, based on some simple kinetic approximations, we may rule out trapping of the ketyl radical as a possible side reaction.

Therefore, we have concluded that it is evident that the persistent carbon-centred radicals investigated by the Scaiano group display antioxidant behaviour towards hydroperoxyl radical, in addition to trapping peroxyl radicals. Again, while these results were interesting for a cursory series of experiments, it is clear that this system is not practical for the preparation of hydroperoxides. In this case, the introduction of transient radical species on the dynamic stability of the dimer ⇆ persistent radical equilibrium remains a mechanistic curiosity, and not a useful synthetic tool.

5.5 Conclusions

The course of the Scaiano Group's investigations into persistent carbon-centred radicals has resulted in a cascade of research projects. While we had originally been examining persistent carbon-centred radicals from lactone derivatives (such as Ciba's HP-136) for their lack of reactivity towards molecular oxygen, the preliminary results

from my Honours Project on the photodecomposition of the pesticide fenvalerate revealed that a new family of nitrile-substituted radicals also displayed this behaviour. This subsequently led to the research described in Chapter 3, and further elucidation of the decomposition mechanism described here in Section 5.2. Next, dimers of the persistent radical species were prepared by M. Frenette, and we have only begun to discover practical uses for these materials. For example, Chapter 4 described convenient carbon-carbon bond formation using the dimers, while this chapter described two other possible examples of applications of these species: the antioxidant potential of the persistent carbon-centred radicals towards hydroperoxyl and peroxyl radicals.

The results included in the preceding chapters reflect only a portion of the remarkable abilities of these intermediates; M. Frenette continues to explore the antioxidant capabilities of the dimers, particularly their inhibition of autoxidation chain reactions. Certainly, the understanding of the behaviour of persistent carbon-centred radicals has come a long way since Gomberg's first description of the triphenylmethyl radical over a century ago, and these species still present exciting opportunities for future researchers...how fortunate we are that enthusiastic chemists did not heed Gomberg's famous plea in his original 1900 publication that he wished to reserve the field of 'trivalent carbon' to himself!

5.6 References

1. Sanjuán, A.; Aguirre, G.; Alvaro, M.; García, H.; Scaiano, J. C.; Chrétien, M. N.; Focsaneanu, K.-S., Product studies and laser flash photolysis of the direct and 2,4,6-triphenylpyrylium-zeolite Y photocatalyzed degradation of fenvalerate. *Photochem. Photobiol. Sci* **2002,** 1, 955-959.

2. No. 90. Fenvalerate. In *WHO/FAO Data Sheets on Pesticides,* World Health Organization and Food and Agriculture Organization of the United Nations: July 1996.

3. Turro, N. J., *Modern Molecular Photochemistry.* University Science Books: Sausalito, 1991.

4. Braden, D. A.; Parrack, E. E.; Tyler, D. R., Solvent cage effects. I Effect of radical mass and size on radical cage pair recombination efficiency. II Is geminate recombination of polar radicals sensitive to solvent polarity? *Coord. Chem. Rev.* **2001,** 211, 279.

5. Chatgilialoglu, C., Electronic Absorption Spectra of Free Radicals. In *Handbook of Organic Photochemistry,* Scaiano, J. C., Ed. CRC Press: Boca Raton, Florida, 1989; Vol. II, pp 3-11.

6. Font-Sanchis, E.; Aliaga, C.; Focsaneanu, K.-S.; Scaiano, J. C., Greatly Attenuated Reactivity of Nitrile-Derived Carbon-centered Radicals toward Oxygen. *Chem. Commun.* **2002,** (15), 1576-1577.

7. Fischer, H., Unusual Selectivities of Radical Reactions by Internal Suppression of Fast Modes. *J. Am. Chem. Soc.* **1986,** 108, (14), 3925-3927.

8. Fischer, H., The Persistent Radical Effect: A Principle for Selective Radical Reactions and Living Radical Polymerizations. *Chem. Rev.* **2001,** 101, 3585-3610.

9. Focsaneanu, K.-S.; Aliaga, C.; Scaiano, J. C., Clean Photochemical Synthesis Mediated by Radical-Radical Reactions: Radical Buffer or the Persistent Free Radical Effect? *Org. Lett.* **2005,** 77, (22), 4979-4982.

10. Ingold, K. U., Peroxyl Radicals. *Acc. Chem. Res.* **1969,** 2, 1.

11. Maillard, B.; Ingold, K. U.; Scaiano, J. C., Rate constants for the reactions of free radicals with oxygen in solution. *J. Am. Chem. Soc.* **1983,** 105, 5095.

12. Denisov, E. T., *Oxidation and antioxidants in organic chemistry and biology.* Taylor & Francis: Boca Raton, 2005.

13. Frenette, M., Private Communication. In 2006.

14. Kornblum, N.; DeLaMare, H. E., The base catalyzed decomposition of a dialkyl peroxide. *J. Am. Chem. Soc.* **1951,** 73, 880.

15. Battino, R., *Solubility Data Series: Oxygen and Ozone.* Pergamon Press: 1981.

16. Murov, S. L.; Carmichael, I.; Hug, G. L., *Handbook of Photochemistry.* Marcel Dekker, Inc.: New York, 1993.

17. Middleton, B. S.; Ingold, K. U., Hydrogen atom abstraction by peroxy radicals. *Can. J. Chem.* **1967,** 45, 191.

18. Bravo, A.; Bjørsvik, H.-R.; Fontana, F.; Liguori, L.; Minisci, F., Ingold-Fischer "Persistent Free Radical Effect", Solvent Effect and Metal Salt Oxidation of Carbon-Centered Radicals in the synthesis of Mixed Peroxides from tert-Butyl Hydroperoxide. *J. Org. Chem.* **1997,** 62, 3849.

19. Frenette, M.; MacLean, P. D.; Barclay, L. R. C.; Scaiano, J. C., Radically Different Antioxidants: Thermally Generated Carbon-Centered Radicals as Chain-Breaking Antioxidants. *J. Am. Chem. Soc.* **2006,** 128, 16432.

20. Frenette, M.; Aliaga, C.; Font-Sanchis, E.; Scaiano, J. C., Bond Dissociation Energies for Radical Dimers Derived from Highly Stabilized Carbon-Centered Radicals. *Org. Lett.* **2004,** 6, (15), 2579-2582.

21. Halliwell, B.; Gutteridge, J. M. C., *Free Radicals in Biology and Medicine.* 3rd ed. ed.; Oxford: 1999.

22. Johnson, J. E., *Free radicals, aging, and degenerative diseases.* Liss: New York, 1986.

23. Knight, J. A., *Free radicals, antioxidants, aging and disease.* AACC Press: Washington, DC, 1999.

24. Reichel, L. W.; Griffin, G. W.; Muller, A. J.; Das, P. K.; Ege, S. N., Photoinduced electron transfer C-C bond cleavage reactions; oxidations and isomerizations. *Can. J. Chem.* **1984,** 62, 424.

25. Konya, K. G.; Paul, T.; Lin, S.; Lusztyk, J.; Ingold, K. U., Laser Flash Photolysis Studies on the First Superoxide Thermal Source. First Direct Measurements of the Rates of Solvent-Assisted 1,2-Hydrogen Atom Shifts and a Proposed New Mechanism for this Unusual Rearrangement. *J. Am. Chem. Soc.* **2000,** 122, 7518.

26. Perkins, M. J., *Radical Chemistry.* Ellis Horwood: New York, 1994.

27. Wiesenfeld, J. R., Atmospheric chemistry involving electronically excited oxygen atoms. *Acc. Chem. Res.* **1982,** 15, 110.

28. Hiatt, R.; Smythe, R. J.; McColeman, C., The reaction of hydroperoxides with triphenylphosphine. *Can. J. Chem.* **1971**, 49, 1707.

29. Howard, J. A.; Ingold, K. U., Absolute rate constants for hydrocarbon oxidation. XI. The reactions of tertiary peroxy radicals. *Can. J. Chem.* **1968**, 46, (2655).

Chapter 6. Pyrene Monomer and Excimer Fluorescence Quenching as a Sensor for Electron-Deficient Molecules

Chapter 6: Pyrene Monomer and Excimer Fluorescence Quenching as a Sensor for Electron-Deficient Molecules

6.1 Introduction

The pyrene fluorophore, along with benzophenone and ruthenium(II) tris(bipyridyl), is one of the most widely-studied molecules in photochemistry; its fluorescence has been used in innumerable sensing or signalling applications. Pyrene fluorescence *quenching* in particular has also been used as an effective analytical tool: some recent examples include detecting NO in NO-releasing oxygen-sensing polymer films,[1] probing the heterogeneous microenvironments of the C18 stationary phase in capillary electrochromatography,[2] measuring intracellular molecular oxygen concentrations,[3] and explosives detection,[4] in an application closely related to the system described in this chapter.

The majority of the pyrene fluorescence quenching applications involve dilute solutions of pyrene or pyrene-based derivatives and thus do not take advantage of excimer formation which occurs in moderately concentrated conditions (*e.g.* ≥ 0.001M in solution).[5, 6] While the monomer-excimer equilibrium has been thoroughly investigated,[7-18] studies on the effect of certain quenchers on the *ratio* of the two species remains limited. Therefore, we decided to investigate further into how the presence of fluorescence quenching agents, specifically electron-deficient compounds, might influence the monomer-excimer equilibrium. We subsequently observed differential excimer and monomer quenching under these conditions, and we have proposed that

this effect may have potential applications as a method to detect electron deficient substrates.

Recall from Chapter 1 that the fluorescence spectra of moderately concentrated solutions of pyrene show two distinct emission bands, where the fine structured band below 400 nm corresponds to emission from the singlet excited state monomer, $^1M^*$. The broad band centred around 470 nm is emission due to the formation of 'excited dimers', or *excimers*. The excimer $^1E^*$ is a relatively stable complex between one excited molecule of pyrene and another in its ground state, with a binding energy of 38-42 kJ/mol in non-viscous solvents.[12, 13, 17, 18]

A variety of molecules are able to quench fluorescence emission from pyrene *via* charge-transfer or electron-transfer mechanisms[19]. In the case of electron-deficient nitromethane, the mechanism of fluorescence quenching was rigorously explored *via* computational studies by McGuffin and coworkers.[20] They concluded that the most likely mechanism is the formation of an excited state ion pair following electron transfer from pyrene to nitromethane. Nitromethane is also known to selectively quench alternant polycyclic aromatic hydrocarbons (by acting as the electron acceptor) whereas alkyl amines act as electron donors and quench non-alternant PAHs.[4, 21-24]

In our investigations, we employed steady-state and time-resolved emission techniques to examine pyrene fluorescence quenching as a way to discriminate between electron-donor and electron-acceptor quenchers. A series of compounds were used as quenchers, ranging from electron-rich to electron-poor molecules. (Appendix 6.A lists the names, structures, and abbreviations for the various quenchers used). We have

proposed that the discrimination of these quenchers *via* differential monomer and excimer quenching may prove useful in analytical applications in the area of explosive detection.

6.2 Steady-State Fluorescence Quenching

The mechanism for the quenching of fluorescence from the monomer and excimer species of pyrene is shown in Scheme 6.1 (adapted from the literature).[25]

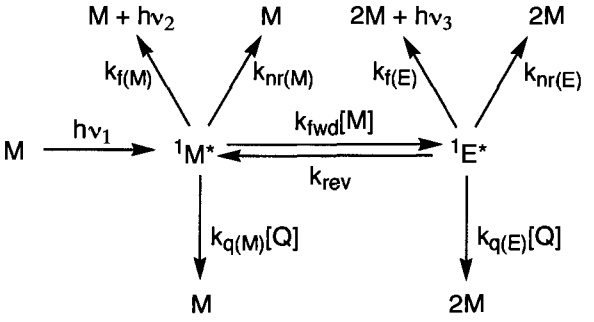

Scheme 6.1. Fluorescence quenching of pyrene. M = monomer form, E = excimer, k_f = fluorescence rate constant, k_q = bimolecular quenching rate constant, k_{nr} = sum of rate constants for non-radiative processes.

In de-aerated alcohols at room temperature, the rate constant for excimer dissociation, k_{rev}, has values around 10^6 s^{-1}.[8, 12] Since the monomer and excimer singlet excited state lifetimes are ~100 ns and ~50 ns respectively under our conditions, we expect excimer dissociation (k_{rev}) to be insignificant: therefore, a stationary-state equilibrium is not established between the monomer and excimer forms. In our experiments, a concentration of pyrene of 3 mM in nitrogen-purged 99% ethanol was used throughout, since comparable emission intensities for monomer and excimer (that

this concentration achieves) ensure the best sensitivity in dual quenching experiments; further, under these conditions the criterion of negligible excimer dissociation is readily achieved (*i.e.*, $k_{fwd}[M] >> k_{rev}$).

We selected a variety of compounds to act as our quenchers, ranging from electron-rich to electron-poor substances. It should be noted that, while we envisioned this method could be used in explosives detection (Section 6.4), for safety and availability reasons, we did not use actual commercial explosives as quenching agents – instead, we approximated the expected results by using other nitrated aromatics (*e.g.* nitrobenzene).

Steady-state fluorescence quenching measurements revealed very clearly that the compounds we had selected could be divided into three categories: non-quenchers, monomer-only quenchers, and monomer-excimer quenchers.

The first group of so-called 'non-quenchers' were electron-rich compounds, such as tribenzylamine and *p*-dimethoxybenzene. These molecules displayed no significant quenching of pyrene fluorescence (data not shown), even at very high quencher concentrations ([Q]), due to their inherently small values of k_q. Thus, we did not pursue any further experiments with these compounds.

The second group of monomer-only quenchers consisted largely of anilines, such as *N,N*-dimethylaniline (DMA, in Figure 6.1A). These molecules displayed a moderate degree of quenching of both emissions, illustrated in the Stern-Volmer plots in Figure 6.1B. The reasons why these molecules are referred to as 'monomer-only' quenchers – in

spite of the fact that they reduce excimer emission - will become apparent as the detailed quenching mechanism is discussed (*vide infra*).

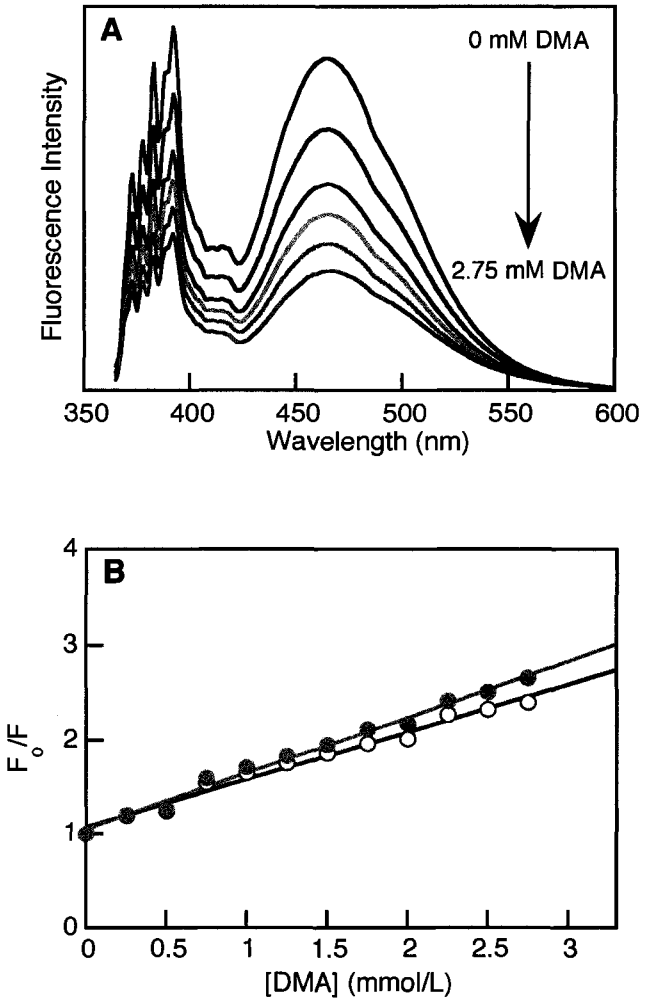

Figure 6.1. Steady-state fluorescence quenching of pyrene (3 mM in nitrogen-purged 99% ethanol, λ_{ex} = 355 nm). A: Q = N,N-dimethylaniline (DMA). Some spectra omitted for clarity. B: Stern-Volmer plots taken at 392 nm to represent the monomer form (O) and 464 nm to represent the excimer form (●); bandpath ~ 3nm.

This dynamic quenching is described by the Stern-Volmer expression, Equation 6.1.[26] In this expression, Φ refers to quantum yields and F to emission intensities in arbitrary units; k_q is the bimolecular quenching rate constant, τ_f^o is the observed fluorescence lifetime for unquenched fluorophore; the product of k_q and τ_f^o may be represented by K_{SV}, called the Stern-Volmer constant.

$$\frac{\Phi_f^o}{\Phi_f} \approx \frac{F_o}{F} = 1 + k_q \tau_f^o [Q] = 1 + K_{SV}[Q] \qquad (6.1)$$

As shown in Figure 6.1B, DMA and the other anilines showed equivalent monomer and excimer quenching. There are in fact two situations in which the slopes for monomer and excimer quenching are expected to be the same: either a) the monomer-excimer equilibrium is maintained at all times, or b) the monomer form is being quenched exclusively, and the observed excimer quenching merely reflects the fact that its precursor is being quenched (*i.e.* a reduced monomer population from which the excimers arise). Since we have already discarded the presence of a stationary-state equilibrium under our conditions, the latter situation must apply for systems where both (monomer and excimer) quenching plots have the same slope. Thus, identical Stern-Volmer plots (*i.e.*, $K_M = K_E$) are expected, as shown in the graph. This behaviour reflects the previously acknowledged effect that excimers are "stabilized" against electron-transfer quenching.[25] Selective monomer quenching by aromatic amines has also been observed by Ottolenghi and coworkers, who measured the monomer-to-excimer fluorescence ratio of pyrene-labeled lipid probes to examine lipid

miscibility in bilayers.[27] Thus, we designated these molecules as 'monomer-only' quenchers.

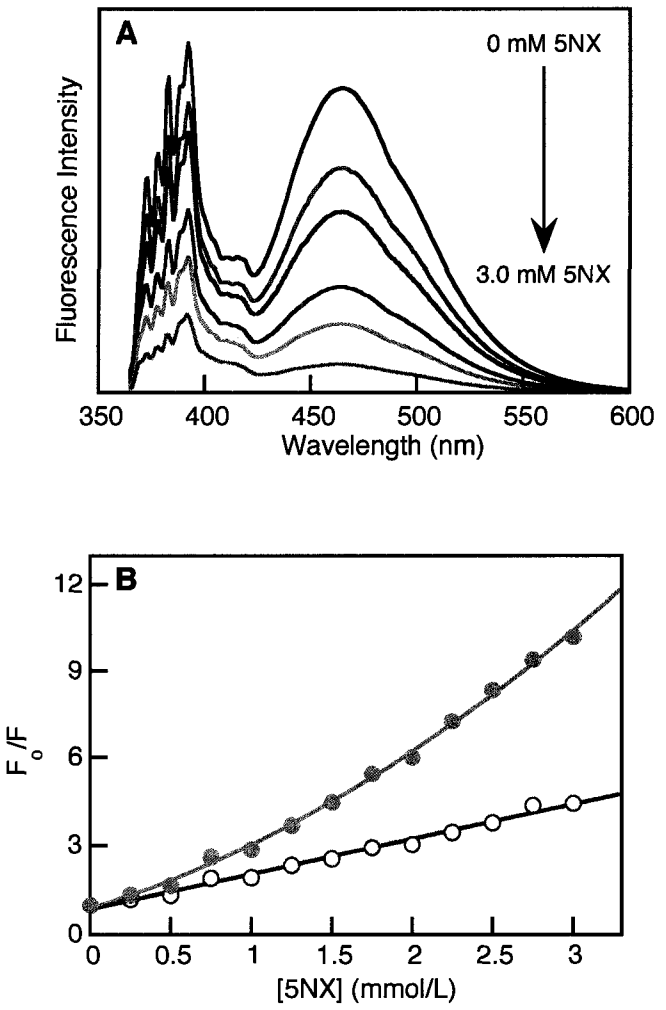

Figure 6.2. Steady-state fluorescence quenching of pyrene (3 mM in nitrogen-purged 99% ethanol, λ_{ex} = 355 nm). A: Q = 5-nitro-*m*-xylene (5NX). Some spectra omitted for clarity. B: Stern-Volmer plots taken at 392 nm to represent the monomer form (O) and 464 nm to represent the excimer form (●); bandpath ~ 3nm. Note the difference between the y-axes in Figures 6.1B and 6.2B.

Interestingly, the electron-deficient compounds displayed behaviour unlike the anilines: these molecules, as exemplified by 5-nitro-*m*-xylene (5NX) in Figure 6.2, had monomer fluorescence quenching which followed the Stern-Volmer relationship.

However, when plotted, the excimer form showed a positive deviation from the expression. In all cases, the excimer fluorescence, while attenuated, showed no significant spectral changes.

Upward-curving Stern-Volmer plots indicate that two possible quenching modes are present in the system; typically, these modes are *dynamic* and *static* quenching.[19] Since both of these modes of quenching manifest a decrease in *steady-state* fluorescence, it is prudent at this point to present a description of these two quenching modes and how they may be differentiated by time-resolved fluorescence measurements.

Dynamic quenching occurs when the quencher is required to diffuse through solution to the location of the fluorophore in order to achieve quenching (Scheme 6.2).

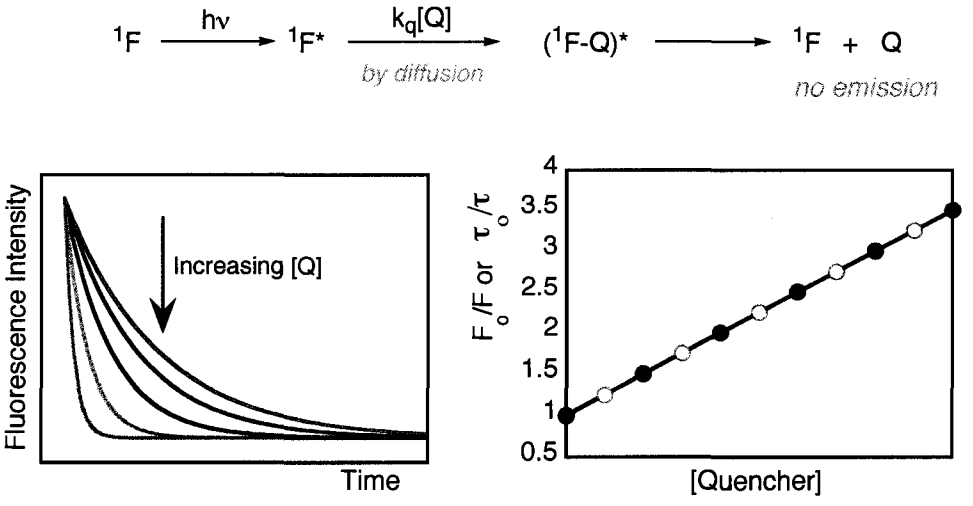

Scheme 6.2. Mechanism of dynamic quenching; an example of the effect of increasing quencher concentration on the observed time-resolved fluorescence; the expected Stern-Volmer plots from steady-state (F_o/F, ●) and time-resolved (τ_o/τ, ○) data.

In other words, following addition of quencher, the initial number of excited state molecules generated by the laser pulse is identical (*i.e.* the amplitude is constant) but the fluorescence *lifetime* is attenuated. When a Stern-Volmer plot is constructed from steady-state (F_o/F) and time-resolved (τ_o/τ) fluorescence data, the slopes are identical.

Conversely, *static* quenching may occur when the quencher forms some sort of pre-association with the fluorophore, such as a ground-state complex. Therefore, it is not necessary for the quencher to diffuse to the substrate: when the fluorophore absorbs a photon a new excited-state is 'born', incorporating the quencher. This new first singlet excited-state may or may not fluoresce; if it does not, then static quenching occurs (Scheme 6.3).

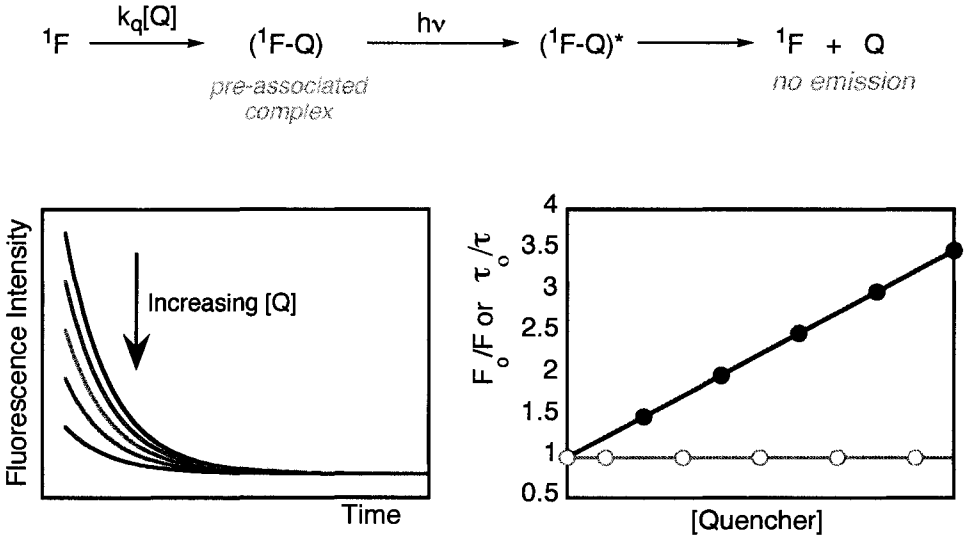

Scheme 6.3. Mechanism of static quenching, and an example of the effect of increasing quencher concentration on the observed time-resolved fluorescence and the expected Stern-Volmer plots from steady-state (F_o/F, ●) and time-resolved (τ_o/τ, ○) data.

Thus, in this case, the actual amount of initial available fluorophore is reduced; however, the molecules that are not participating in a pre-association with the quencher moiety still fluoresce with the same intrinsic fluorescence lifetime. Therefore, for pure static quenching, as the concentration of quencher is increased, the amplitude of the fluorescence decreases, while the observed lifetime remains unchanged. In this case, the resulting Stern-Volmer plot is a flat line for the time-resolved (τ_o/τ) fluorescence data, while F_o/F is linear and non-zero.

Therefore, if a quencher is capable of both static and dynamic quenching, then both the fluorescence intensity and lifetime are attenuated. Consequently, when plotted, (τ_o/τ) is linear with a non-zero slope, while F_o/F displays upward curvature, as illustrated in Scheme 6.4.

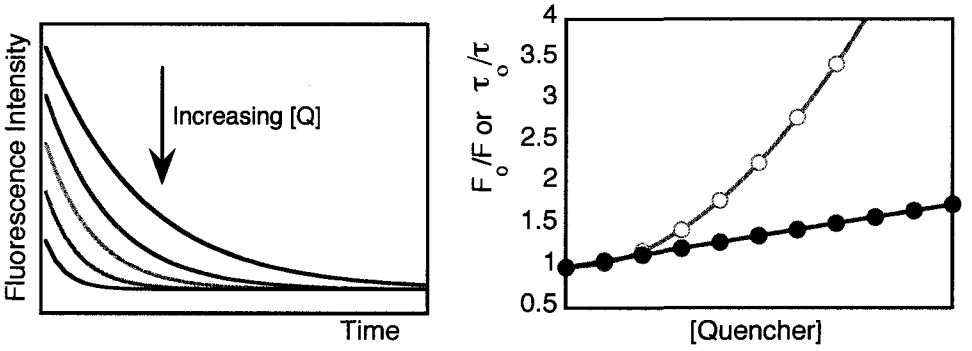

Scheme 6.4. Time-resolved fluorescence measurements and the resulting Stern-Volmer plots under static and dynamic quenching conditions.

This new curve may be fitted with a parabolic expression involving two Stern-Volmer constants, representing the static and dynamic quenching components:[19]

$$\begin{aligned}\frac{F_o}{F} &= (1 + K_{SV,s}[Q])(1 + K_{SV,d}[Q]) \\ &= 1 + (K_{SV,s} + K_{SV,d})[Q] + (K_{SV,s}K_{SV,d})[Q]^2\end{aligned} \tag{6.2}$$

If the fluorescence lifetime of the fluorophore is known, fitting the curve to this second-order polynomial expression can yield the bimolecular rate constants for both modes.

While this explanation is sufficient for most positive deviations from ideal Stern-Volmer behaviour, it became clear that our system did *not* involve static quenching. Ground-state absorption studies of pyrene showed no spectral shifts upon addition of the various quenchers, suggesting that there is no pre-association between the fluorophore and quencher. Also, time-resolved fluorescence measurements for both the monomer and excimer species (Section 6.3) showed only attenuation of the fluorescence lifetimes, and not the fluorescence intensity, with increasing quencher concentration.

Thus, we were convinced that another mechanism was responsible for the observed upward curvature. We determined that this deviation was the result of a combination of two-state quenching resulting from a reduced $^1M^*$ population, and dynamic fluorescence quenching of the excimer itself. In other words, the nitroaromatic compounds, which displayed the largest deviations from ideal Stern-Volmer behaviour, are strong enough to deactivate the excimer complex, with bimolecular quenching rate

constants approaching diffusion-control. Consequently, the electron-deficient compounds were placed in a third category: 'monomer *and* excimer quenchers'. This conclusion will be discussed more thoroughly in the following section (as the explanation requires time-resolved fluorescence data); for now, let us return to the steady-state fluorescence quenching measurements, and their potential analytical applications.

The results exemplified by Figure 6.2 above add a new dimension to the application of pyrene fluorescence quenching to analyze electron-deficient molecules, particularly nitroaromatics.[28] By recording the *ratio* of monomer-to-excimer emission intensities, it is possible to have a detection method that is only sensitive to electron-deficient molecules, suggesting possible methodologies for explosives detection.

Simultaneous monomer and excimer quenching allows the generation of calibration curves by plotting the ratio of the fluorescence intensities of the two forms (F_M/F_E) as a function of quencher concentration. As a result, quantification of unknown samples will be possible. Representative example curves of three quenchers with different responses, *N,N*-dimethylaniline (DMA), nitroethane (NE) and 5-nitro-*m*-xylene (5NX), are shown in Figure 6.3.

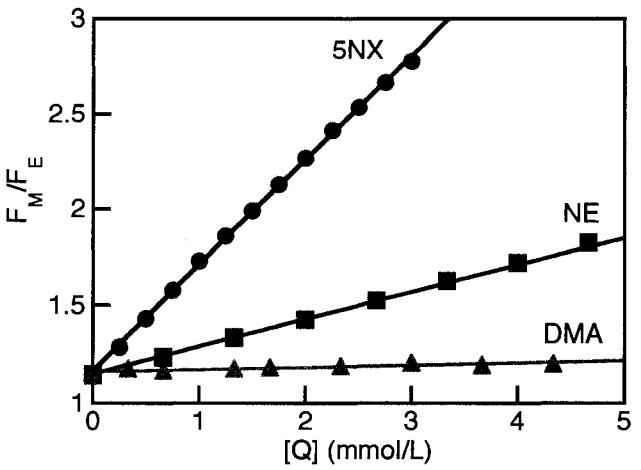

Figure 6. 3. Representative calibration curves constructed by taking the ratio of fluorescence intensities of 3 mM pyrene (in ethanol) at 392 nm and 464 nm (F_M/F_E) as quencher is added: (●) Q = 5-nitro-*m*-xylene; (■) Q = nitroethane; (▲) Q = *N,N*-dimethylaniline.

Table 1 includes the values of the slopes of the calibration curves constructed for the various quenchers. From this, three groupings can be discerned. As the anilines were found to be 'monomer-only' quenchers, their attenuation of the excimer fluorescence signal is solely due to depletion of the monomer precursor; hence their graphs of F_M/F_E are nearly horizontal. Conversely, since the electron-deficient compounds are capable of quenching both the monomer and excimer species, a distinct response is acquired when plotting F_M/F_E. For the nitroaliphatics, this response is quite significant, with slopes around 150 to 200 M^{-1}. However, it is the explosive analogues, the nitroaromatics, that displayed the greatest degree of quenching, leading to slopes in the 550-to-650 M^{-1} range. Therefore, assuming a value of 600±50 M^{-1} will allow the

estimation of an approximate concentration, even for molecules where a sample of the authentic material is not available.

Table 6.1. Slope values from the plots of F_M/F_E for various quenchers.[a]

Quencher	Slope (M^{-1})
p-dicyanobenzene, DCB	652
nitrobenzene, NB	618
p-dinitrobenzene, pDNB	595
5-nitro-*m*-xylene, 5NX	588
m-dinitrobenzene, mDNB	572
2,4-dinitrofluorobenzene, DNFB	558
nitromethane, NM	191
nitroethane, NE	170
N,*N*-dimethylaniline, DMA	11.1
trioctylamine, TOA	6.0
N,*N*-dimethylaminopyridine, DMAP	5.5
N,*N*-dimethyl-2,6-diisopropylaniline, DDA	-5.3

[a]Typical errors are <5%.

This effect may be more dramatically illustrated in the bar graph of Figure 6.4: here, the three groupings are clearly visible, with the nitroaromatics providing the largest response to the dual fluorescence quenching. The average value for the response obtained from these compounds, 600 M^{-1}, is indicated on the graph. With such an evident discrimination between electron-poor and electron-rich compounds, we anticipate that this effect can be exploited in the identification and quantification of other electron-deficient molecules, such as explosives (see Section 6.4).

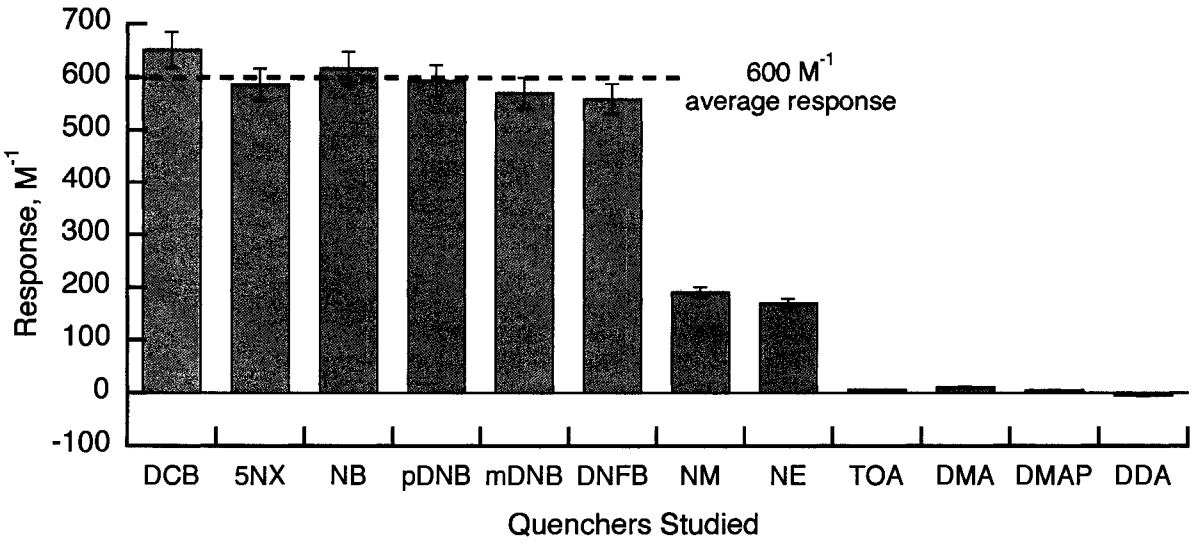

Figure 6.4. Bar graph indicating the dual fluorescence quenching response for the quenchers studied. See Appendix 6A for abbreviations and structures.

6.3 Time-Resolved Fluorescence Quenching

In order to establish a more thorough understanding of the mechanistic details of this system, we pursued time-resolved studies of monomer and excimer quenching. However, it should be noted that these measurements would not be required for possible analytical applications, as described in the next Section, where only steady state fluorescence at two separate wavelengths would be required.

Figure 6.5A shows the time-resolved fluorescence spectrum for 3mM pyrene in nitrogen-purged 99% ethanol following excitation by a 355 nm nanosecond laser pulse; Figure 6.5B displays the transient fluorescence decays for the monomer and excimer species, as monitored at 392 and 464 nm, respectively.

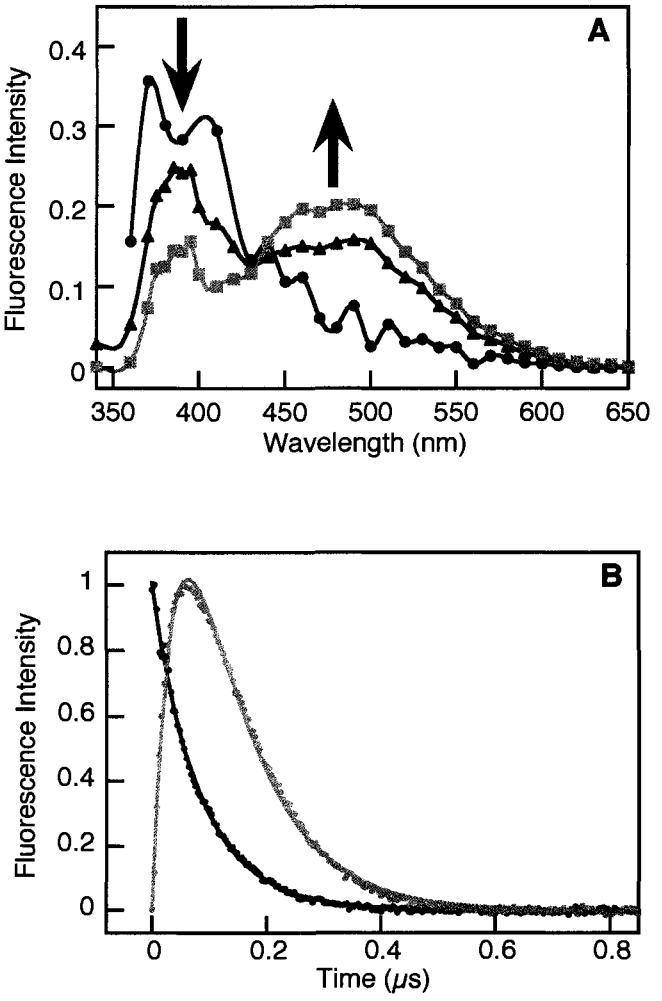

Figure 6.5. A: Time-resolved fluorescence spectrum of pyrene, 3mM in 99% ethanol solution following 355 nm nanosecond laser excitation (●) 0.008 μs; (■) 0.032 μs; and (▲) 0.068 μs after the laser pulse. B: Transient fluorescence decays, as monitored at (●) 392 nm (monomer species) and (●) 464 nm (excimer species). For details on the curve fittings, see text.

Under these conditions, the pyrene monomer fluorescence displays a monoexponential decay with a lifetime of 105 ± 2 ns, confirming that dissociation from the excimer is negligible; the excimer species' fluorescence may be fitted with a first-order growth + first-order decay expression, Equation 6.3:[29, 30]

$$I_t = A_o \frac{k_1}{k_2 - k_1}\left(\left(\exp(-k_1 t)\right) - \left(\exp(-k_2 t)\right)\right) \qquad (6.3)$$

In this equation, I_t is the fluorescence intensity at time t, and A_o is the pre-exponential factor. The rate constants k_1 and k_2 represent the growth and decay of the excimer species; however, since the monomer is the precursor for the excimer species, the growth of the excimer simply reflects the decay of the monomer. Thus, k_1 and k_2 correspond to τ_M^{-1} and τ_E^{-1}, respectively.

In the presence of the same quenchers used in the preceeding section, the time-resolved fluorescence quenching results for the monomer confirmed that quenching of this species under our conditions is in fact a dynamic process. As mentioned previously, the lifetimes, and not intensities, of the observed fluorescence were attenuated. This rules out any static quenching, and so at the concentrations employed pyrene-quencher pre-association is negligible.

The monomer fluorescence decays in the presence of quencher were fitted with monoexponential expressions, where the observed decay rate constant is a combination of the intrinsic fluorescence decay and bimolecular quenching (Equation 6.4):

$$I_t = A_o\left(\exp(-k_{obs} t)\right) \quad , \quad k_{obs} = k_o + k_q[Q] \qquad (6.4)$$

Plotting the observed rate constant (τ^{-1}) against the quencher concentration thus yields values for k_q; Figure 6.6 shows a sample quenching plot for *m*-dinitrobenzene, and the values for the quenching rate constants for the monomer species are reported in

Table 6.2. Not surprisingly, other electron-deficient substrates besides the nitroaromatics (such as 1,4-dicyanobenzene) also behaved as excellent quenchers.

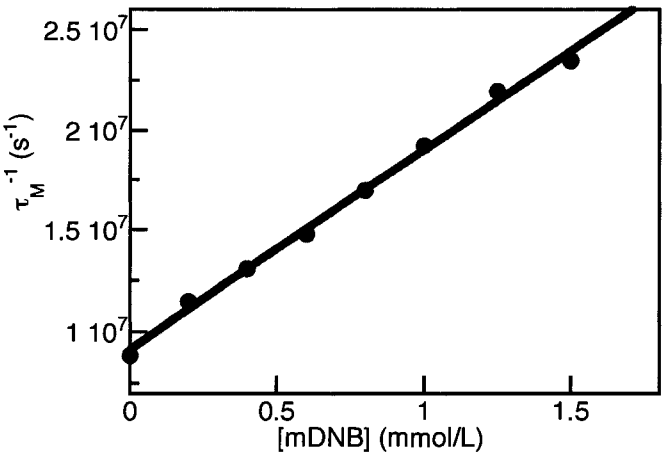

Figure 6.6. Quenching of fluorescence at 392 nm from 3 mM pyrene in nitrogen-purged 99% ethanol by mDNB, following laser excitation at 355 nm.

Table 6.2. Quenching rate constants for pyrene monomer fluorescence in ethanol at room temperature.[b]

Quencher	k_q, $M^{-1}s^{-1}$
DCB	9.7×10^9
5NX	8.0×10^9
NB	7.7×10^9
pDMB	1.0×10^{10}
mDNB	9.9×10^9
DNFB	6.8×10^9
NM	3.6×10^9
NE	3.2×10^9
DMA	4.6×10^9
TOA	4.1×10^9
DMAP	1.2×10^9
DDA	4.4×10^9

[b]Typical errors are <5%. See Appendix 6A for structures and abbreviations.

Figure 6.7 shows the Stern-Volmer plots based on emission intensity (F_0/F) and on lifetimes (τ_0/τ), derived from steady-state and time-resolved fluorescence measurements, respectively.

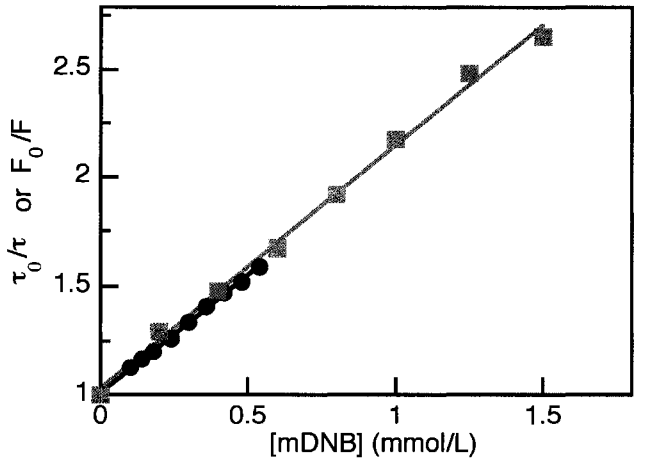

Figure 6.7. Stern-Volmer plots based on steady-state measurements (●) and time-resolved studies (■) for the quenching of the pyrene monomer (monitored at 392 nm).

As explained in Section 6.2, the excellent agreement between the two techniques is another confirmation that only dynamic quenching is occurring.[19] Identical results were obtained with the other quenchers. Thus, along with the previous evidence, we were able to conclude that the anilines and nitro-compounds were all quenching pyrene monomer fluorescence in a dynamic fashion with rates approaching diffusion-control, and that any ground-state association between these molecules may be ruled out.

We also examined the effect of quenchers on the pyrene excimer fluorescence lifetimes. The resulting luminescence growth and decay could also be fitted using Equation 6.3; however, in order to improve the fitting, the growth component (k_1) was fixed to values calculated according to the linear fit shown in Figure 6.6 to minimize

error from the actual experimental data points. As a representative example, all three sets of values for the quenching of pyrene excimer by mDNB (k_1 expt'l, k_1 calc'd, and the resulting k_2 from Equation 6.3) are shown in Table 6.3.

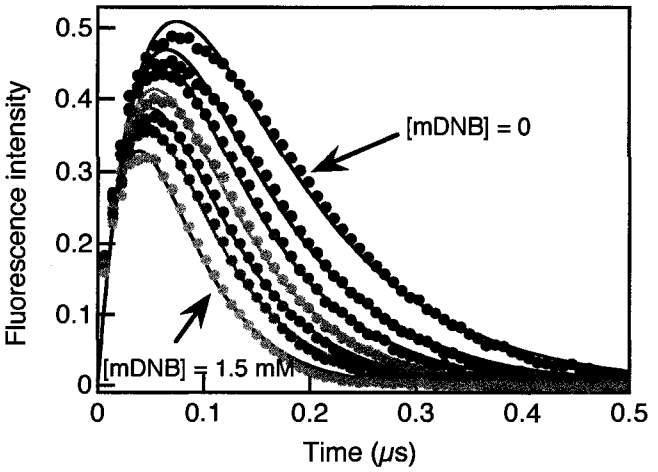

Figure 6.8. Time-resolved excimer fluorescence quenching of 3mM pyrene in nitrogen-purged 99% ethanol by mDNB, monitored at 464 nm following excitation at 355 nm.

Table 6.3. Experimental and calculated rate constants for pyrene fluorescence quenching by mDNB in nitrogen-purged 99% ethanol at room temperature.

[mDNB], mmol/L	k_1 (expt'l)[a], x10^7s^{-1}	k_1 (calc'd)[b], x10^7s^{-1}	k_2(expt'l)[c], x10^7s^{-1}
0.00	0.88	0.91	1.89
0.20	1.14	1.11	2.08
0.40	1.31	1.31	2.20
0.60	1.48	1.50	2.25
0.80	1.70	1.70	2.35
1.00	1.92	1.90	2.53
1.25	2.19	2.15	2.74

[a] Data shown in Figure 6.6.
[b] Values calculated according to the linear fit shown in Figure 6.6.
[c] Values obtained by fitting Figure 6.8 with Equation 6.3 and k_1 (calc'd).

Therefore, it is possible to generate quenching plots analogous to Figure 6.6 for the excimer species using the obtained values of τ_E^{-1}. Figure 6.9 shows the resulting relationship for mDNB (*i.e.* using the first and fourth columns in Table 6.3). This analysis was repeated for the other highly electron-deficient compounds, as these were the molecules that were able to appreciably quench the excimer species (as reflected in the decreasing values of τ_E). The values for the bimolecular quenching rate constants for the pyrene excimer are listed in Table 6.4. As expected, the electron-poor molecules all quench with rates approaching diffusion control: this is reasonable, as the quenching must compete with the rapid deactivation of the excimer (~50 ns), as well as overcome the high degree of 'stabilization' towards charge-transfer experienced by the excimer.

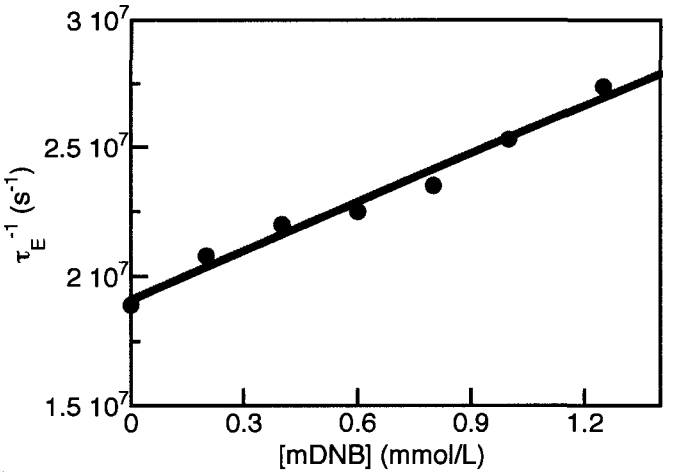

Figure 6.9. Quenching of fluorescence at 464 nm from 3 mM pyrene in nitrogen-purged 99% ethanol by mDNB, following laser excitation at 355 nm. Data points taken from Table 6.3.

Table 6.4. Quenching rate constants for pyrene excimer fluorescence in ethanol at room temperature.[c]

Quencher	k_q, $M^{-1}s^{-1}$
DCB	1.0×10^{10}
5NX	5.5×10^{9}
NB	6.4×10^{9}
pDMB	9.8×10^{9}
mDNB	6.3×10^{9}
DNFB	4.8×10^{9}

[c]Typical errors are <5%.

Since the integrals under the emission curves shown in Figure 6.8 are proportional to the emission intensity under steady state conditions, a Stern-Volmer plot, analogous to Figure 6.7 can also be constructed for the excimer, as shown in Figure 6.9. The plot based on τ_0/τ, is linear as expected, since it only reflects excimer quenching.

In contrast, mirroring the results from steady-state measurements, the plot of I_0/I (based on the integrals under the curves) displays positive deviation from ideal Stern-Volmer behaviour. Therefore, like the excimer quenching shown in Figure 6.2, this curve may be fitted with the second-order polynomial expression of Equation 6.2.[19] Note that only small curvature is introduced by the excimer term in this case.

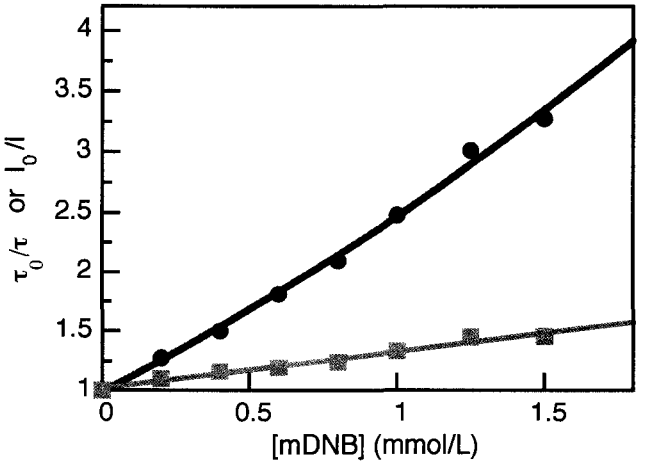

Figure 6.10. Stern-Volmer plots based on steady-state measurements (●) and time-resolved studies (■) for the quenching of the pyrene excimer (monitored at 464 nm).

Since τ_0/τ is linear with a non-zero slope, we may conclude that the excimer species is also being quenched in a dynamic fashion by mDNB. Therefore, *both* the pyrene monomer and excimer undergo dynamic quenching by nitroaromatic compounds. Thus, the excimer species does experience two modes of depletion by quencher: while it is being quenched, its precursor is being removed as well. This effect would manifest as mathematically identical to a combination of static and dynamic quenching, where the 'static' component is actually due to the suppression of the feed of excimer. As such, the Stern-Volmer plots from steady-state and time-resolved fluorescence measurements in this case resemble that described in Scheme 6.4.

We found this system to be intriguing, from both a mechanistic point of view and as a potential analytical technique. The following Section will describe how we anticipate differential pyrene fluorescence quenching could be used as a method to detect electron-deficient compounds, particularly explosives.

6.4 Potential Analytical Applications

The use of fluorescence spectroscopy to detect explosives is not new; an example is modification of environmental or forensic sample analysis: currently, samples are generally analyzed according to the EPA8330 protocol developed by the U.S. Environmental Protection Agency.[31] Recall from Chapter 1 that, in this method, samples are injected into a reverse-phase HPLC with UV-vis detection (Figure 6.11, A).[32] Similar methods employ capillary liquid chromatography to separate and identify sample mixtures.[33] Although sensitivity is high, it offers little selectivity towards explosives (electron-deficient compounds), especially when these compounds are part of complex mixtures. The addition of a fluorescence spectrophotometer as a detection system has previously been explored and has been proven to be an effective method: a fluorophore (pyrene) is introduced post-column *via* a mixing tee and the resulting fluorescence quenching by separated components is monitored,[4] resulting in a significant increase of the signal-to-noise ratio (Figure 6.11, B).

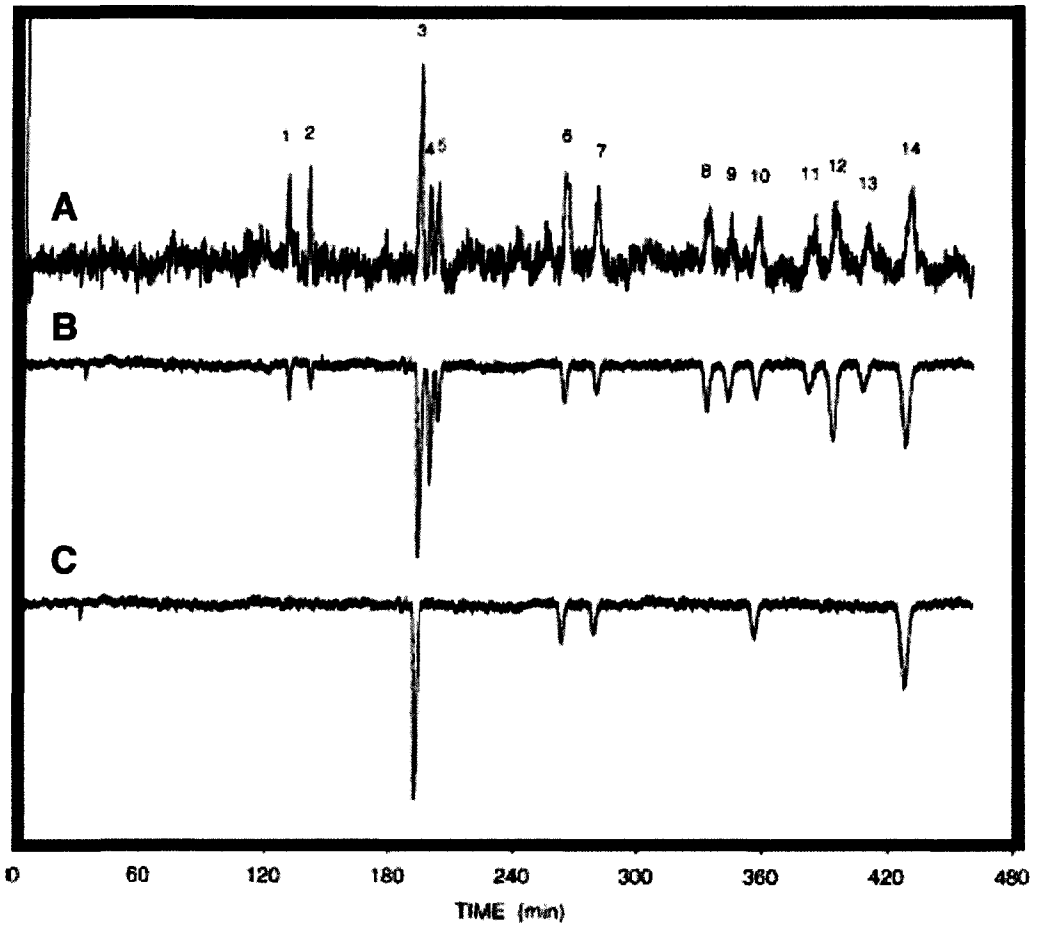

Figure 6.11. Comparison of the sensitivity and selectivity of various detection techniques, for a theoretical environmental or forensic sample containing explosives, following separation by HPLC. A) UV-visible absorbance detection. B) Fluorescence quenching detection. C). Hypothetical F_M/F_E response we anticipate from dual wavelength fluorescence quenching acquisition (generated artificially using chromatograph B).

We propose that recording the monomer fluorescence quenching, as reported by Goodpaster and McGuffin,[4] concurrent with acquisition of the F_M/F_E ratio will allow clear discrimination between general and specifically electron-deficient quenchers.

Experimentally this would require the use of a multi-wavelength fluorescence detector (such as a diode array), rather than a single wavelength detector.

Application of the ideas illustrated here to conventional LC analysis (*i.e.* F_M/F_E acquisition) should lead to chromatograms that highlight those peaks which are due to electron deficient molecules such as nitrated compounds, including explosives (Figure 6.11, C). While complete quantification would be possible with authentic samples, approximate values (±15%) could be obtained by assuming a representative value for the F_M/F_E response. The fact that nitrated aromatics cluster with slopes around 600±50 M^{-1} is partly due to the fact that the monomer and excimer quenching approaches diffusion control for these samples (*i.e.* the F_M/F_E response is limited by the fact that the excimer is quenched through two nearly diffusion-controlled processes). Finally, it should be noted that while this technique would require higher concentrations of fluorophore (to facilitate excimer formation), quenching does not require significantly larger concentrations of substrate.

Due to the high sensitivities associated with fluorescence detection, we anticipate that the experimental method described above would have a detection limit at or below 10 ppm, for molecules with typical molecular weights. For example, using the approximate response value of 600 M^{-1}, a 10 ppm (or 44 μM) solution of trinitrotoluene (TNT, 227.1 g/mol) would result in a 2% change in the F_M/F_E ratio, easily detectable by most modern fluorescence spectrometers.

Finally, it must be noted that the method does respond to electron-deficient molecules other than explosives, thus being prone to some false positives; however,

more importantly, the method is very unlikely to lead to *false negatives*, a desirable characteristic in security-related applications. Therefore, we envisioned this method would be useful as a screening technique to environmental or forensic laboratories processing large numbers of samples: if an obtained chromatogram shows no response during F_M/F_E acquisition, then it is highly unlikely that explosives are present in the sample. Consequently, analysts can instead focus on those samples which *do* elicit a response (with approximate concentrations in hand), thus saving both time and resources.

6.5 Conclusions

While the monomer-excimer photophysics of pyrene have been extensively studied in all manner of media, studies on the effect of certain quenchers on the *ratio* of the two species were somewhat limited. Thus, we undertook an investigation into how the presence of a variety of fluorescence quenching agents, from electron-rich to electron-poor compounds, might influence the monomer-excimer equilibrium. In the case of electron-deficient molecules, specifically nitroaromatics, we subsequently observed non-ideal Stern-Volmer quenching for the excimer under these conditions.

Through extensive steady-state and time-resolved fluorescence spectroscopy, we were able to elucidate the overall quenching mechanism responsible for the observed behaviour: electron-rich quenchers, such as *N,N*-dimethylaniline, quench the monomer species only, and thus the observed excimer quenching merely reflects the reduced population of its precursor. Conversely, electron-deficient molecules efficiently quench

both monomer and excimer emission with bimolecular rate constants approaching diffusion control; thus, the excimer experiences two modes of quenching: 'static'-type quenching of the excimer's precursor along with dynamic quenching of the excimer itself. As a consequence of this dual quenching mechanism, the monomer-to-excimer fluorescence ratio (F_M/F_E) is linearly proportional to the concentration of electron-deficient quenchers.

We have proposed that this effect may have potential applications as a method to detect electron deficient substrates: two-wavelength analysis of the quenching of pyrene fluorescence can unequivocally sense electron deficient molecules and also provide approximate concentration information even in the absence of authentic samples. We anticipate that this interesting characteristic could be employed in the detection of explosives.

6.6 References

1. Schoenfisch, M. H.; Huiping, Z.; Frost, M. C.; Meyerhoff, M. E., Nitric Oxide-Releasing Fluorescence-Based Oxygen Sensing Polymeric Films. *Anal. Chem.* **2002,** 74, (23), 5937-5941.

2. He, Y.; Geng, L., In Situ Time-Resolved Fluorescence Spectroscopy in the Frequency Domain in Capillary Electrochromatography. *Anal. Chem.* **2002,** 74, (8), 1819-1823.

3. Ji, J.; Rosenzweig, N.; Jones, I.; Rosenzweig, Z., Molecular Oxygen-Sensitive Fluorescent Lipobeads for Intracellular Oxygen Measurements in Murine Macrophages. *Anal. Chem.* **2001,** 73, (15), 3521-3527.

4. Goodpaster, J. V.; McGuffin, V. L., Fluorescence Quenching as an Indirect Detection Method for Nitrated Explosives. *Anal. Chem.* **2001,** 73, (9), 2004-2011.

5. Gilbert, A.; Baggott, J., *Essentials of Molecular Photochemistry.* Blackwell: Oxford, 1991.

6. Turro, N. J., *Modern Molecular Photochemistry.* University Science Books: Sausalito, 1991.

7. Birks, J. B., *Photophysics of Aromatic Molecules.* Wiley-Interscience: New York, 1970.

8. Birks, J. B.; Alwattar, A. J. H., Influence of Environment on the Radiative and Radiationless Transition Rates of the Pyrene Excimer. *Chem. Phys. Lett.* **1971,** 11, (1), 89-92.

9. Birks, J. B.; Christophorou, L. G., *Spectrochim. Acta* **1963,** 19, 401.

10. Birks, J. B.; Dyson, D. J.; Munro, I. H., 'Excimer' fluorescence II. Lifetime studies of pyrene solutions. *Proceedings of the Royal Society of London. Series A, Mathematical and Physical Sciences* **1963,** 275, 575-588.

11. Birks, J. B.; Seifert, H. G., Double-Photon Excitation of Excimer Fluorescence of Pyrene Solutions. *Phys. Lett.* **1965,** 18, (2), 127-128.

12. Duhamel, J.; Winnik, M. A.; Baros, F.; André, J. C.; Martinho, J. M. G., Diffusion Effects on Pyrene Excimer Kinetics: Determination of the Excimer Formation Rate Coefficient Time Dependence. *J.Phys. Chem.* **1992,** 96, (24), 9805-9810.

13. Duhamel, J.; Yekta, A.; Winnik, M. A., Excimer Lifetime Recovery: Application to Microheterogeneous Systems. *J. Phys. Chem.* **1993,** 97, 2759-2763.

14. Förster, T.; Kasper, K., Der Konzentrationsumschlag des Fluoreszenz des Pyrens. *Z. Phys. Chem. (N.F.)* **1954**, 1, 274.

15. Förster, T.; Kasper, K., Ein Konzentrationsumschlag der Fluoreszenz des Pyrens. *Z. Electrochim.* **1955**, 59, 976.

16. Stevens, B., *Spectrochim. Acta* **1962**, 18, 439.

17. Stevens, B., Influence of Environment on the Radiative and Radiationless Transition Rates of the Pyrene Excimer. *Adv. Photochem.* **1971**, 8, 161.

18. Winnik, F. M., Photophysics of Preassociated Pyrenes in Aqueous Polymer Solutions and in Other Organized Media. *Chem. Rev.* **1993**, 93, 587-614.

19. Lakowicz, J. R., *Principles of Fluorescence Spectroscopy, 2nd Ed.* Kluwer Academic: New York, 1999; p 9-10.

20. Goodpaster, J. V.; Harrison, J. F.; McGuffin, V. L., Ab Initio Study of Selective Fluorescence Quenching of Polycyclic Aromatic Hydrocarbons. *J. Phys. Chem. A* **2002**, 106, 10645-10654.

21. Goodpaster, J. V.; Howerton, S. B.; McGuffin, V. L., Forensic Analysis of Commercial Petroleum Products Using Selective Fluorescence Quenching. *J. Forensic. Sci.* **2001**, 46, (6), 1358-1371.

22. Howerton, S. B.; Goodpaster, J. V.; McGuffin, V. L., Characterization of polycyclic aromatic hydrocarbons in environmental samples by selective fluorescence quenching. *Anal. Chim. Acta* **2002**, 459, 61-73.

23. Pandey, S.; Fletcher, K. A.; Powell, J. R.; McHale, M. E. R.; Kauppila, A.-S. M.; Acree, W. A.; Fetzer, J. C.; Dai, W.; Harvey, R. G., Spectrochemical investigations of fluorescence quenching agents Part 5. Effect of surfactants on the ability of nitromethane to selectively quench fluorescence emission of alternants PAHs. *Spectrochim. Acta Part A* **1997**, 53, 165-172.

24. Sawicki, E.; Stanley, T. W.; Elbert, W. C., Quenchofluorometric Analysis for Fluoranthenic Hydrocarbons in the Presence of Other Types of Aromatic Hydrocarbon. *Talanta* **1964**, 11, 1433-1441.

25. Caldwell, R. A.; Creed, D.; DeMarco, D. C.; Melton, L. A.; Ohta, H.; Wine, P. H., Charge-Transfer Quenching of Singlet Excited Complexes. *J. Am. Chem. Soc.* **1980**, 102, (7), 2369-2377.

26. Stern, O.; Volmer, M., Uber Die Abklingzeit Der Fluoreszenz. *Phys. Z.* **1919**, 20, 183.

27. Barenholtz, Y.; Cohen, T.; Haas, E.; Ottolenghi, M., Lateral organization of Pyrene-labeled Lipids in Bilayers as Determined from the Deviation from Equilibrium between Pyrene Monomers and Excimers. *J. Bio. Chem.* **1996,** 271, (6), 3085-3090.

28. Focsaneanu, K.-S.; Scaiano, J. C., Potential analytical applications of differential fluorescence quenching: pyrene monomer and excimer emissions as sensors for electron deficient molecules. *Photochem. Photobiol. Sci.* **2005,** 4, 817.

29. Laidler, K., *Chemical Kinetics*. McGraw-Hill: New York, 1965.

30. Van Dyke, D. A.; Pryor, B. A.; Smith, P. G.; Topp, M. R., Nanosecond time-resolved fluorescence spectroscopy in the physical chemistry laboratory: Formation of the pyrene excimer in solution. *J. Chem. Ed.* **1998,** 75, 615.

31. Method 8330: Nitroaromatics and Nitramines by High Performance Liquid Chromatography (HPLC). In EPA, U. S., Ed. 1994.

32. Weisberg, C. A.; Ellickson, M. L., Practical modifications to U.S. EPA Method 8330 for the analysis of explosives by high performance liquid chromatography (HPLC). *Am. Lab.* **1998,** 30, (4), 32N-32V.

33. Goodpaster, J. V.; McGuffin, V. L., Separation of Nitramine and Nitroaromatic Explosives by Capillary Liquid Chromatography. *J. Liq. Chrom.* **2001,** 24, (13), 1965-1978.

Appendix 6.A. Quenchers Evaluated in This Chapter

Name	Abbreviation	Structure
p-dicyanobenzene, DCB	DCB	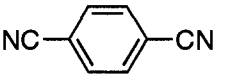
nitrobenzene, NB	NB	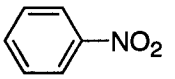
p-dinitrobenzene, pDNB	pDNB	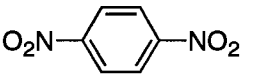
5-nitro-*m*-xylene, 5NX	5NX	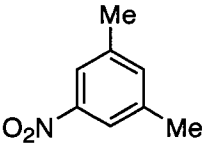
m-dinitrobenzene, mDNB	mDNB	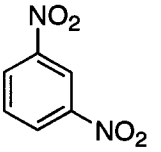
2,4-dinitrofluorobenzene, DNFB	DNFB	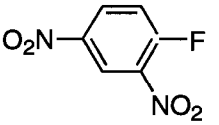
nitromethane, NM	NM	CH_3NO_2
nitroethane, NE	NE	$CH_3CH_2NO_2$
N,N-dimethylaniline, DMA	DMA	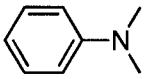
trioctylamine, TOA	TOA	$(CH_3(CH_2)_7)_3N$
N,N-dimethylaminopyridine, DMAP	DMAP	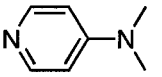
N,N-dimethyl-2,6-diisopropylaniline, DDA	DDA	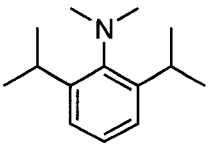
tribenzylamine	TBA	$(C_6H_5CH_2)_3N$
p-dimethoxybenzene	DMB	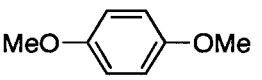

Chapter 7. Other Applications of Differential Pyrene Fluorescence Quenching

Chapter 7. Other Applications of Differential Pyrene Fluorescence Quenching

7.1 Introduction

While we were originally examining differential pyrene fluorescence quenching for quantification of nitrated compounds in solution, we soon discovered other practical uses for this phenomenon.

Thus, the concept of acquisition of the monomer-to-excimer fluorescence ratio was then extrapolated to other systems that we found intriguing. In this chapter, a few of the many other possible examples of such applications will be outlined, including the development of a sensor for dissolved oxygen, and explorations into potential solid-state sensors using gas-permeable silicone films and supramolecular materials (*i.e.* zeolites).

7.2 Pyrene Fluorescence Quenching by Oxygen

Following our elucidation of the mechanistic details of pyrene monomer and excimer fluorescence quenching by nitrated compounds, we were curious whether other highly electrophilic species would also display such behaviour in solution, specifically dissolved molecular oxygen. As in the case of nitroaromatic quenchers, monitoring the F_M/F_E fluorescence ratio could thus serve as a potential oxygen sensor as well.

Multiple laboratory techniques for *in situ* oxygen sensing are currently available. Two of the many examples, situated at either end of the 'accessibility' spectrum, are the

widely commercially-available oxygen electrodes and optrodes *versus* the custom-built oxygen-uptake systems originally built by Howard and Ingold.

Most commonly used oxygen sensors for measuring dissolved oxygen are based on a Clark-type electrode[1] or their modern equivalents, 'optrodes'. In the conventional Clark electrode, oxygen diffuses to the sensor through a permeable membrane, and is reduced to water at the cathode, creating a measurable electrical current, which is proportional to the dissolved oxygen concentration. Optrodes, such as the FOXY sensor manufactured by Ocean Optics[2], employ fiber optic technology to transmit light from a pulsed blue LED (~475 nm) to a sol-gel membrane containing an organometallic complex, which fluoresces at ~600 nm. When oxygen diffuses through the membrane, it quenches the complex's fluorescence and the resulting decrease in the detected fluorescence signal is also proportional to the dissolved oxygen concentration.[3] In both techniques, oxygen is consumed locally at the sensor tip during the measurement; hence samples must be stirred in order to obtain accurate values of $[O_2]$.

Conversely, oxygen consumption over the course of a reaction can be measured with remarkable accuracy and precision using oxygen uptake systems.[4-6] These can be very elaborate devices, using a dual-channel stainless steel apparatus: one chamber holds the experimental sample while the other holds a blank sample (*e.g.* it contains all the 'ingredients' for an autoxidation chain reaction except the initiator). This set-up is fitted with a sensitive pressure transducer, and the experiment works by measuring the differences in pressures above the two solutions as time progresses. This difference in pressure can then be converted to $\Delta[O_2]$.

However, these two techniques have disadvantages. Oxygen electrodes and optrodes are generally only useful for aqueous systems, as the polymer membranes used to form the sensing tips are usually soluble in organic solvents (an observation rather unfortunately made by a younger version of the present author). Furthermore, while the oxygen-uptake system is very precise, it is time-consuming to construct and calibrate, and its reporting method has yet to be digitized (the system uses a strip-chart recorder for data output). Therefore, given the sensitivity and ease of fluorescence measurements, we were enthused about the possibility of developing an *in situ* oxygen sensor using pyrene fluorescence quenching.

Samples containing 3 mM pyrene in 99% ethanol were purged with mixtures of nitrogen and oxygen or nitrogen and air using a calibrated flowmeter. Steady-state fluorescence measurements of these samples revealed that the quenching of pyrene monomer and excimer fluorescence by dissolved molecular oxygen does indeed follow the same behaviour as that shown by the nitroaromatic compounds in Chapter 6: the monomer quenching follows the linear Stern-Volmer equation for dynamic quenching, while the excimer shows an upward curvature which can be fitted with the polynomial expression of Equation 6.2.

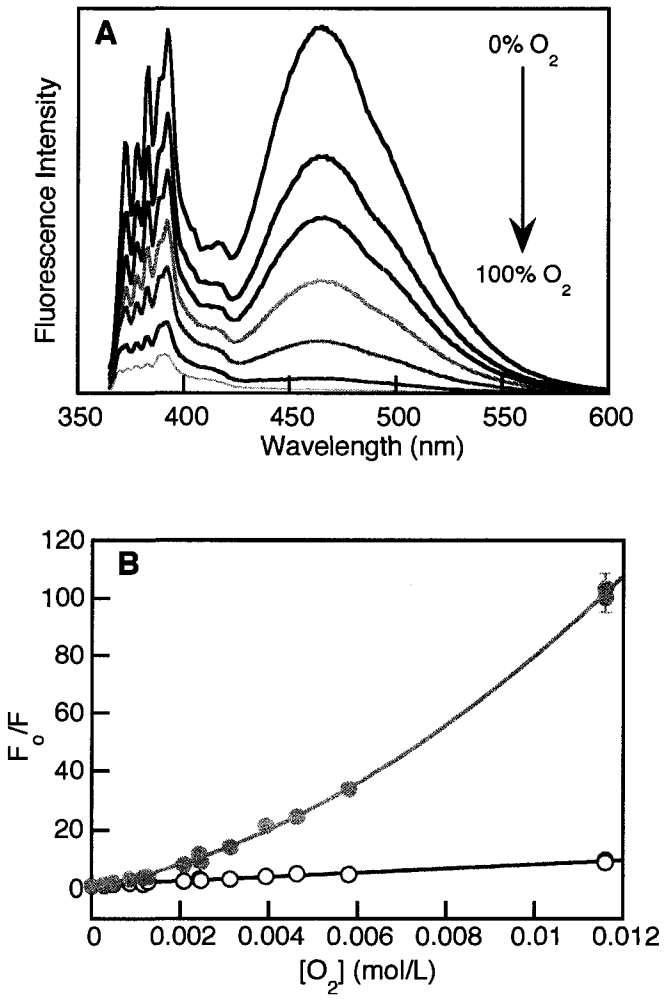

Figure 7. 1. A. Steady-state fluorescence quenching of pyrene 3 mM in 99% ethanol by dissolved oxygen; λ_{ex} = 355 nm. Some spectra omitted for clarity. B: Stern-Volmer plots taken at 392 nm to represent the monomer form (O) and 464 nm to represent the excimer form (●); bandpath ~ 3nm.

Again, while Equation 6.2 is commonly applied to systems involving a combination of static and dynamic quenching,[7] in this case, the positive deviation for the excimer form is due to the fact that it experiences two modes of quenching: both itself and its precursor are quenched dynamically with rates approaching diffusion control.

Therefore, by plotting the ratio of monomer-to-excimer fluorescence (F_M/F_E) as a function of the concentration of oxygen, a linear calibration curve is obtained.

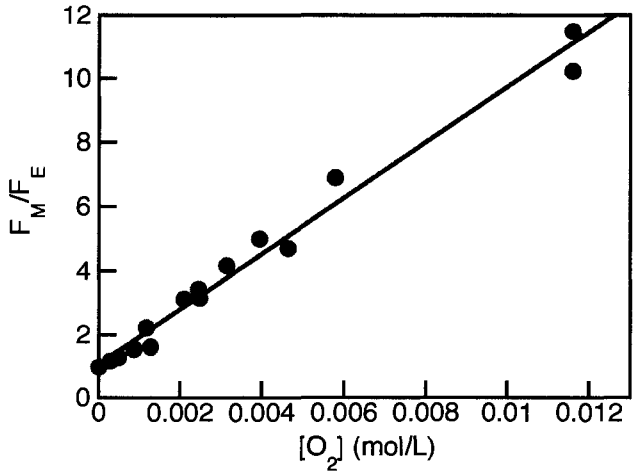

Figure 7.2. Calibration curves constructed by taking the ratio of fluorescence intensities of 3 mM pyrene (in 99% ethanol) quenched with oxygen at 392 nm and 464 nm (F_M/F_E).

In the preceding chapter, we were careful to mention that samples were thoroughly purged with nitrogen before analysis, and Figure 7.2 perfectly illustrates why this precaution is necessary: any oxygen present would contribute to a false positive response for the F_M/F_E signal.

Time-resolved fluorescence measurements of 3 mM pyrene in 99% ethanol quenched with oxygen (data not shown) were subjected to the same analysis as for the nitroaromatic quenchers in Chapter 6, yielding bimolecular quenching rate constants for the monomer and excimer species of 6.7×10^9 $M^{-1}s^{-1}$ and 1.0×10^{10} $M^{-1}s^{-1}$ respectively. Thus, we may conclude that the quenching of concentrated solutions of pyrene by oxygen follows the mechanism described for nitrated compounds.

With this result, we anticipate that pyrene differential fluorescence quenching is an innovative technique to measure dissolved oxygen in organic solvents. As a proof-

of-concept, we attempted to mimic the autoxidation of cumene used by Barclay and others to determine inhibition rate constants and stoichiometric factors for potential antioxidants.[4-6, 8, 9]

In this system, cumene is dissolved in aerated chlorobenzene along with a radical initiator, usually azobisisobutyronitrile (AIBN), which thermally decomposes with known rates to two carbon-centred radicals, commencing the autoxidation chain reaction (Scheme 7.1).

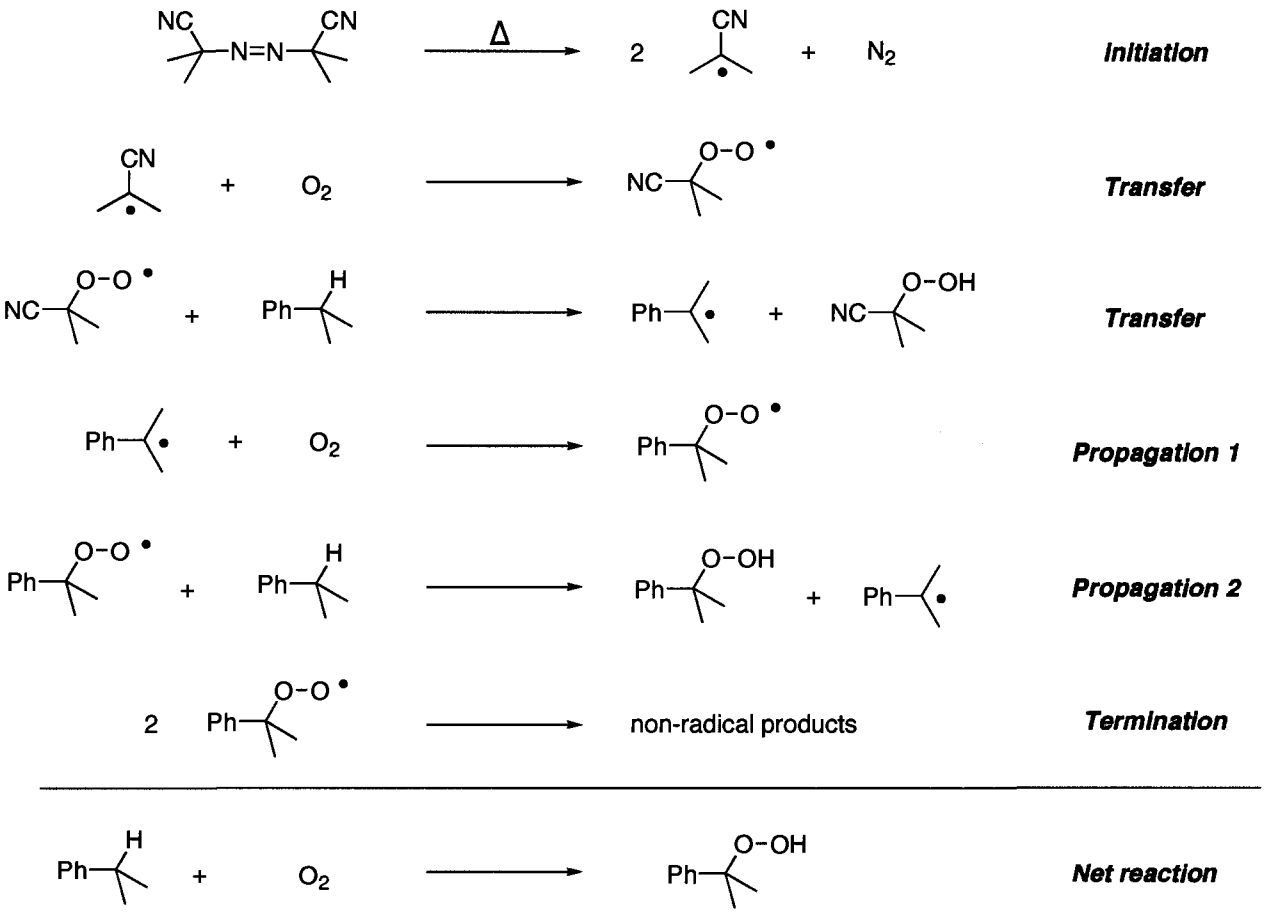

Scheme 7. 1. Chain reaction mechanism for the autoxidation of cumene, using AIBN as the initiator.

Samples were therefore prepared containing 5.35 M cumene, 3 mM pyrene and 8.5mM AIBN in chlorobenzene, and rapid steady-state fluorescence spectra were recorded at ~45°C every few minutes (Figure 7.3).

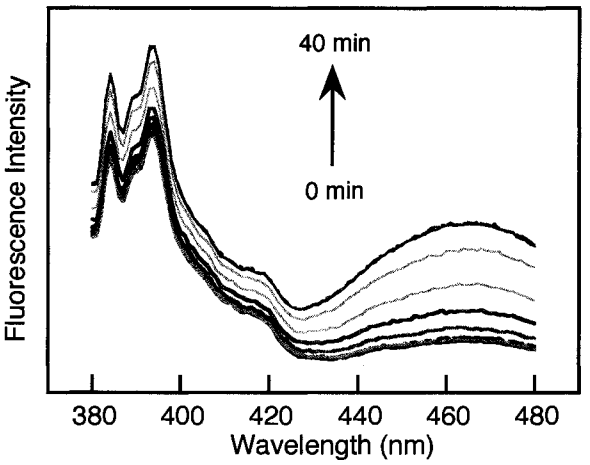

Figure 7. 3. Steady-state fluorescence spectra (λ_{ex}=355 nm) of an aerated chlorobenzene solution of 5.35 M cumene, 3mM pyrene, and 8.5 mM AIBN at ~45°C, recorded every few minutes after being placed in the thermo-stated fluorimeter. Control experiments (*i.e.* in the absence of either AIBN or oxygen) showed negligible fluorescence change with time.

Firstly, we must note the decreased amount of excimer in this system with respect to ethanol solution: this is due to the increased interactions between the pyrene monomer and aromatic solvent and hence a decreased value for the bimolecular rate constant for excimerization.[10-12] Secondly, a lag time of 3 to 4 minutes was observed, likely due to the time required for the sample to adjust to the temperature inside the fluorimeter. Thirdly, note that in this case the fluorescence is increasing, as the quencher, dissolved oxygen, is being consumed in the autoxidation reaction; the fluorescence reaches a plateau around 30 minutes, indicating that the total dissolved oxygen has been depleted and the chain reaction has stopped.

When the F_M/F_E ratio is plotted, the course of the autoxidation is clearly visible (Figure 7.4).

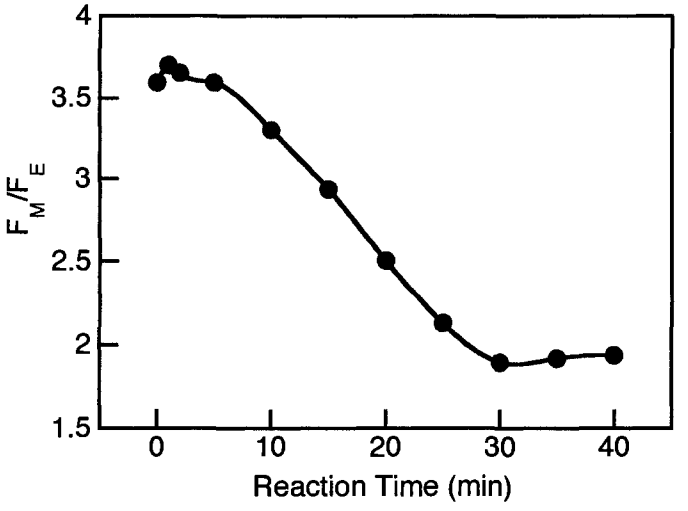

Figure 7.4. The ratio of fluorescence intensities of 3 mM pyrene (in 99% ethanol) at 392 nm and 464 nm (F_M/F_E), measured during the course of the autoxidation of cumene.

Recently, an oxygen-uptake system, used earlier by Barclay's group, was introduced in the Scaiano Group's facilities at the University of Ottawa, and we are now looking forward to further experiments to compare the pyrene fluorescence quenching method with this system. We anticipate that, once calibrated and tested, this novel method could also be used to monitor oxygen consumption and determine inhibition rate constants and stoichiometric factors for potential antioxidants in organic solvents. Furthermore, acquisition of the F_M/F_E ratio, rather than the quenching of the monomer alone, may also have the advantage of reduced sensitivity to any minute amounts of pyrene degradation that may occur during oxidation.

In summary, dissolved molecular oxygen effectively quenches emission from both the monomer and excimer forms of pyrene with rates approaching diffusion control. We believe that this characteristic could be employed in the development of a sensor for dissolved oxygen in organic solvents.

7.3 Pyrene Fluorescence Quenching in Silicone Films

Since we had thoroughly examined the effect of nitroaromatic quenchers in ethanol solution, we were intrigued about the possibility of the development of solid state sensors. To that end, we explored the use of silicone films as a means of immobilizing pyrene and creating a cheap, disposable sensor for nitroaromatics.

Swager has been a forerunner in the field of thin films in the detection of explosives. Originally constructed as a means to detect the minute amounts of vapours existing over buried landmines, he and his colleagues have developed a variety of films that are responsive to explosives, in particular, trinitrotoluene, TNT.[13-17] These films consist of pentiptycene-based highly-conjugated fluorescent polymers with rigid, three-dimensional backbones that are widely spaced apart. When exposed to TNT vapours, the TNT molecules can penetrate the film and settle within the pockets between polymer chains. Electron transfer from the electron-rich polymer to the electron-poor guest thus causes a highly amplified quenching of fluorescence. This amplification lends to sensitivities in the parts-per-quadrillion range; Swager has since developed these materials for use in handheld detection devices under the commercial name "Fido" with ICx Technologies, Inc.

While we did not anticipate that a simple system of pyrene in silicone films would provide sensitivities comparable to these materials, we nonetheless were intrigued to determine whether such films would respond to quencher vapours. We thus carried out a few exploratory experiments to assuage our curiosity.

Polydimethylsiloxane (PDMS) films loaded with 15% (w/w%) pyrene were prepared using commercially available silicones and cast onto glass microscope slides, with final film thicknesses of < 1mm. The slides were then placed in a sealed jar containing a 2x2 cm^2 wad of tissue that had been soaked in (neat) liquid quencher. Exposure times were measured with a stopwatch, and steady-state fluorescence spectra of the films were taken following exposure. Figure 7.5 shows the steady state spectra and resulting F_M/F_E plot for a pyrene-PDMS film exposed to nitrobenzene (NB) vapours.

In the film, molecular diffusion is sufficiently attenuated such that two distinct populations of monomers and excimers are present; the excimers must therefore arise from pre-existing aggregates in the film.

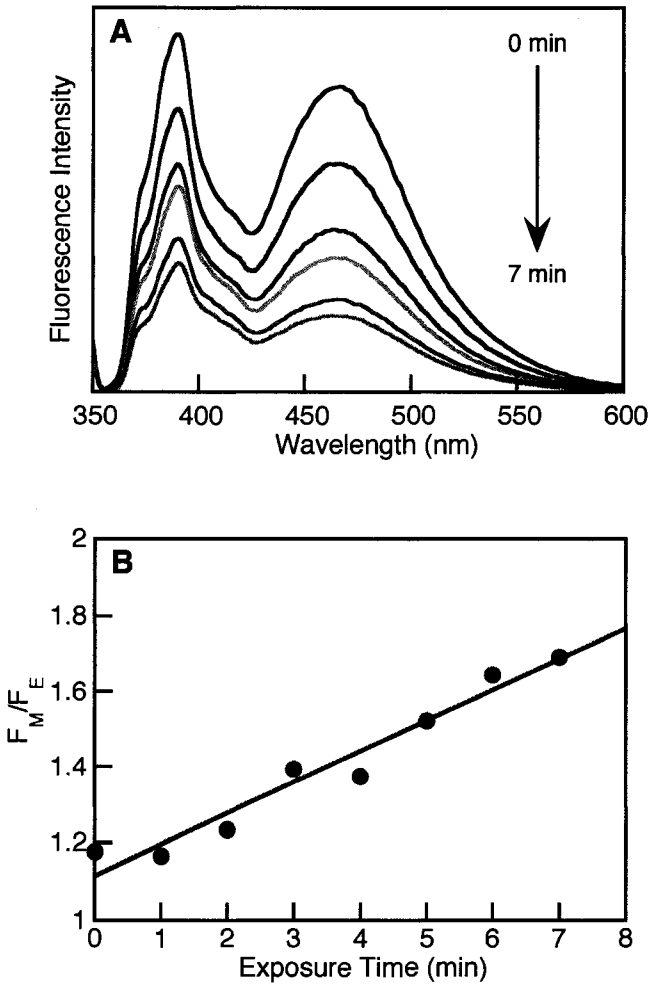

Figure 7.5. A: Steady-state fluorescence quenching of a pyrene-loaded PDMS film (15% w/w) exposed to nitrobenzene vapours; λ_{ex}= 340 nm. B: The ratio of fluorescence intensities at 392 nm and 464 nm (F_M/F_E) as a function of exposure time.

It is surprising, then, that differential quenching is indeed observed under these conditions, with a reasonable degree of linearity for a heterogeneous system, even though the F_M/F_E response is much less pronounced (*i.e.* compare the y-axes of Figure 7.5 and 7.2, for example). Since, in this case of a 'frozen' equilibrium, there is no 'precursor' for the excimers; thus the observed dual quenching is most likely due to the

competition of dynamic quenching a the surface with static-like quenching from nitrobenzene molecules that have penetrated the silicone film.

Nevertheless, we were pleased to see that our system could be extended to easy-to-prepare PDMS films. Using the vapour pressure of nitrobenzene (0.245 mmHg at 25°C), the volume of liquid quencher (~0.1 mL) and the volume of the sealed jar (~200 mL), we can obtain a rough approximation of 160 ppm for the concentration of NB in the jar. We thus concluded that, while this system is interesting as an extension of our previous work in solution, it certainly is no threat to Swager's fascinating fluorescent conjugated polymers.

7.4. Pyrene Fluorescence Quenching in Zeolite Y

A third possible application of differential monomer-to-excimer fluorescence quenching that we explored was the encapsulation of pyrene into supramolecular materials, namely zeolites.

Zeolites are synthetically prepared porous crystalline aluminosilicates with a continuous framework of AlO_4 and SiO_4 tetrahedra linked by their oxygen atoms. They can be represented by the formula: $M_{2/n}O \bullet AlO_2 \bullet xSiO_2 \bullet yH_2O$ where M is a group I or II cation.[18] Different zeolites have different Si/Al ratios and different types of cavities. For example, faujasites such as NaX and NaY (Figure 9) have 13 Å cavities interconnected with four neighbours in a tetrahedral arrangement through ~7.5 Å windows (for a full description of these materials, including their physical and chemical properties, consult reference 19).

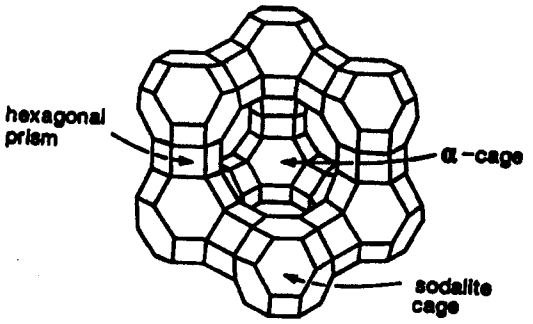

Figure 7.6. The structure of the cavity of faujasite NaY. From reference 18.

Since these cavities are of molecular dimensions, zeolites have the capacity to form 'guest-host' complexes, where substrates are encapsulated in the host's channels of cavities.[19] The incorporation of guest molecules into the zeolite interior is controlled by both the size of the zeolite cavity and the size of the entrance aperture: if the guest molecule has a kinetic diameter smaller than the pore opening, it can be directly included *via* either vapour phase or solution inclusion. Zeolite 'guest-host' complexes are designated by the abbreviation 'guest@zeolite', and the average loading, or *occupancy*, is the number of molecules per supercage and is denoted by <S>.

The incorporation of pyrene into zeolite materials has been extensively studied, and it has been demonstrated that the behaviour of pyrene in supramolecular systems is far more complex than in solution, exhibiting severe dependence on variables such as aging and sample preparation.[20-28] In particular, pyrene@Y has been a commonly used guest-host complex, as the cavities of zeolite Y are just large enough to accommodate the pyrene excimer. The excimer formed within such a doubly-occupied supercage arises in 7 to 14 picoseconds (depending on the composition of the zeolite), presumably

corresponding to the time required for the two molecules to achieve the face-to-face orientation required for the excimer.[20]

As an example of the importance of sample preparation, Cozens *et al.* prepared samples where <S>=0.1 (*i.e.* there is ~1% chance of double occupancy)[21]: early emission spectra were dominated by the excimer species, but after about 30 days, the fluorescence spectra indicated primarily monomer emission. Thus, it had taken the sample 4 weeks for the pyrene to percolate through the pores of the zeolite and achieve a random distribution.

In light of our fluorescence quenching results in solution, we were somewhat intrigued by a publication from Zhang and Thomas.[28] In this report, the authors examined the quenching of pyrene by *N,N*-dimethylaniline (DMA) in neutral zeolite Y (USY). They observed pyrene monomer fluorescence quenching, concurrent with the appearance of an emission centred around 460 nm (Figure 7.7). The authors surmised that this band was due to dynamic quenching of the pyrene monomer resulting in the formation of the pyrene-DMA exciplex, a phenomenon well established in non-polar solution.[29, 30]

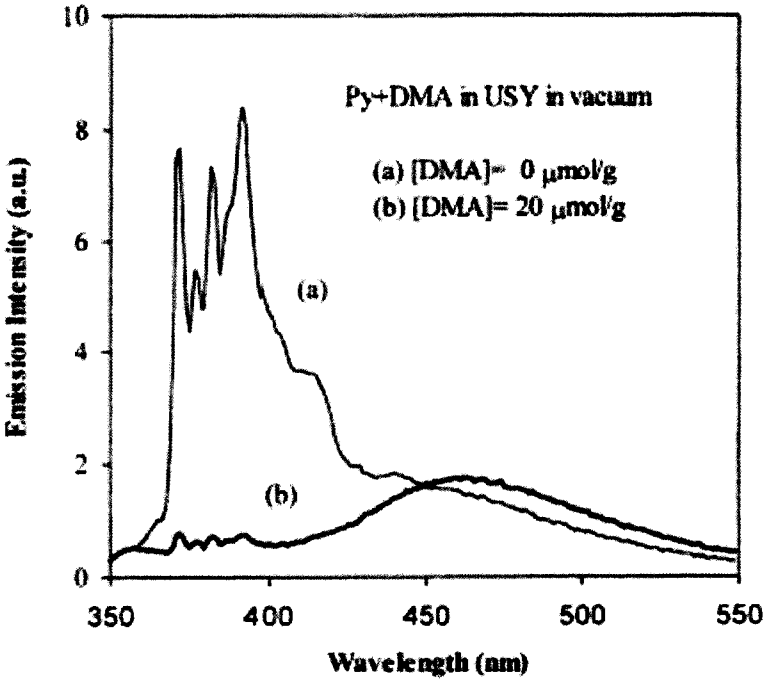

Figure 7.7. Steady-state measurements of pyrene fluorescence quenching by DMA in zeolite USY. [Py] = 1.0 x 10^{-7} mol/g; [DMA] = 2.0 x 10^{-5} mol/g. From reference 28.

While the loadings of pyrene are sufficiently low as to preclude the formation of excimer in a randomly distributed sample (<S> = 0.0002), the authors do not mention whether the samples were, in fact, aged as needed to achieve the necessary percolation of pyrene. Thus, it is possible that, if these are measurements performed on freshly prepared samples, the emission observed above 400 nm is due to pyrene excimers formed on the surface of the zeolite particles, as reported by Cozens *et al.* In this case, the spectrum of (Py+DMA)@USY would represent selective quenching of the pyrene monomer only by DMA - this seems reasonable, as we would not expect DMA to be able to quench excimer emission efficiently due to size constraints (*i.e.* the zeolite cavity cannot simulateously contain two molecules of pyrene and a molecule of DMA). We

employed time-resolved and steady-state fluorescence techniques to investigate this possibility, and a portion of these results are reported here. Based on our results in solution, we expected DMA to be a poor excimer quencher when encapsulated in Py@Y, while nitro compounds would show appreciable excimer quenching.

We prepared samples of (Py+DMA)@Y, but aged the samples in two different fashions: in Type A aging, pyrene and DMA were included together, and then aged in a vacuum desiccator for 20 days; in Type B aging, pyrene is included first, allowed to age for 20 days, and then DMA is added. Therefore, we expect situation A will require more work to reach statistical distribution because of the extra presence of the quencher molecules. On Day 0, all of the samples were sealed either under vacuum, nitrogen, or NO•; on Day 20, all of the samples were either sealed under vacuum, nitrogen, or oxygen. Final loadings of pyrene and DMA were determined to be <S>~0.7 and <S>~0.06.

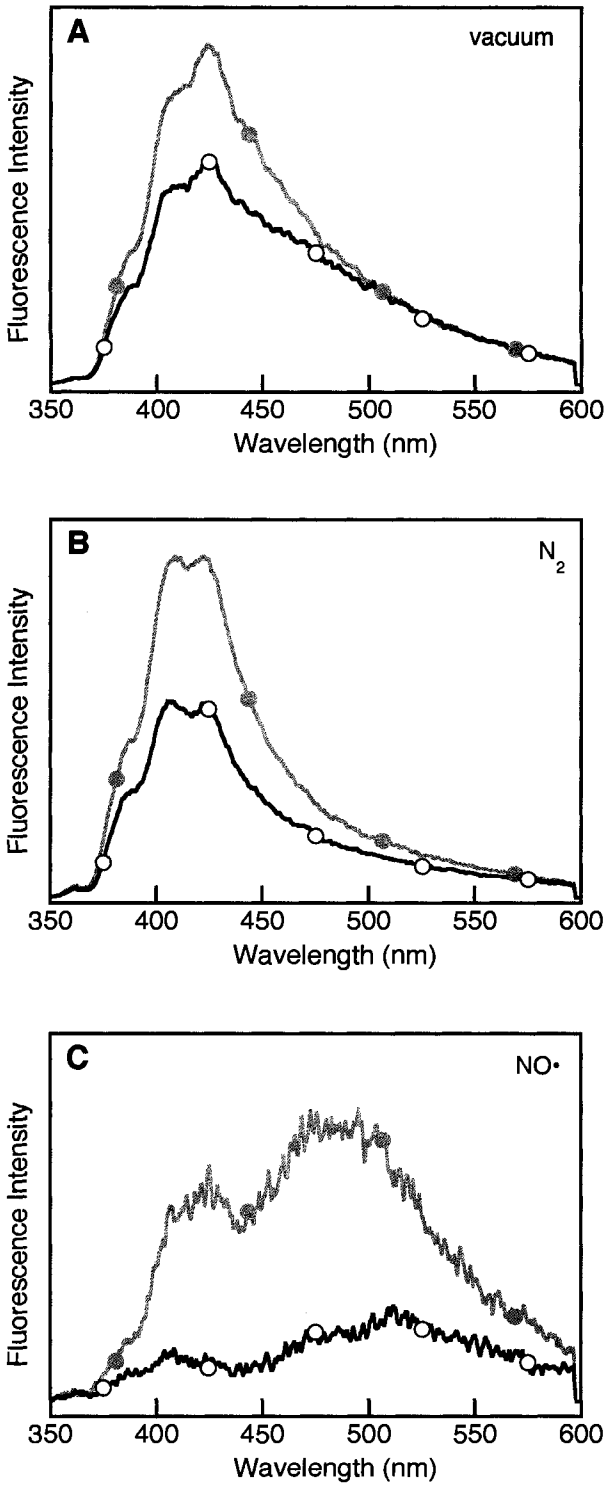

Figure 7. 8. Steady-state fluorescence spectra of Py@Y (●) and (Py+DMA)@Y (○) on Day 0, sealed under (A) vacuum, (B) nitrogen, and (C) NO•.

Figure 7.8 shows the steady-state fluorescence spectra recorded for the samples on Day 0. A number of observations may be made from these spectra. First, note that, as reported in the literature, the presence of nitrogen acts as a 'lubricant', accelerating the distribution of pyrene through the zeolite particle (as evidenced by the higher monomer-to-excimer ratio in B). Next, the spectra in Figure 7.8A suggest that the DMA is preferentially quenching the monomer species, just as we had speculated. Lastly, gaseous paramagnetic NO•, a highly potent fluorescence quencher, appears to readily percolate through the pores of zeolite Y and efficiently quench both species (the absolute intensities in Figure 7.8C are greatly reduced with respect to the other measurements).

Time-resolved fluorescence acquisition revealed that the co-inclusion of DMA resulted in no significant dynamic quenching of either the monomer or excimer species (only static quenching was found; data not shown). Conversely, NO• displayed both static and dynamic quenching modes.

Following the twenty days of two types of aging, the steady-state and time-resolved fluorescence was re-measured. The resulting spectra for the samples sealed under vacuum for the two types of aging are shown along with the Day 0 results in Figure 7.9.

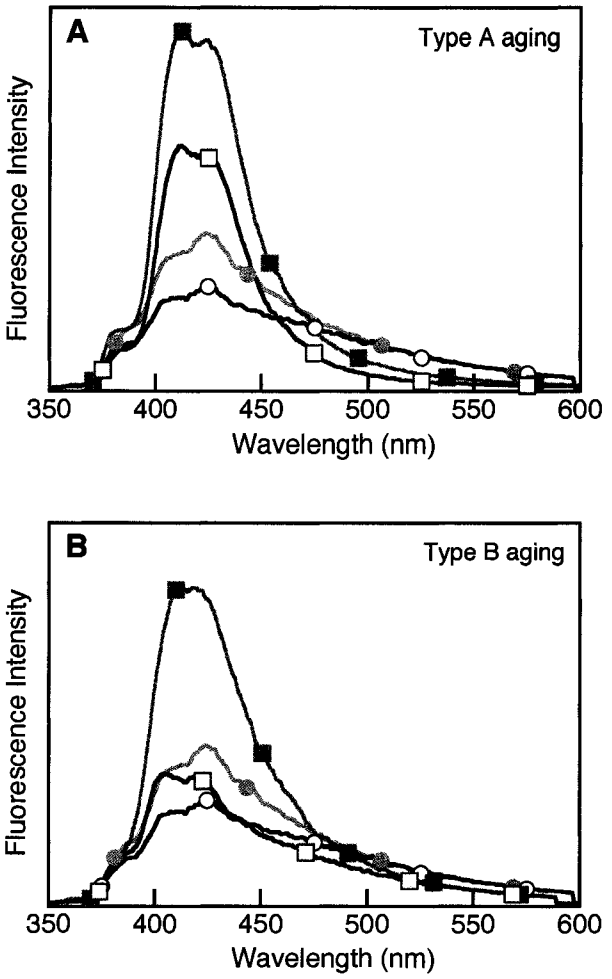

Figure 7. 9. Steady-state fluorescence spectra of Py@Y (●) and (Py+DMA)@Y (○) on Day 0 and Py@Y (■) and (Py+DMA)@Y (□) on Day 20, all sealed under vacuum, for Type A aging (A) and Type B aging (B).

Figure 7.9 shows that pyrene randomly distributes through the zeolite network over time, as greater proportion of monomer emission is obtained following twenty days of Type A aging and Type B aging (*vide infra*). This effect is also observed for DMA itself: note that the pyrene monomer is more efficiently quenched on Day 20 when the DMA has been freshly added, rather than co-included with pyrene on Day 0.

We repeated this experiment, using a nitroaromatic quencher, 5-nitro-*m*-xylene (5NX), which displayed differential monomer-to-excimer pyrene fluorescence

quenching in solution. Thus, rather than display all of the numerous permutations of comparing individual spectra, let us instead focus our attention on the ratio of monomer-to-excimer fluorescence intensities for each sample: would we observe DMA or 5NX quenching behaviour that differs from in solution? Figure 7.11 shows the F_M/F_E fluorescence intensity ratio for all the samples.

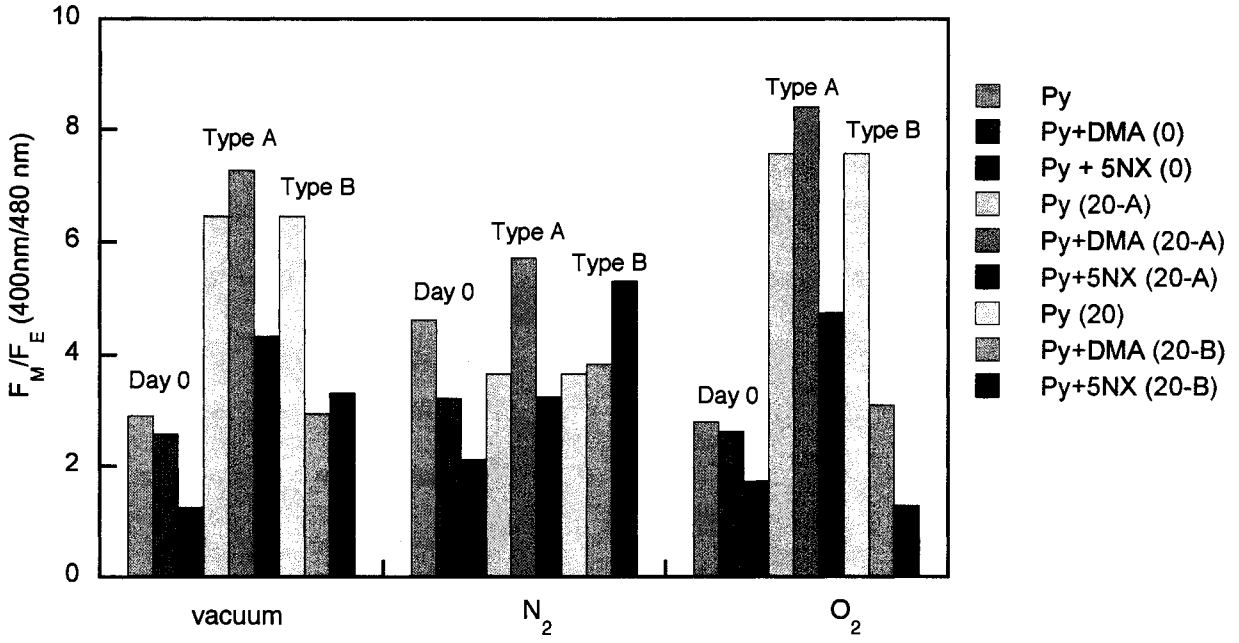

Figure 7. 10. F_M/F_E ratio for the steady-state fluorescence spectra of all samples. Note that on Day 0, the samples were treated with vacuum, N_2, and NO•, while on Day 20, the samples were treated with vacuum, N_2, and O_2.

From this complex graph, a few trends may be discerned in addition to those described above:

1. The amount of monomer emission increases with respect to the values recorded on Day 0, *i.e.* as pyrene percolates through the zeolite particle, the proportion of monomer increases.

2. On Day 0, under all conditions, F_M/F_E ratio *decreases* with respect to Py@Y when Q = DMA, and decreases further when Q = 5NX. If neither of these molecules quench the excimer species (due to size constraints), then this indicates that 5NX is a more efficient quencher of monomer fluorescence than DMA (as seen in solution).

3. If the F_M/F_E ratio *increases* with respect to Py@Y after aging, then it must be due to either an increase in the population of monomer or to quenching of the excimer species. Surprisingly, this occurs with DMA after Type A aging under vacuum, N_2, and O_2, and for 5NX after Type B aging under vacuum and N_2. Scaiano *et al.* demonstrated that triplet energy transfer from xanthone to 1-methylnaphthalene in zeolite NaY can occur between neighbouring supercages.[31] Thus, it may be possible that inter-cage electron transfer from DMA to the pyrene excimer is occurring, a phenomenon that is not observed in solution. However, this explanation could suffice for 5NX: based on rate constants observed in solution, we may not rule out the possibility that a nitroaromatic could undergo charge transfer with a pyrene molecule in a neighbouring cavity. In fact, Ellison *et al.* have proposed an electron-tunnelling mechanism for the quenching of singlet excited state anthracene by nitroalkanes in supramolecular materials.[23] Therefore, further study into electron-exchange processes between pyrene and electron-rich *vs.* electron-poor quenchers in supramolecular materials is needed to clarify this problem.

Again, time-resolved fluorescence measurements indicated that, in all cases, DMA and 5NX display only static quenching of the pyrene fluorescence emission. Thus, our observed quenching must be due to a quencher molecule either sharing a supercage with pyrene or a neighbouring cage. Finally, no evidence for exciplex formation between the pyrene monomer and DMA was observed under these conditions.

In summary, extensive steady-state and time-resolved spectroscopy of these materials (of which, only a portion was described here) revealed that pyrene fluorescence quenching within zeolite Y by electron-rich (DMA) and electron-poor (5NX) substrates is a complex process, depending on factors such as sample loading, order of sample loading, aging, and atmosphere. However, in all cases, both DMA and 5NX were found to quench monomer fluorescence in a static fashion; it is possible that 5NX may quench excimer fluorescence as well. Finally, while we found this system intriguing for its photophysical aspects, it is clear that the quenching mechanism of Py@Y is simply too inconsistent for these materials to be developed into a useful and reliable detection device.

7.5 Conclusions

Following our original investigation into the mechanism of differential pyrene fluorescence quenching by nitrated compounds in solution, we were eager to explore its other possible applications. Thus, the concept of acquisition of the monomer-to-excimer fluorescence ratio was then extrapolated to other systems that we found intriguing.

The chapter has described three of the many other possible examples of such applications. In the first section, we discovered that dissolved oxygen displayed

quenching behaviour identical to the nitroaromatics; thus, we have proposed that acquisition of the F_M/F_E ratio could potentially be developed into a sensor for dissolved oxygen in organic solvents. The second and third sections detailed our explorations into the effects of constrained media *e.g.* gas-permeable silicone films and supramolecular materials (*i.e.* zeolites) on the quenching behaviour. These heterogeneous systems proved to be obviously much more complex than in solution; and while they show interesting photophysics, a solid state sensor for nitroaromatics based on these techniques is likely impractical.

7.6 References

1. Clark, L. C.; Wolf, R.; Granger, D.; Taylor, Z., Continuous recording of blood oxygen tensions by polarography. *J. Appl. Physiol.* **1953,** 6, 189.

2. Fiber Optic Oxygen Sensors: Theory of Operation. www.oceanoptics.com/products/sensortheory.asp

3. Wang, W.; Reimers, C. E.; Wainwright, S. C.; Shahriari, M. R.; M.J., M., Applying Fiber-Optic Sensors for Monitoring Dissolved Oxygen. *Sea Technology* **1999,** 40, 69.

4. Burton, G. W.; Doba, T.; Gabe, E. J.; Hughes, L.; Lee, F. L.; Prasad, L.; Ingold, K. U., Autoxidation of biological molecules. 4. Maximizing the antioxidant activity of phenols. *J. Am. Chem. Soc.* **1985,** 107, 7053.

5. Howard, J. A.; Ingold, K. U., Absolute rate constants for hydrocarbon autoxidation. XVII. The oxidation of some cyclic ethers. *Can. J. Chem.* **1969,** 47, 3809.

6. Wayner, D. D. M.; Burton, G. W., *Handbook of Free Radicals and Antioxidants in Biomedicine.* CRC Press: Boca Raton, FL, 1989; Vol. Vol. III.

7. Lakowicz, J. R., *Principles of Fluorescence Spectroscopy, 2nd Ed.* Kluwer Academic: New York, 1999; p 9-10.

8. Barclay, L. R. C.; Baskin, K. A.; Kong, D.; Locke, S. J., Autoxidation of model membrane. The kinetics and mechanism of autoxidation of mixed phospholipid bilayer. *Can. J. Chem.* **1987,** 65, 2541.

9. Barclay, L. R. C.; Baskin, K. A.; Locke, S. J.; Schaefer, T. D., Benzophenone-photosensitized autoxidation of linoleate in solution and sodium dodecyl sulfate micelles. *Can. J. Chem.* **1987,** 65, 2529.

10. Birks, J. B., *Photophysics of Aromatic Molecules.* Wiley-Interscience: New York, 1970.

11. Birks, J. B.; Alwattar, A. J. H., Influence of Environment on the Radiative and Radiationless Transition Rates of the Pyrene Excimer. *Chem. Phys. Lett.* **1971,** 11, (1), 89-92.

12. Birks, J. B.; Dyson, D. J.; Munro, I. H., 'Excimer' fluorescence II. Lifetime studies of pyrene solutions. *Proceedings of the Royal Society of London. Series A, Mathematical and Physical Sciences* **1963,** 275, 575-588.

13. McQuade, D. T.; Pullen, A. E.; Swager, T. M., Conjugated Polymer-Based Chemical Sensors. *Chem. Rev.* **2000,** 100, 2537.

14. Swager, T. M., The molecular wire approach to sensory amplification. *Acc. Chem. Res.* **1998,** 31, 201.

15. Williams, V. E.; Swager, T. M., Iptycene-Containing Poly(aryleneethynylene)s. *Macromol.* **2000,** 33, 4069.

16. Yang, J.-S.; Swager, T. M., Porous Shape Persistent Fluorescent Polymer Films: An Approach to TNT Sensory Materials. *J. Am. Chem. Soc.* **1998,** 120, (120).

17. Yang, J.-S.; Swager, T. M., Fluorescent Porous Polymer Films as TNT Chemosensors: Electronic and Structural Effects. *J. Am. Chem. Soc.* **1998,** 120, 11864.

18. Leigh, W. J.; Johnston, L. J., Properties of surfactants, liquid crystals, and solid supports. In *Handbook of Organic Photochemistry, Volume II,* Scaiano, J. C., Ed. CRC Press: Boca Raton, 1989.

19. Chrétien, M. N. Photochemical, Photophysical, and Photobiological Studies of Zeolite Guest-Host Complexes. Doctoral Thesis, University of Ottawa, Ottawa, 2005.

20. Cheng, K. A. W. Y.; Schepp, N. P.; Cozens, F. L., Ultrafast dynamics of pyrene excimer formation in Y zeolites. *J. Phys. Chem. A* **2004,** 108, 7132.

21. Cozens, F. L.; Régimbald, M.; García, H.; Scaiano, J. C., Intrazeolite photochemistry. 15. Influence of aging, inert gases, and water on the mobility of pyrene molecules on the faujasite NaY. *J. Phys. Chem.* **1996,** 100, 18165.

22. Ellison, E. H., Effects of coadsorbed water on the mobility of polyaromatic hydrocarbons in zeolite Y. *J. Phys. Chem. B* **1999,** 103, 9314.

23. Ellison, E. H.; Thomas, J. K., Enhanced quenching of anthracene fluorescence by nitroalkanes in zeolite X and Y. *Langmuir* **2001,** 17, 2446.

24. Iu, K.-K.; Thomas, J. K., Photophysical properties of pyrene in zeolites. 2. Effects of coadsorbed water. *Langmuir* **1990,** 6, 471.

25. Liu, X.; Iu, K.-K.; Thomas, J. K., Photophysical properties of pyrene in zeolites. *J. Phys. Chem.* **1989,** 93, 4120.

26. Suib, S. L.; Kostapapas, A., Intermolecular Pyrene Excimer Formation in Zeolites. Decay Parameters and Ground-State Association. *J. Am. Chem. Soc.* **1984,** 106, (7705).

27. Thomas, A.; Polarz, S.; Antonietti, M., Influence of spatial restrictions on eqilibrium reactions: A case study about the excimer formation of pyrene. *J. Phys. Chem. B* **2003**, 107, 5081.

28. Zhang, G.; Thomas, J. K., Effects of Charge Stabilization on Electron Transfer Reactions in Zeolites. *J. Phys. Chem. B* **2003**, 107, 7254.

29. Gilbert, A.; Baggott, J., *Essentials of Molecular Photochemistry*. Blackwell: Oxford, 1991.

30. Turro, N. J., *Modern Molecular Photochemistry*. University Science Books: Sausalito, 1991.

31. Scaiano, J. C.; Camara de Lucas, N.; Andraos, J.; García, H., Intrazeolite Photochemistrty. 10. Determination of the distance for triplet energy transfer in the faujasite NaY. *Chem. Phys. Lett.* **1995**, 233, 5.

Chapter 8. Final Comments and Future Directions

Chapter 8. Final Comments and Future Directions

8.1 Final Comments

The work presented in this thesis is exemplary of recent shifts in the field of physical organic chemistry from basic to applied research. However, it represents only two small facets in the ever-increasing and exciting potential applications of fundamental concepts, in areas such as supramolecular chemistry, molecular recognition, materials chemistry and nanotechnology.

This thesis described two successful applications of physical organic chemistry. The first project investigated persistent carbon-centred radicals and the possible application of a kinetic phenomenon to deliberate and selective carbon-carbon bond formation mediated by recombination reactions using these species. The second project involved employing knowledge about pyrene, a highly-studied fluorophore, to a novel methodology to detect electron-deficient materials.

While examining the photodecomposition of the pesticide fenvalerate, we were stunned at the remarkable purity of the primary decomposition product. Subsequent investigation revealed that, of the two radical intermediates formed during the photolysis, one was a *stabilized yet transient* secondary benzylic radical, while the other was a *stabilized and persistent* nitrile-substituted secondary benzylic radical. Thus, we realized that the kinetic phenomenon known as the Fischer-Ingold Persistent Free Radical Effect (PFRE) was operating in this system and was responsible for the observed product selectivity.

The discovery of a persistent nitrile-substituted secondary benzylic radical was surprising. At the time, members of the Scaiano Group had been evaluating persistent carbon-centred radicals generated from lactone derivatives and their antioxidant potentials. A list of factors influencing attenuated reactivity towards molecular oxygen - a key criterion for both persistent and antioxidant behaviour - was compiled from careful studies of these lactones, and it was found that the α-cyanobenzylic radicals also displayed some of these characteristics. Thus, we were able report on an entirely new family of persistent carbon-centred radicals, where the elevated unpaired electron spin delocalization on the nitrogen atom and electron-withdrawing effects added to stabilization achieved by resonance through the aromatic ring.

Soon after these discoveries, M. Frenette was able to prepare head-to-head dimers of several of the persistent carbon-centred radicals examined in the group. When these dimers were found to be in thermal equilibrium with the radical species, we hastened to explore possible applications for these materials, such as their use as high-temperature antioxidants (to be detailed in M. Frenette's upcoming thesis).

A successful application of these dimers involved their use to achieve novel organic synthesis *via* radical-radical recombination reactions as controlled by the PFRE. We found it was possible to exploit this effect as a synthetic tool through the use of a "radical buffer", in which persistent radicals are generated thermally from the dimer starting materials; when a transient radical is then introduced photochemically, it will recombine selectively with the persistent radical species. This process was demonstrated in this thesis through the steady-state photolysis and laser flash

photolysis studies of dibenzyl ketone with 2,2,3,3-tetraphenylsuccinonitrile to produce 2,3,3-triphenylproprionitrile. Most remarkably, the obtained product mixtures were very clean, containing only two head-to-head recombination products. Also notable was the fact that this system was the first example to allow for complete independent control over the supply of the two radicals, and hence the proportion of the two observed products, simply by varying the temperature and light intensity. Thus, we were able to demonstrate that, by carefully choosing persistent/transient radical pairs, this method may be applied as a simple and effective route to novel carbon-carbon bond formation.

The second project described in this thesis involved the use of pyrene fluorescence quenching as a technique to detect electron-deficient compounds. In this case, the research was inspired by a publication reporting a novel modification to the generally accepted laboratory method to detect and quantify explosives (in brief: HPLC coupled with UV-vis detection). In that report, the authors described replacing the absorption spectrophotometer detection system with single-wavelength fluorescence detection; introduction of a constant flow of pyrene following separation by HPLC but prior to detection resulted in fluorescence quenching chromatograms with higher signal-to-noise ratios.

The authors had used a very dilute solution of pyrene; we were curious as to what quenching behaviour would be observed if a higher concentration of pyrene – facilitating the formation of pyrene excimer -- was used instead. Thus, from that speculation, the topic of the second project described in this thesis was developed.

Since the photophysical properties of pyrene in dilute and concentrated solutions had been a topic of intense research interest for many years, the dynamic equilibrium between the monomer and excimer forms has been largely elucidated. However, we realized that the effect of certain fluorescence quenchers on the *ratio* of emission from the two species remained largely unexplored. Thus, we carried out extensive time-resolved and steady-state fluorescence measurements to study the quenching behaviour of concentrated pyrene solutions.

It was found that certain quenchers, namely very electron-poor compounds, were able to efficiently and dynamically quench both the monomer and excimer species, with bimolecular quenching rate constants approaching diffusion control. As a consequence, by monitoring the monomer-to-excimer fluorescence ratio, we have reported that it is possible to identify and even (roughly) quantify these compounds. Therefore, we have anticipated that this characteristic can allow for potential security-related applications, including the detection of explosives and for rapid screening of complex samples suspected of containing explosives.

The concept of differential monomer-to-excimer fluorescence quenching was then extrapolated to other systems that we found intriguing. For example, it was found that, in addition to nitroaromatics, molecular oxygen also quenches both species with rate constants approaching diffusion-control; thus, this methodology can also feasibly be applied to sensing dissolved oxygen. As well, we explored the effect of constrained media on differential quenching, including the use of gas-permeable silicone films and supramolecular materials (zeolites), both heavily-loaded with pyrene. It was found that,

in this media, differential quenching is maintained, and thus these materials could potentially be developed as cheap and disposable sensor materials.

While the two concepts of physical organic chemistry we explored seem utterly dissimilar, in essence, this thesis has actually described two successful applications of 'weakly-bound dimers'. In the first project, covalently bonded dimers of persistent carbon-centered radicals were used in the deliberate and selective carbon-carbon bond formation mediated by the Persistent Free Radical Effect, while the second project involved employing fluorescence quenching of the excited-state dimer of pyrene to develop a novel methodology to detect electron-deficient materials.

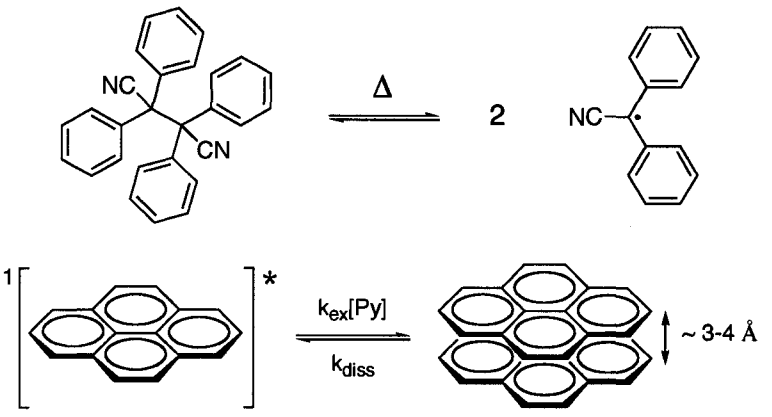

Scheme 8.1. The 'weakly-bound dimers' examined in this thesis. Top: Thermal equilibrium between persistent carbon-centred radicals and their head-to-head dimer precursor. Bottom: Excited-state dimer, or excimer, formed in concentrated solutions of pyrene.

Ultimately, these two projects demonstrate how fundamental concepts of physical organic chemistry may be applied to practical uses, from organic synthesis to molecular detection.

8.2 Future Directions

1. In the context of the persistent carbon-centred radicals, a thorough EPR study of these species is needed; M. Frenette is currently undertaking these measurements. Obtaining knowledge of the *g*-factors and hyperfine coupling constants for the nitrile-substituted benzylic radicals can give further information about the radical centre's electronic structure. Thus, such studies would complement the steady-state and time-resolved absorption spectra reported in this thesis, and complete the characterization of these species.

2. The exploration of antioxidant potential of the dimers of persistent carbon-centred radicals was briefly described in this thesis; specifically, the reactivity of these intermediates towards the trapping of benzylperoxyl and hydroperoxyl radicals. Obviously, more thorough investigation into their antioxidant behaviour towards other reactive oxygen species (such as alkoxyl radicals) is now prudent. Such experiments are currently being undertaken by M. Frenette, as well as the assessment of the rate constants for inhibition of the autoxidation reaction by comparison with established antioxidants, e.g. α-tocopherol.

3. While carbon-carbon bond formation via the combination of thermal and photochemical sources for persistent and transient radicals has been shown here to be a useful synthetic tool, we anticipate that the system described in Chapter 4 could be applied to other, innovative tandem-trapping type mechanisms. For example, one could

envision trialkylsilyl radicals ($R_3Si\bullet$) being trapped by an alkene or ketone, which is then subsequently trapped the persistent radical. Similarly, one could conceive systems involving competing reactions. For example, where a unimolecular rearrangement of a radical precursor competes with trapping by persistent radical: at low temperature one would trap the rearranged radical and at high temperatures the unrearranged one (as long as the rearrangement itself has a lower activation energy than the bond dissociation energy of the dimer). Finally, this section proved that the Persistent Free Radical Effect can effectively direct product formation in reactions involving radical intermediates: perhaps, then, there are a number of examples buried in the literature that could benefit from a re-interpretation, based on these observations!

4. In the context of the differential quenching of pyrene monomer and excimer quenching, an obvious departure would be the construction and testing of a modified EPA8330 method. This would involve the modification of a conventional LC separations module to include multi-wavelength fluorescence detection, for instance, through the addition of a photo-diode array detection system. Following the reverse-phase column but prior to the detector, a mixing tee is also added, into which a continuous stream of a moderately concentrated solution of pyrene (at least 1 mM) is introduced. Software controlling the apparatus would have to be manipulated such that single-wavelength quenching is simultaneously acquired with the monomer-to-excimer fluorescence ratio, thus supplying the analyst with two chromatographs for each injected sample. We anticipate that this would be an effective screening technique for

high-throughput analytical laboratories, as samples which give signals in the F_M/F_E chromatograph may be suspected of containing explosive compounds (with approximate concentrations) and thus may be selected for further analysis.

5. Experiments exploring the sensitivity of pyrene monomer and excimer fluorescence to the presence of dissolved oxygen shown in this thesis lend to a further investigation of the differential quenching method as a possible oxygen sensor. Recently, an oxygen-uptake system (identical to that used by L. R. C. Barclay to determine autoxidation inhibition rate constants) was established in the Scaiano Group; thus experiments comparing the oxygen-sensing capabilities of the two systems would be highly valuable.

8.3. Claims to Original Research

8.3.1. Results included in this thesis

1. Reactivities towards alkoxyl radicals of a family of nitrile-substituted hydrogen donors. Steady-state and time-resolved spectroscopy of the resulting α-cyanobenzylic radicals; examination of their persistence and reactivities towards molecular oxygen. Computational investigations into the geometries and spin delocalizations of the carbon-centred radicals to further understand the reasons behind their persistent nature and attenuated reactivity towards oxygen

2. Development of a novel synthetic route to carbon-carbon bond formation between transient and persistent radicals *via* application of the Persistent Free Radical Effect. Demonstration of the sensitivity of the resulting product distribution to the supply of the individual radicals (*i.e.* light intensity for the photochemically generated transient species and solution temperature for the thermally generated persistent species). Characterization of the radical intermediates by steady-state and time-resolved absorption spectroscopy and quantum mechanical calculations.

3. Characterization of the radical intermediates involved in the photodecomposition of the pesticide fenvalerate by steady-state and time-resolved absorption spectroscopy.

4. Demonstration of the antioxidant behaviour of dimers of persistent carbon-centred radicals towards benzylperoxyl and hydroperoxyl radicals to form unsymmetric peroxides and hydroperoxides, respectively.

5. Extensive steady-state and time-resolved fluorescence spectroscopy of concentrated solutions of pyrene in the presence of a variety of fluorescence quenchers, ranging from electron-rich to electron-poor compounds. Elucidation of the quenching mechanism, including bimolecular quenching rate constants. Development of a novel identification and quantification technique exploiting the differential pyrene monomer-to-excimer fluorescence quenching induced by electron-deficient molecules: construction of calibration curves by plotting the monomer-to-excimer fluorescence ratio as a function of quencher concentration.

6. Steady-state and time-resolved fluorescence spectroscopy of concentrated solutions of pyrene in the presence of molecular oxygen; development of a possible solution-phase oxygen sensor.

7. Investigation into the effect of constrained media on differential quenching, including the use of pyrene-loaded gas-permeable silicone films and supramolecular materials (zeolites).

8.3.2. Results not included in this thesis

1. Investigation into hydrogen-abstraction from the unsaturated fatty acid docosahexenoic acid by alkoxyl radicals; confirmation of a formula for hydrogen abstraction from fatty acids. Use of the benzhydrol probe technique to capture the growth of the resulting doubly-allylic fatty acid radical intermediate.

2. Investigation into carbon-centred radicals derived from indoles; determination of absolute rate constants for hydrogen abstraction by alkoxyl radical and subsequent characterization of the radical intermediates by time-resolved absorption techniques (with C. Aliaga).

3. Steady-state and time-resolved absorption and fluorescence spectroscopy of $[Ir(ppy)_2(vpy)Cl]$ and other similar derivatives: determination of fluorescence quantum yields and lifetimes (with M. De Rosa and published in *Inorg. Chem.* – see Section 8.4.2).

4. Investigation into the stabilization of polyurethane foams incorporated with HP-136, a lactone-based antioxidant. Photodegradation studies using both continuous (lamp) and pulsed (laser) irradiation (with M. Frenette). Unfortunately, this project, commissioned by Ciba Specialty Chemicals, Inc., was dropped as our results indicated that premature yellowing of the polyurethane was not decelerated by embedded amounts of HP-136.

5. Steady-state and time-resolved fluorescence quenching of 1,10-bis-(1-pyrenyl)decane (DPD) by electron-rich and electron-poor compounds and dissolved oxygen. Unlike the results shown in this thesis for pyrene in solution, fluorescence quenching of DPD does not show any discrimination between anilines and

nitroaromatics; it is, however, responsive to the presence of dissolved oxygen (akin to the results shown in Section 7.2), yet requires much lower concentrations than pyrene to excimerize (40 μM *vs.* 3 mM). Therefore, while DPD also shows potential for as an *in situ* oxygen sensor, its relatively high cost may unfortunately hinder its applicability in this field.

6. Steady-state and time-resolved fluorescence quenching of pyrene in micellar solutions by electron-rich and electron-poor compounds, specifically within micelles of sodium dodecyl sulfate (SDS). Again, unlike the results shown in this thesis for pyrene in solution, fluorescence quenching of pyrene in the micellar phase does not show any clear discrimination between anilines and nitroaromatics; instead, erratic and unreliable results were obtained, with no distinguishable trends.

8.4. Publications

8.4.1. Publications resulting from work presented in this thesis

- **Focsaneanu K.-S.**; Scaiano, J. C. The Persistent Free Radical Effect: From Mechanistic Curiosity to Synthetic Tool. *Helv. Chim. Acta*, **2006**, 89 (10), 2473.

- **Focsaneanu K.-S.**; Aliaga, C.; Scaiano, J. C. Photochemical Synthesis Mediated by Radical-Radical Reactions: Radical Buffer or the Persistent Free Radical Effect? *Org. Lett.*, **2005**, *7*(22), 4979-4982.

- **Focsaneanu K.-S.**; Scaiano, J. C. Potential analytical applications of differential fluorescence quenching: pyrene monomer and excimer emissions as sensors for electron deficient molecules. *Photochem. Photobiol. Sci.*, **2005**, *4*(10), 817.

- Scaiano, J. C.; Aliaga, C.; Chrétien, M. N.; Frenette, M.; **Focsaneanu, K.-S.**; Mikelsons, L. Fluorescence Sensor Applications as Detectors for DNA Damage, Free Radical Formation, and in Microlithography. *Pure and Applied Chemistry*, **2005**, *77*, 1009-1018.

- Sanjuàn, A.; Aguirre, G.; Alvaro, M.; Chrétien, M. N.; **Focsaneanu K.-S.**; Garcià, H.; Scaiano, J. C. Product Studies and laser flash photolysis of the direct and 2,4,6-triphenylpyrylium-zeolite Y photocatalyzed degradation of fenvalerate. *Photochem. Photobiol. Sci.*, **2002**, *1*, 955–959.

- Font-Sanchis, E.; Aliaga, C.; **Focsaneanu K.-S.**; Scaiano, J. C. Greatly attenuated reactivity of nitrile-derived carbon-centered radicals toward oxygen. *Chem. Commun.*, **2002**, 1576-1577.

8.4.2. Publications resulting from work not presented in this thesis

- DeRosa, M. C.; Mosher, P. J.; Yap, G. P. A.; **Focsaneanu K.-S.**; Crutchley, R. J.; Evans, C. E. B. Synthesis, Characterization, and Evaluation of $[Ir(ppy)_2(vpy)Cl]$ as a Polymer-Bound Oxygen Sensor. *Inorg. Chem.*, **2003**, *42*, 4864-4872.

- Cosa, G.; **Focsaneanu K.-S.**; McLean, J. R. N.; Scaiano, J. C. Photophysical Properties of DNA stain Dyes Bound to Double and Single Stranded DNA in Aqueous Buffered Solution. *Photochem. Photobiol.*, **2001**, *73*, 585-601.

- Cosa, G.; **Focsaneanu K.-S.**; McLean, J. R. N.; Scaiano, J. C. Direct Determination of Single-to-Double Stranded DNA Ratio in Solution Applying Time-resolved Fluorescence Measurements of Dye-DNA Complexes. *Chem. Commun.*, **2000**, 689-670.